Investigating resistance mechanisms to ATR inhibitors

Samantha Jan Olyha

Oriel College, University of Oxford

Thesis submitted for the degree of Master of Science by Research
Trinity Term 2016



CRUK/MRC Oxford Institute for Radiation Oncology
Department of Oncology, University of Oxford



OXFORD INSTITUTE FOR RADIATION ONCOLOGY



Investigating resistance mechanisms to ATR inhibitors

Samantha Jan Olyha
Oriel College, University of Oxford
Thesis submitted for the degree of Master of Science by Research
Trinity Term 2016

Abstract

The kinase activity of Ataxia-Telangiectasia and Rad3 related (ATR) protein plays a key role in controlling the DNA damage response (DDR) by acting through downstream targets to stabilise DNA replication forks, induce a transient cell cycle arrest to facilitate the repair of DNA, and thereby prevent premature mitosis in cells with unrepaired or unreplicated DNA. ATR is activated when single stranded DNA arises, for example, from stalled DNA replication forks or during the intermediate steps of double strand DNA break repair, and it is thought to mediate most of its responses through the downstream checkpoint kinase 1, CHK1. As ATR plays an important role in intra-S phase and G2/M cell cycle checkpoints, it has been proposed that inhibition of ATR activity selectively targets tumour cells that have defects in DNA damage-induced G1 cell cycle checkpoints by causing the accumulation of DNA damage and cell death.

AZD6738 is a selective ATR kinase inhibitor that is currently in early clinical development (phase 1). Since development of resistance has been universally observed with long-term use of kinase inhibitors in the clinic, we aimed to identify potential mechanisms of acquired resistance to AZD6738. In this study, we used an in vitro assay system using PC-9 human non-small cell lung cancer cells to generate independent clonal cell lines (SO25, SO45, and SO46) that were resistant to AZD6738. The resistant cells have increased relative cell viability in the presence of AZD6738 compared to the parental cells and, surprisingly, grow better in the presence of the inhibitor than in its absence. AZD6738 resistant cells are also cross-resistant to other chemically unrelated ATR inhibitors (VE-821 and VE-822) as well as CHK1/2 and WEE1 inhibitors, but not ataxia telangiectasia mutated (ATM) inhibitors. Together, cell cycle, DNA fibre, and RNA-sequencing analyses all point towards differential cell cycle regulation in the resistant clones while western blot analysis revealed activation of ATM signalling in the presence of AZD6738 in parental PC-9, but not in the resistant cells.

Western blot and RNA-sequencing analyses demonstrated that cyclins A2 and E1 are downregulated in the resistant cells. Knockdown of cyclin A2 and/or cyclin E1 using siRNA in parental PC-9 cells increased cell viability in the presence of AZD6738. We conclude that downregulation of cyclins A2 and E1 can confer resistance to ATR kinase inhibitors, and may also confer cross-resistance to other inhibitors targeting certain pathways downstream of ATR signalling (CHK1, WEE1).

Acknowledgements

Firstly, I would like to thank my supervisor, Dr. Anderson Ryan, for providing me with invaluable guidance, knowledge, experience, and moral support throughout my years in the lab and beyond. I have come a long way from the first days when I had to be reminded that science was more like an art than a science, and along the way have picked up a great deal of British trivia and a deep fondness for the United Kingdom.

Sincere thanks to all members of the Ryan lab: Fiona Cahill, Süreyya Çorbacioglu, Neele Drobnitzky, Marcus Green, Yanyan Jiang, Luiza Madia Lourenço, John Moore, Amalina Mumin, Agata Patel, Yasmin Shanneik, and Anika Weber, who have taught me a great deal both inside and outside of the lab, and who have become a dear second family to me. I cherished our lunchtime chats, trivia teams, and lab dinners, though I am still not clear on the differences between scones/cookies/biscuits. A special thanks to Anika for her extensive guidance and to Agata for taking the time to help me tie up loose ends, navigate the Oxford system, and put many anxieties to rest once I had returned to the United States for medical school.

I am extremely grateful to Jonas Harnau for his unending friendship, love, and support, and helping me to retain my sanity (and good posture) throughout the long process. Not to mention his statistical advice, willingness to hear all about my cells, and ability to track down paperwork and printers from across the ocean, without which this thesis would not exist.

And of course, none of this could have been possible without the unfailing love and support of Mom, Dad, Mandy, and Jim. For giving me up for two years to move across the pond, dealing with early morning phone calls, providing airport shuttle service during interview season, and everything in between, thank you very, very much.

Word Count: 29,616

Contents

1 INTRODUCTION 12
1.1 THE DNA DAMAGE RESPONSE 12
1.2 THE ROLE OF ATR IN RESPONSE TO DNA DAMAGE 13
1.3 ATR AS A TARGET FOR CANCER THERAPY 16
1.4 CURRENT ATR INHIBITORS 18
1.5 RESISTANCE TO ATR INHIBITORS 24
1.6 AIM OF THIS STUDY 25
2 MATERIALS AND METHODS 26
2.1 MAMMALIAN CELL CULTURE 26
2.1.1 Maintenance of cell lines 26
2.1.2 Cell counting and seeding 27
2.1.3 Cryostorage and thawing of cells 28
2.2 CLONE SELECTION 28
2.3 DRUG TREATMENTS 29
2.4 CELL VIABILITY ASSAY 29
2.5 PICOGREEN CELL PROLIFERATION ASSAY 30
2.6 PROTEIN DETECTION BY WESTERN BLOTTING (IMMUNOBLOTTING) 32
2.6.1 Preparation of cell extracts, gel electrophoresis, and transfer 32
2.6.2 Immunoblotting and chemiluminescent detections 33
2.6.3 Two-colour detection with infrared fluorescence 36
2.7 LIVE CELL IMAGING 37
2.8 CLONOGENICS 38
2.8.1 Clonogenic survival assay 38
2.8.2 Colony forming assay 38
2.9 TP53 GENE SEQUENCING 39
2.10 RNA-SEQUENCING 40
2.11 FLOW CYTOMETRY 42
2.11.1 DNA content analysis/cell cycle analysis 42
2.11.2 BrdU chase assay 43
2.12 IMMUNOFLUORESCENCE 44

2.12.1 Quantitative γH2AX, 53BP1, and RPA32 foci staining 45
2.12.2 Quantitative cyclin A2 and cyclin E1 staining 46
2.13 DNA Fibre Assay 46
2.13.1 Labelling and spreading fibres 46
2.13.2 Staining 47
2.13.3 Imaging 48
2.13.4 Analysis 49
2.14 siRNA Transfections 49
2.15 Data Analysis and Statistics 50
3 ATR Resistant Clones 52
3.1 Isolation of ATR inhibitor resistant clones 52
3.2 Response to ATR inhibitors 53
3.3 Proliferation of ATR inhibitor resistant clones 57
3.4 Colony forming ability of ATR inhibitor resistant cells 59
3.5 Clonogenic survival of ATR inhibitor resistant clones in the presence of increasing concentrations of AZD6738 61
3.6 Cross-resistance of ATR inhibitor resistance cells to other classes of DNA damage response modulators 62
3.7 Sensitivity to standard cancer chemotherapies 64
3.8 TP53 mutation status of resistant clones 65
3.9 Key pathway analysis 67
3.10 Key Findings 70
4 Mechanism of ATR Resistance 71
4.1 Cell cycle analysis 71
4.2 DNA fibre analysis 73
4.3 Analysis of RPA32 and γH2AX 75
4.4 Effect of endogenous replication stress on sensitivity to ATR inhibitors 78
4.5 Further pathway analysis 80
4.6 Confirmation of cyclin A2 and E1 levels with RNA-sequencing 86
4.7 Effect of knockdown of cyclins A2 and E1 86
5 Discussion 91
6 References 101
7 Supplemental Information 113

List of Figures

FIGURE 1.1: ATR ACTIVATION IN RESPONSE TO REPLICATION STRESS THAT LEADS TO LONG STRANDS OF SSDNA. 15

FIGURE 1.2: ATR- INDUCED CELL CYCLE ARREST IS MEDIATED THROUGH CHK1. 16

FIGURE 2.1: OUTLINE OF METHOD FOR ANALYSIS OF RNA-SEQUENCING DATA. 42

FIGURE 3.1: GENERATION OF AZD6738 RESISTANT PC-9 CLONES. 52

FIGURE 3.2: APPEARANCE OF PARENTAL PC-9 AND SO25, SO45, AND SO46 RESISTANT CLONES. 54

FIGURE 3.3: RESPONSE OF PC-9 CELLS AND SO25, SO45, AND SO46 RESISTANT CLONES TO INCREASING CONCENTRATIONS OF AZD6738. 54

FIGURE 3.4: REPONSES OF PC-9, SO25, SO45, AND SO46 CELLS TO ATR INHIBITION BY VE-821 AND VE-822. 56

FIGURE 3.5: VISUALISATION OF THE UP-TAKE OF VE-822 INTO PC-9 AND RESISTANT CELLS. 58

FIGURE 3.6: RELATIVE GROWTH OF PC-9 AND ATR RESISTANT CELLS. 59

FIGURE 3.7: PLATING EFFICIENCY OF PC-9 AND SO25 CELLS IN THE PRESENCE OF ATR INHIBITORS. 60

FIGURE 3.8: CLONOGENIC SURVIVAL ASSAY WITH INCREASING CONCENTRATIONS OF AZD6738. 61

FIGURE 3.9: RESPONSES OF PC-9 AND RESISTANT CLONES TO DIFFERENT CLASSES OF DNA DAMAGE RESPONSE MODULATORS. 63

FIGURE 3.10: SENSITIVITY OF PC-9 AND ATR INHIBITOR RESISTANT CELLS TO INCREASING DOSES OF GEFITINIB. 66

FIGURE 3.11: SO25 CELLS EXPRESS MUTANT TP53. 66

FIGURE 3.12: SCHEMATIC SHOWING KEY PATHWAY ANALYSIS OF DIFFERENTIAL EXPRESSION OF CELL CYCLE REGULATED IN ATR INHIBITOR RESISTANT SO25 CELLS AND PARENTAL PC-9 CELLS. 69

FIGURE 4.1: AZD6738 LEADS TO EARLY S-PHASE ARREST IN PC-9 CELLS. 72

FIGURE 4.2: TREATMENT WITH AZD6738 FOR 24 H CAUSES MORE S-PHASE INCORPORATION OF BRDU IN SO25 CELLS. 73

FIGURE 4.3: CLDU TRACT LENGTH DISTRIBUTION IN PC-9 AND SO25 CELLS FOLLOWING TREATMENT WITH AZD6738. 75

FIGURE 4.4: AVERAGE RPA32 PER CELL FOCI UPON TREATMENT WITH AZD6738. 76

FIGURE 4.5: AVERAGE γH2AX FOCI PER CELL AND PAN-NUCLEAR γH2AX UPON TREATMENT WITH AZD6738. 77

FIGURE 4.6: CO-LOCALISATION OF 53BP1 AND γH2AX FOCI. 77

FIGURE 4.7: A549, CALU-6, H1975, AND NBE1 LACK AN EARLY S-PHASE ARREST FOLLOWING TREATMENT WITH AZD6738. 79

FIGURE 4.8: INCREASE IN PAN-NUCLEAR γH2AX, BUT NOT IN γH2AX FOCI, UPON TREATMENT WITH AZD6738 CORRELATES WITH SENSITIVITY. 80

FIGURE 4.9: ATR SIGNALLING IN PC-9 AND RESISTANT CELLS. 82

FIGURE 4.10: ATM SIGNALLING IS ACTIVATED IN PC-9 CELLS, BUT NOT RESISTANT CELLS, IN RESPONSE TO ATR INHIBITION. 83

FIGURE 4.11: RESISTANT CLONES HAVE LOWER LEVELS OF CYCLIN A2 AND E1. 85

FIGURE 4.12: RNA-SEQUENCING CONFIRMS SIGNIFICANTLY LOWER LEVELS OF CYCLINS A2 AND E1 IN SO25 CELLS COMPARED TO PARENTAL PC-9. 86

FIGURE 4.13: CYCLIN A2, BUT NOT CYCLIN E1 SHOWED SUFFICIENT KNOCKDOWN WITH SIRNA. 87

FIGURE 4.14: CYCLIN A2 AND E1 KNOCKDOWN IN PC-9 CELLS CONFERS RESISTANCE TO AZD6738 TREATMENT. 89

FIGURE 4.15: CYCLIN A2 AND E1 – TREATED PC-9 CELLS HAVE A SIMILAR APPEARANCE TO RESISTANT CELLS. 90

SUPPLEMENTARY FIGURE 1: LEGEND FOR CELL CYCLE SCHEMATIC. 120

List of Tables

TABLE 1.1: ATR INHIBITORS. 20

TABLE 2.1: CELL LINES USED IN THIS STUDY....27

TABLE 2.2: DNA LYSIS BUFFER COMPOSITION....31

TABLE 2.3: LYSIS BUFFER STOCK COMPONENTS FOR WESTERN BLOT CELL EXTRACT COLLECTION. 33

TABLE 2.4: BUFFERS AND SOLUTIONS USED IN IMMUNOBLOTTING. 34

TABLE 2.5: PRIMARY ANTIBODIES USED FOR IMMUNOBLOT ANALYSIS. 34

TABLE 2.6: SECONDARY ANTIBODIES USED FOR IMMUNOBLOT ANALYSIS. 36

TABLE 2.7: SECONDARY ANTIBODIES USED FOR TWO-COLOUR DETECTION WITH INFRARED FLUORESCENCE. 37

TABLE 2.8: PCR REACTION COMPONENTS. 40

TABLE 2.9: PLATING CONDITIONS FOR RNA-SEQUENCING. 41

TABLE 2.10: PRIMARY ANTIBODIES USED IN IMMUNOFLUORESCENCE. 45

TABLE 2.11: SPREADING BUFFER COMPONENTS FOR DNA FIBRE ASSAY....47

TABLE 2.12: PRIMARY ANTIBODIES USED IN THE DNA FIBRE ASSAY....48

TABLE 2.13: SECONDARY ANTIBODIES USED IN THE DNA FIBRE ASSAY....48

TABLE 3.1: PERCENT RELATIVE CELL VIABILITY AT 1.11 MM AZD6738....55

TABLE 3.2: PERCENT RELATIVE CELL VIABILITY AT 1 MM VE-821 AND 1.11 MM VE-822. 56

TABLE 3.3: DOUBLING TIME OF PC-9 AND SO25 CELLS....57

TABLE 3.4: SENSITIVITY OF PC-9 AND RESISTANT CELLS TO MK-1775....63

TABLE 3.5: SENSITIVITY OF PC-9 AND ATR INHIBITOR RESISTANT CELLS TO AZD7762....64

TABLE 3.6: SENSITIVITY OF PC-9 AND ATR INHIBITOR RESISTANT CELLS TO CHEMOTHERAPY AGENTS ALONE AND IN COMBINATION WITH AZD6738. 65

TABLE 3.7: SAMPLES FOR RNA-SEQUENCING....68

TABLE 3.8: COMPARISONS OF RNA-SEQUENCING EXPRESSION[1] 68

TABLE 4.1: MEAN CLDU FIBRE TRACT LENGTHS IN PC-9 AND RESISTANT CELLS. 74

TABLE 4.2: SENSITIVITY OF VARIOUS CELL LINES TO AZD6738. 78

TABLE 4.3: PC-9 CELLS TREATED WITH CYCLIN A2 AND/OR E1 HAVE INCREASED RELATIVE CELL VIABILITY AT 1.11 MM AZD6738.....90

SUPPLEMENTARY TABLE 1: TOP 200 DIFFERENTIALLY EXPRESSED GENES BETWEEN CONDITIONS #1 (PC-9) AND #4 (SO25) RANKED ON Q VALUE (LOW TO HIGH), P VALUE (LOW TO HIGH) AND ABS (TEST STATISTIC) (HIGH TO LOW).....113

SUPPLEMENTARY TABLE 2: KEY PATHWAYS DIFFERENTIALLY REGULATED BETWEEN PC-9 AND SO25 CELLS.....118

Abbreviations

53BP1	tumour protein p53 binding protein 1
A	adenine
ADP	adenosine diphosphate
ALT	alternative lengthening of telomeres
ANOVA	analysis of variance
A-T	Ataxia-telangiectasia
ATCC	American Type Culture Collection
ATM	ataxia-telangiectasia mutated
ATP	adenosine triphosphate
ATR	ataxia-telangiectasia and Rad3-related
ATRIP	ATR interacting protein
BRCA2	breast cancer type 2 susceptibility protein
BrdU	bromodeoxyuridine
BSA	bovine serum albumin
C	Celsius or cytosine
CCNA2	cyclin A2
CCNE1	cyclin E1
CDC2	cell-division cycle 2
CDC25	cell division cycle 25
CDK	cyclin dependent kinase
CDT1	chromosome licensing and DNA replication factor 1
CFP	cyan fluorescent protein
CHK1	CHEK1, checkpoint kinase 1
CHK2	CHEK2, checkpoint kinase 2
CldU	5-chlorodeoxyuridine
CLL	chronic lymphocytic leukaemia
CO_2	carbon dioxide
CRISPER	clustered regularly interspaced short palindromic repeats
CV	crystal violet
DAPI	4’,6-diamidino-2-phenylindole
DDR	DNA damage response
dH_2O	distilled water
DMEM	Dulbecco's modified Eagle's medium
DMSO	dimethyl sulfoxide
DNA	deoxyribonucleic acid
DNA-PK	DNA-dependent protein kinase
DNA-PKcs	DNA-dependent protein kinase catalytic subunit
dNTP	deoxynucleotide triphosphate
DSB	double-strand break
E	glutamate
EDTA	ethylenediaminetetraacetic acid
EGFR	epidermal growth factor receptor
FACS	fluorescence-activated cell sorting
FBS	foetal bovine serum
FPKM	Fragments per kilobase of transcript per million mapped reads
G	guanine

g	gram(s)
Gln	glutamine
G1-phase	gap phase of cell cycle before DNA replication
G2-phase	gap phase of cell cycle before mitosis
Gy	Gray
h	hour(s)
H_2O	water
HCl	hydrochloric acid
HER2	human epidermal growth factor receptor 2
HR	homologous recombination
HRP	horseradish peroxidase
HU	hydroxyurea
HUS1	HUS1 checkpoint clamp component
I	isoleucine
IC_{50}	half-maximal inhibitory concentration
IdU	5-iododeoxyuridine
IR	ionising radiation
KAP1	Krüppel-associated box-associated co-repressor 1
kDa	kilo-Dalton
KPA	key pathway analysis
L	litre
M	molarity or methionine
m	metre
min	minute(s)
M-phase	mitosis
MTOR	mechanistic target of rapamycin
Na_3VO_4	sodium orthovanadate
NaCl	sodium chloride
NAE	Nedd8-activating enzyme
NaF	sodium fluoride
NaOH	sodium hydroxide
NER	nucleotide-excision repair
NGS	normal goat serum
NSCLC	non-small cell lung cancer
P	proline
p53 (TP53)	tumour protein 53
PARP	poly(ADP-ribose)-polymerase
pATM	phospho-ATM
PBS	phosphate buffered saline
PBS-T	phosphate buffered saline with Tween 20
pCHK1	phospho-CHK1
pCHK2	phospho-CHK2
PCR	polymerase chain reaction
PE	plating efficiency
PFA	Paraformaldehyde
pHH3	phospho-histone H3
PI	propidium iodide
PI3K	phosphatidylinositol-3-OH kinase
PIKK	phosphatidylinositol 3-kinase-related kinase
pKAP1	phospho-KAP1

PLL	prolymphocytic leukaemia
PPIB	peptidyl-prolyl cis-trans isomerase B (Cyclophilin B)
pTP53	phospho-tumour protein 53
Q	glutamine
R	arginine
RAD1	radiation sensitivity abnormal 1
RAD17	radiation sensitivity abnormal 17
RAS	rat sarcoma
RFC	replication factor C
RNA	ribonucleic acid
RPA	replication protein A
RT	room temperature
S	serine
S-phase	DNA replication or synthesis phase of the cell cycle
SchB	Schisandrin B
SDS	sodium dodecyl sulphate
sec(s)	second(s)
SEM	standard error of the mean
Ser	serine
siRNA	small interfering ribonucleic acid
SMARCAL1	SWI/SNF related, matrix associated, actin dependent regulator of chromatin, subfamily A-like 1
ssDNA	single-stranded DNA
T	thymidine or threonine
t	time
TBS	tris-buffered saline
TBS-T	tris-buffered saline with Tween 20
Thr	threonine
TLS	translesion synthesis
TOPBP1	DNA topoisomerase 2-binding protein 1
Tyr	tyrosine
UV	ultraviolet
V	volt
x g	times gravity
XRCC	X-ray cross complementing protein
Y	tyrosine
γH2AX	phosphorylated histone H2AX

CHAPTER 1

1 Introduction

1.1 The DNA damage response

The DNA contained in every cell has limited chemical stability and is inflicted with thousands of lesions on a day-to-day basis (Lindahl, 1993). This damage to DNA plays a role in mutagenesis, carcinogenesis, and ageing, and arises from both endogenous and exogenous sources (De Bont & van Larebeke, 2004). Endogenous DNA damage can stem from spontaneous hydrolysis, base depurination or deamination, and exposure to reactive oxygen species or other reactive cellular metabolites which can cause up to 10^5 lesions per day (Barnes & Lindahl, 2004; Hoeijmakers, 2009; Helleday *et al*, 2014). Alternatively, exogenous DNA damage can be caused by environmental exposure to non-ionising ultraviolet radiation, ionising radiation (IR), chemicals, or other genotoxic agents (Helleday *et al*, 2014). Unrepaired or aberrantly repaired DNA lesions can lead to senescence, cell death, or mutations that can give rise to cancer (Hoeijmakers, 2009).

Due to the grave consequences to both individual cells and to the organism that are associated with damage of genetic material, cells have evolved a DNA damage response (DDR) in order to ameliorate these effects. The DDR consists of a series of interconnected and specialised pathways whose role is to detect and repair DNA damage. A large number of proteins are involved that engage signal transduction pathways that will determine whether a cell will undergo apoptosis, senescence, or transient growth arrest mediated through cell cycle checkpoints in order to allow for DNA repair to maintain cell viability and genomic stability (Ciccia & Elledge, 2010; Jackson & Bartek, 2010). At the core of this extensive DDR network are members of the phosphatidylinositol-3 kinase-related kinase (PIKK) family of

serine/threonine protein kinases that recognize and phosphorylate Ser-Gln (SQ) and Thr-Gln (TQ) motifs in proteins (Kastan & Bartek, 2004; Cimprich & Cortez, 2008). DNA-dependent protein kinase (DNA-PK) is required for DNA double strand break (DSB) repair, whereas ATM (Ataxia Telangiectasia Mutated) and ATR (Ataxia Telangiectasia and Rad3 related) are primarily involved in DDR signalling and cell cycle arrest (Lovejoy & Cortez, 2009). ATM is recruited to sites of DNA double strand breaks that may arise after exposure to ionising radiation, while ATR is recruited to single stranded DNA (ssDNA) coated with replication protein A (RPA) that arises in response to stalled replication forks, resected DSBs, or as repair intermediates following exposure to DNA-damaging agents (Zou & Elledge, 2003; Glover *et al*, 2005). ATR responds to replication stress induced by UV light, chemotherapeutic agents, radiation, hydroxyurea, and hypoxia; conditions where helicases continue to unwind DNA during replication even when the polymerase has stalled, leading to long strands of ssDNA (Zou & Elledge, 2003; Cimprich & Cortez, 2008; Dai & Grant, 2010). While these two kinases share many substrates and overlapping pathways, the remainder of this chapter will focus on ATR.

1.2 The role of ATR in response to DNA damage

ATR is a large protein of 2644 amino acids with a molecular weight of 301 kDa and is the functional homologue of Rad3 and Mec1 checkpoint proteins from *Schizosaccharomyces pombe* and *Saccharomyces cerevisiae*, respectively (Bentley *et al*, 1996; Cimprich *et al*, 1996; Cimprich & Cortez, 2008). Although ATM can be recruited to DNA DSBs, in order activate ATR, DNA DSBs must first be resected to create ssDNA which is then bound by RPA. ATRIP (ATR-interacting protein) interacts with ssDNA-bound RPA and the N-terminus of ATR in order to localise ATR to sites of replication stress and DNA damage. Since the loss of either ATR or ATRIP cause similar phenotypes, ATRIP may be considered a subunit of an ATR

'holoenzyme' (Cimprich & Cortez, 2008). RPA on the ssDNA also enables the binding of the RAD17/RFC2-5 clamp loader complex at the junction of ds- and ssDNA and facilitates the loading of the RAD9-HUS1-RAD1 (9-1-1) heterotrimeric ring complex onto the DNA (Figure 1.1). The 9-1-1 complex is loaded to DNA with 5'-recessed ends, which generally occurs at replication forks with sites of damage, recombination sites, and nucleotide-excision repair (NER) sites (Ellison & Stillman, 2003). The complex then recruits TOPBP1 (DNA topoisomerase 2-binding protein 1) that in turn stimulates the ATR-ATRIP kinase activity (Kumagai *et al*, 2006; Delacroix *et al*, 2007; Mordes *et al*, 2008). Both the 9-1-1 and ATR-ATRIP complexes are recruited independently, which may be an additional regulatory mechanism to ensure that the ATR signalling pathway is only active when both complexes are present and thus that the ATR pathway is not aberrantly triggered during normal DNA replication (Kondo *et al*, 2001; Melo *et al*, 2001).

Downstream targets of ATR then initiate a transient cell cycle arrest and stabilisation of stalled replication forks to promote the repair of damaged DNA and subsequent restart of DNA replication (Cimprich & Cortez, 2008; Errico & Costanzo, 2012). Claspin, which is normally associated with active replication forks, is recruited by RAD17, phosphorylated by ATR and, once modified, recruits CHK1, which is activated by ATR-dependent phosphorylation at serine 317 (S317) and S345 (Jeong *et al*, 2003; Kumagai & Dunphy, 2003; Lee *et al*, 2003; Kumagai *et al*, 2004). The TIMELESS/TIPIN complex is also involved in bringing ATR and CHK1 together (Kemp *et al*, 2010). Activated CHK1 can autophosphorylate at S296 and is released from the chromatin where it then mediates many of the downstream functions of ATR. One such function is enforcing the intra-S-phase checkpoint in normal S-phase and in the presence of DNA damage (Sørensen *et al*, 2003; Xiao *et al*, 2003; Dai & Grant, 2010). This is accomplished through CHK1 phosphorylation-dependent ubiquitination of CDC25A, thus inhibiting the firing of replication origins because the inhibitory phosphate on CDK2 is not

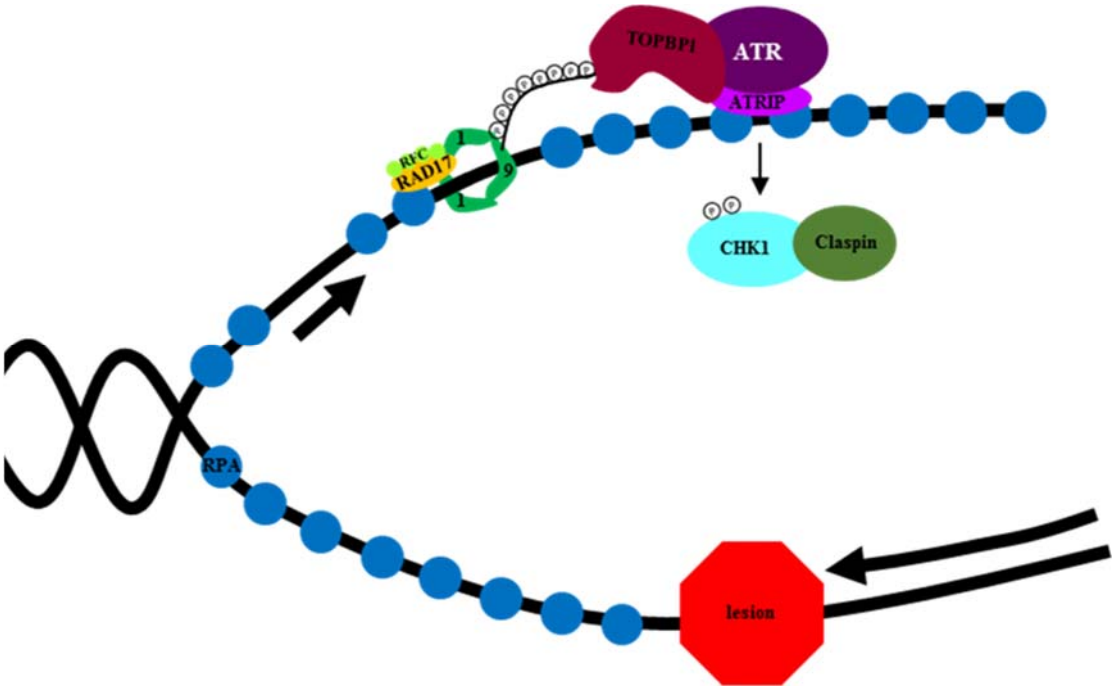


Figure 1.1: ATR activation in response to replication stress that leads to long strands of ssDNA.

Black lines represent DNA, and the red octagon represents a DNA lesion. The RAD17/RFC2-5 clamp loader complex binds RPA on ssDNA and facilitates the loading of the RAD17-HUS1-RAD1 (9-1-1) heterotrimeric ring complex onto the DNA. The complex then recruits TOPBP1 that stimulates the ATR-ATRIP kinase activity. Claspin recruits CHK1, which is activated by ATR-dependent phosphorylation at S317 and S345, and can autophosphorylate at S296. It is then released from the chromatin and mediates many of the downstream functions of ATR. See text for details. Adapted from Wagner & Kaufmann, 2010.

removed by CDC25A, cyclin E/A complexes are inhibited, and the CDC45 initiation factor is not loaded to chromatin (Figure 1.2). In normal replication, this prevents re-replication of DNA, whereas in instances of DNA damage, it slows down replication allowing time for the damage to be resolved (Bartek & Lukas, 2003; Donzelli & Draetta, 2003; Sørensen *et al*, 2003; Xiao *et al*, 2003).

ATR also plays a key role in the G2/M checkpoint to prevent cells from prematurely entering mitosis in the presence of DNA damage or incomplete replication. This is mediated through the degradation of CDC25A that leads to a G2 arrest since it is unable to remove the inhibitory phosphate from CDK1/cyclin B, and through CHK1's phosphorylation of CDC25C at S216 so

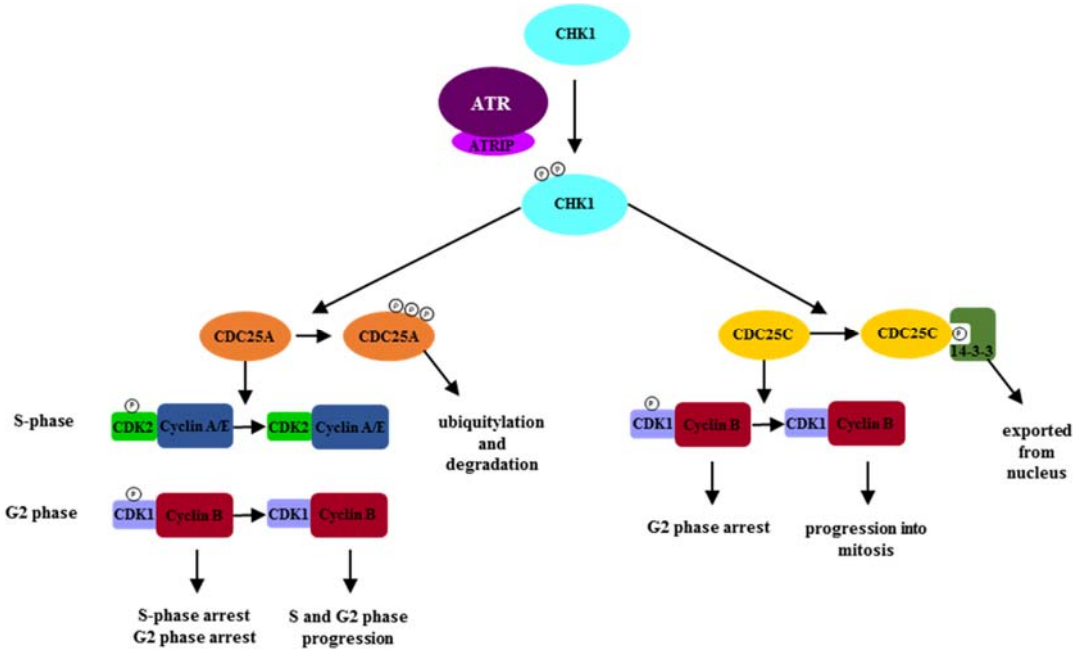


Figure 1.2: ATR- induced cell cycle arrest is mediated through CHK1.
See text for details. Adapted from Wagner & Kaufmann, 2010.

that it is exported from the nucleus via 14-3-3 proteins (Zhao *et al*, 2002; Xiao *et al*, 2003; Dai & Grant, 2010). CDC25C is then sequestered in the cytoplasm and unable to dephosphorylate nuclear CDC2, which is then unable to allow entry into mitosis (Peng *et al*, 1997). CHK1-mediated phosphorylation can also stimulate WEE1 kinase activity (Lee *et al*, 2001).

1.3 ATR as a target for cancer therapy

Cancer therapies such as radio-and chemotherapy rely on DNA damage being selectively toxic to proliferating cancer cells in order to be effective. However, the effects of these therapies are not completely selective to cancer cells, which leads to normal tissue toxicity and side effects that limit the dose that can be administered (Karnitz *et al*, 2005; Myers *et al*, 2009; Woods & Turchi, 2013). In addition, treatment resistance can emerge as the tumour cells alter the regulation of their DDR components in order to circumvent the effects of DNA damage. As a

result, targeting the DDR has become an attractive therapeutic approach either as a radio- or chemo-sensitizer to prevent the development of resistance, or as a synthetic lethal approach targeting genetic defects in DDR pathways (Bao *et al*, 2006; Oliver *et al*, 2010; Bouwman & Jonkers, 2012; Weber & Ryan, 2015). As ATR is involved in the response to radiation and many chemotherapies, and has been found to be constitutively activated in fast proliferating cancers that have increased replication stress, it has become an attractive target for the development of enzyme (kinase) inhibitors (López-Contreras & Fernandez-Capetillo, 2010). ATR inhibition is also an attractive therapeutic approach where toxicity to tumour cells is enhanced with respect to normal tissues; for example in cells with p53 (a substrate of ATM, and important for G2/M and G1 arrest after DNA damage) mutations, one of the most frequent alteration in cancers. Loss of p53 function increases replication stress and sensitises cells to ATR inhibition as they rely more heavily on the ATR pathway compared to normal cells (Nghiem *et al*, 2001; Murga *et al*, 2009; Ruzankina *et al*, 2009). Defects in the DNA damage-induced G1 checkpoint leads to a greater reliance on the intra-S and G2/M checkpoints for cell survival. ATR inhibition leads to loss of both these DNA damage-induced cell cycle checkpoints, accumulation of DNA damage, premature entry into mitosis, and cell death (Nghiem *et al*, 2001; Kaelin, 2005; Gabrielli *et al*, 2012). ATR inhibitors could therefore enhance the cytotoxicity of certain chemotherapies in p53-defective tumour cells, perhaps allowing these chemotherapies to be used at lower doses with less toxicity to normal (p53 wild-type) tissue. Clinical trials observing combination treatments with CHK1 inhibitors and cytotoxic agents have also had some positive clinical responses, which points to a potential similar outcome with combination ATR inhibitors and cytotoxic agents (Garrett & Collins, 2011; Sakurikar & Eastman, 2015).

ATR and CHK1 are considered to be essential genes. In mice, genetic loss of function leads to chromosome breaks and early embryonic lethality (Brown & Baltimore, 2000; De Klein *et al*,

2000; Liu *et al*, 2000; Cortez *et al*, 2001). Depletion of ATR in adult mice leads to aging-related phenotypes, defects in tissue homeostasis, cellular loss in rapidly proliferating tissues, reductions in stem cells, and exhaustion of tissue renewal and homeostatic capacity (Ruzankina *et al*, 2007). In humans, hypomorphic mutations in ATR resulting in partial loss of gene function cause Seckel syndrome, which is characterised by growth and mental retardation, osteoskeletal abnormalities, and severe microcephaly. There are no viable complete loss of function mutations reported in ATR, only heterozygous or hypomorphic mutations (O'Driscoll *et al*, 2003). In a mouse model of Seckel syndrome, there are high levels of replicative stress in embryogenesis and accelerated aging in adult life (Murga *et al*, 2009). ATR function is required in unperturbed S-phase cells to regulate DNA replication and maintain genome stability. Replication forks can stall during normal replication, especially at repetitive DNA sequences and chromosomal fragile sites (regions of DNA that replicate in late S-phase, are difficult to replicate, and are prone to gaps and breaks) (Mirkin & Mirkin, 2007). ATR appears crucial for maintaining the stability of these chromosomal fragile sites, since cells deficient in ATR have a marked increase in both observable fragile sites and chromosome breakage at fragile sites (Casper *et al*, 2002; Cha & Kleckner, 2002).

There are concerns about the potential side effects of ATR inhibition in proliferative tissues, especially in conditions of high levels of replication stress. The embryonic lethality of loss of ATR gene function may have played a role in delaying the development and exploitation of ATR inhibitors, and may in part be a reason for the relative paucity of ATR inhibitors in clinical development.

1.4 Current ATR inhibitors

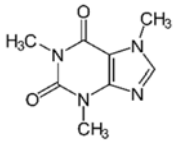
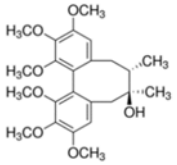
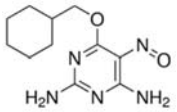
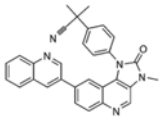
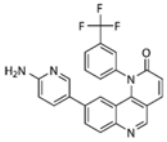
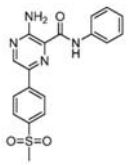
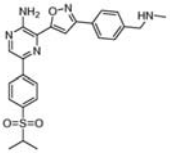
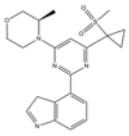
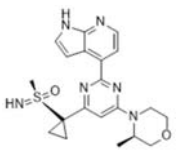
Caffeine has been shown to be a weak inhibitor of both ATR and ATM that sensitises cells to ionising radiation and genotoxic stress (Lau & Pardee, 1982; Blasina *et al*, 1999; Hall-Jackson

et al, 1999; Sarkaria *et al*, 1999). This led to the search for more potent and selective ATR inhibitors, with schisandrin B (SchB) being the first reported ATR-selective small-molecule inhibitor (Table 1.1). It is a dibenzocyclooctadiene derivative isolated from *Fructus Schisandrae* (fruit of *Schisandra chinensis*) that is commonly used in Chinese medicine. It has been found to increase sensitivity of A549 non-small cell lung cancer (NSCLC) cells to UV radiation by abrogating the S and G2/M checkpoints and inhibiting CHK1 phosphorylation. However, it is only effective at high concentrations (30 μM) where it can also inhibit ATM activity.

Although NU6027 was identified as an ATR inhibitor, it was originally developed as a CDK2 inhibitor and is therefore not selective for ATR. It attenuated G2/M arrest after DNA damage in breast and ovarian cancer cell lines, and sensitised cells to chemotherapy agents such as cisplatin and temozolomide (Peasland *et al*, 2011, Sultana *et al*, 2013). It also exhibited synthetic lethality in XRCC1-deficient ovarian cancer cells that resulted in cytotoxicity, accumulation of DSBs, G2/M cell cycle arrest, and increased apoptosis.

NVP-BEZ235 was identified in a cell-based screen to identify compounds that inhibit ATR kinase activity in the nanomolar concentration range (Toledo *et al*, 2011). It was originally developed as a dual phosphatidylinositol-3-OH kinase (PI3K) and MTOR kinase inhibitor, but was subsequently found to be a potent inhibitor of ATM and DNA-PKcs, and to radiosensitise RAS-overexpressing tumours (Maira *et al*, 2008; Konstantinidou *et al*, 2009). The screen also led to the discovery of a non-selective ATR inhibitor, ETP-46464, which was shown to be toxic for p53-deficient cells and in conditions that increase replication stress, such as the over-expression of cyclin E (Toledo *et al*, 2011). More recently, a chemically-related and non-selective inhibitor of PIKK-family kinases and MTOR (Torin2) has been described (Liu *et al*, 2013).

Table 1.1: ATR inhibitors.

Compound	Structure
Caffeine	
Schisandrin B	
NU6027	
NVP-BEZ235	
Torin 2	
VE-821	
VE-822 (VX-970)	
AZ20	
AZD6738	

Vertex Pharmaceuticals carried out a high-throughput screen to identify selective ATR inhibitors, which led to the discovery of VE-821. VE-821 is an ATP-competitive inhibitor of ATR, with good selectivity and minimal cross-reactivity with related PIKK family members (ATM and DNA-PK), or MTOR (Reaper *et al*, 2011). VE-821 blocked pCHK1 S345 phosphorylation and showed strong synergy in HCT116 colorectal cancer cells with genotoxic agents like gemcitabine, camptothecin, and etoposide, as well as with IR and DNA cross-linking drugs cisplatin and carboplatin (Reaper *et al*, 2011; Jossé *et al*, 2014). Cells deficient in p53 or ATM, or cells treated with the ATM inhibitor KU55933 were especially sensitive to the combination of VE-821 and cisplatin. Importantly, this cytotoxic synergy with cisplatin was observed in most cancer cell lines, but not in non-tumour cell lines which experienced only a transient and reversible growth arrest (Reaper *et al*, 2011). VE-821 has also been shown to be a radiosensitiser in human cancer cells that have undergone replication arrest induced by hypoxic conditions (Pires *et al*, 2012). This is notable, as hypoxic tumour cells are known to be more resistant to radiotherapy (Gray *et al*, 1953; Wouters & Brown, 1997). Pancreatic and resistant head and neck cancer cells were also found to have increased sensitivity to chemotherapy when co-treated with VE-821 (Prevo *et al*, 2012; Luong *et al*, 2016). Mohni *et al*, 2014 found a synthetic lethal interaction of VE-821 and cisplatin in cells with loss of TLS polymerase ζ and 53BP1, but not in cells that have deficiencies in the homologous recombination (HR) or mismatch repair pathways. They also observed the re-sensitisation of cisplatin-resistant cell lines and synergy with PARP inhibition, even in HR-proficient cells. Previously, the same group found synthetic lethal interactions of VE-821 in cells with reduced function in the ATR pathway and in cells with loss of the structure-specific endonuclease ERCC1-XPF, especially in triple negative breast cancer and NSCLC cells (Mohni *et al*, 2014). Defects in ATM, BRCA2, XRCC3, XRCC1, and Ku80 (XRCC5), and cells with high levels of DNA-PKcs (associated with replication stress and DDR activation) have also all been found

to confer sensitivity to VE-821 and could be potential biomarkers of ATR response in future clinical studies (Middleton *et al*, 2015). In addition, cancer cells that rely on the alternative lengthening of telomeres (ALT) pathways appear to be hypersensitive to, and selectively killed by, VE-821 (Flynn *et al*, 2015), while the levels of VE-821- induced ssDNA have been found to correlate with ATR inhibitor sensitivity in a panel of cell lines (Buisson *et al*, 2015). Finally, IGF-1R tyrosine kinase inhibitor BMS-754807 has recently been reported to be synergistic with VE-821 in breast cancer cells (O'Flanagan *et al*, 2016).

VE-822, an analogue of VE-821, has enhanced potency and selectivity for ATR, as well as increased solubility and superior pharmacokinetic properties (Charrier *et al*, 2011). It has also been shown to sensitise human pancreatic cancer cells to radiation and gemcitabine, leading to abrogated checkpoints, increased DNA damage, and blocked HR repair, but without increased non-tumour cell or tissue toxicity (Fokas *et al*, 2012). In addition, VE-822 sensitised lung cancer cells and a panel of primary tumour cell lines, but not non-tumour cells, to DNA damaging drugs. In particular, loss of p53 function sensitised tumour cells, and there was enhanced response to cisplatin in primary patient-derived lung tumour xenograft models (Hall *et al*, 2014). Furthermore, VE-822 (also known as VX-970) was the first selective ATR inhibitor to enter clinical development, and patients are currently being recruited in a phase I clinical trial to assess safety, tolerability, and pharmacokinetics in combination with cytotoxic chemotherapy (ClinicalTrials.gov: NCT02157792, EUDRACT: 2012-003126-25).

AZD6738, developed by AstraZeneca, is the second ATR inhibitor to enter clinical studies. It is an analogue of AZ20, a potent and selective ATR inhibitor that has a synergistic effects with the ATM inhibitor KU-60019 (Jacq *et al*, 2012). As a monotherapy, AZ20 was shown to inhibit growth of DDR-defective (MRE11A-mutant) LoVo colorectal adenocarcinoma xenografts grown in nude mice at doses that are well tolerated (Foote *et al*, 2013). AZD6738 has much improved solubility compared to AZ20, good potency and selectivity, and pharmacokinetic and

biopharmaceutical properties suitable for oral dosing (Jones *et al*, 2013; Vendetti *et al*, 2015). In cells, AZD6738 treatment inhibits the phosphorylation of CHK1 and increases the phosphorylation of ATM-dependent CHK2 and γH2AX (a marker for DNA damage) – both consistent with an impaired intra-S-phase checkpoint. Furthermore, AZD6738 was effective both as a single agent and was synergistic in vivo with gemcitabine, cisplatin, and IR. In in vivo xenografts of ATM-deficient tumours, AZD6738 halted or regressed tumour growth at tolerated doses both as a single agent and in combination with carboplatin or IR. Importantly, when used in vivo, there was only a transient increase in γH2AX staining in the bone marrow or gut, suggesting a favourable therapeutic index (Guichard *et al*, 2013). Vendetti *et al*, 2015 found AZD6738 induced cell death and senescence in NSCLC lines, causing cells to accumulate at the G1/S border and in early S-phase. The inhibitor also enhanced cytotoxicity with cisplatin and gemcitabine in NSCLC cells with functioning ATM kinase, and synergised with cisplatin in ATM-deficient NSCLC. The inhibitor was also well tolerated in mice for 14 consecutive days and, strikingly, the combination of cisplatin and AZD6738 caused marked regressions of ATM-deficient lung cancer xenografts (Vendetti *et al*, 2015). Furthermore, in vitro, AZD6738 was selectively toxic to both p53- and ATM-defective chemoresistant chronic lymphocytic leukaemia (CLL) cells, and was synthetically lethal with chemotherapy. Primary xenograft models of these cells also had decreased tumour load (Kwok *et al*, 2015, 2016). A first time in patient multiple ascending dose study with AZD6738 to assess pharmacokinetics in CLL, PLL, and B cell lymphoma patients (ClinicalTrials.gov: NCT01955668) was completed after only two patients were recruited. However, there are two trials currently recruiting patients. A phase I clinical trial is assessing the safety of AZD6738 alone and in combination with radiotherapy in patients with solid tumours (NCT02223923; EUDRACT: 2013-003994-84 and 2014-002233-66) and another trial is evaluating the combination of

AZD6738 with carboplatin, olaparib, or MED14736/durvalumab, a monoclonal antibody against PD-L1 (NCT02264678).

1.5 Resistance to ATR inhibitors

Resistance to chemotherapy, characterised by a lack of response to drug-induced growth inhibition, is one of the major reasons for failure of cancer treatments. In the 1990s, it was estimated that nearly 50% of patients with cancer have tumours that are resistant to chemotherapy (Pinedo & Giaccone, 1998). Resistance is either intrinsic, arising from heterogeneity in the tumour, or acquired in response to drug exposure via e.g. the expression of transporters, insensitivity to drug-induced apoptosis, or the development of drug-detoxifying mechanisms (Gottesman, 2002; Luqmani, 2005; Lippert *et al*, 2011; Zahreddine & Borden, 2013). Unfortunately, it appears inevitable that resistance will develop to most cancer therapeutics. As a result, it is important to understand mechanisms of resistance in order to combat it when it arises in patients, and to design rational combination strategies that delay or prevent the development of resistance (Garraway & Jänne, 2012).

To date, there has been no reports of resistance to ATR inhibitors in the clinic. However, it has been reported that Chinese hamster ovary cells with loss of DNA-PKcs were not sensitive to VE-821 (Middleton *et al*, 2015). A genome-wide CRISPR-Cas9 screen was carried out in murine embryonic stem cells in order to identify mutations that might confer resistance to ATR inhibitors, and CDC25A was identified as a major determinant of ATR sensitivity, with CDC25A levels in human cancer cell lines correlating with response to ATR inhibitors. It was reported that cells deficient in CDC25A could tolerate high doses of ATR inhibitor because these cells prematurely entered mitosis. Notably, treatment with a WEE1 inhibitor forced these cells in mitosis and re-sensitised them to ATR inhibition (Ruiz *et al*, 2016).

1.6 Aim of this study

The aim of this study was to isolate and characterise cells resistant to ATR inhibitors, and to identify potential mechanisms of resistance.

CHAPTER 2

2 Materials and Methods

2.1 Mammalian Cell Culture

2.1.1 Maintenance of cell lines

The cell lines used in this study are listed in Table 2.1). Cells were cultured in 75 and 150 cm^2 tissue culture flasks (Corning Incorporated; Corning, NY, USA) and incubated in a standard humidified incubator at 37 °C and 7.5% CO_2. Cells were cultured in Advanced Dulbecco's modified eagle medium (DMEM)/F12 (Life Technologies, Carlsbad, CA, USA) and supplemented with 5% foetal bovine serum (FBS; Sigma-Aldrich; St. Louis, MO, USA), 2 mM GlutaMAX™ (Life Technologies), and 50 U penicillin / 50 μg/mL streptomycin (Life Technologies). SO25 and SO46 cells lines were cultured in 1 μM AZD6738 (AstraZeneca; Macclesfield, UK), with SO45 in 2 μM AZD6738. The cells were passaged at sub-confluence (70-80%), the culture medium was changed every two to five days, and cells were not passaged more than 25 passages. Passaging involved aspiration of medium, washing with PBS, and trypsinisation with Trypsin/EDTA (Life Technologies; strength shown in Table 2.1) for three to seven minutes. Growth medium was then added to inactivate the trypsin activity and cells were split between 1:4 and 1:10.

Authenticated cell lines obtained from the ATCC were cultured continuously for no more than 4 months, or 20 passages, whichever came first. All cell lines were additionally identified by sequencing highly polymorphic loci in mitochondrial DNA as described in Hutter *et al*, 2004.

Table 2.1: Cell lines used in this study.

The designation used throughout the study for each cell line is in bold. All cell lines used are of human origin.

Cell Line	Histological Subtype	Obtained from	Trypsin
A549	lung carcinoma not specified (NSCLC)	ATCC[1] #CCL-185	0.25%
Calu-6	Lung carcinoma, anaplastic	ATCC #HTB-56	0.025%
LIMM-**NBE1** (Stead *et al*, 2012)	Telomerase immortalised normal bronchial epithelial cells	[2]	0.025%
NCI-**H1975**	lung adenocarcinoma (NSCLC)	ATCC #CRL-5908	0.025%
NCI-**H23**	lung adenocarcinoma (NSCLC)	ATCC #CRL-5800	0.025%
PC-9	lung adenocarcinoma (NSCLC)	[3]	0.25%
SO25	lung adenocarcinoma (NSCLC)	This work	0.25%
SO45	lung adenocarcinoma (NSCLC)	This work	0.25%
SO46	lung adenocarcinoma (NSCLC)	This work	0.25%

2.1.2 Cell counting and seeding

Cell density and viability were measured using the Countess® automated cell counter (Life Technologies). A 1:1 mixture of cell suspension and 0.4% trypan blue solution (Life

[1] ATCC = American type culture collection (Manassas, VA, USA)
[2] Kindly provided by Dr. Pamela Rabbitts, Leeds Institute of Molecular Medicine, University of Leeds, UK
[3] Kindly provided by Dr. Kazuto Nishio, Kinki University, Osaka, Japan

Technologies) were added to a Countess® cell counting chamber slide and inserted into the Countess® automated cell counter for standard counting. The desired numbers of cells were then seeded in fresh culture media prior to any experiments. SO25, SO45, and SO46 cell lines were always plated without the presence of AZD6738. 1 or 2 μM AZD6738 was added after approximately 24 h.

2.1.3 Cryostorage and thawing of cells

Cells were stored in the vapour phase above liquid nitrogen. To thaw cells from liquid nitrogen storage, the cells were first rapidly thawed at 37 °C. These cells were diluted in 6 mL of 37 °C complete culture medium and pelleted by centrifugation (225 x g, 5 min). The supernatant was then aspirated and the cell pellet was re-suspended in 12 mL of 37 °C complete culture medium and transferred to a 75 cm^2 flask.

For cryostorage, cells were grown until they reached 85-95% confluency and then trypsinised and resuspended in growth medium as described in section 2.1.1. The cells were pelleted by centrifugation (225 x g, 5 min), the supernatant was aspirated, and the cells were re-suspended in 5 mL of complete culture medium with 10% (v/v) dimethyl sulfoxide (DMSO; Fisher Scientific; Waltham, MA, USA). 1 mL aliquots were then transferred to cryogenic tubes (Corning Incorporated) and frozen at -80 °C overnight in an isopropanol Mr. Frosty™ Freezing Container (Thermo Scientific; Waltham, MA, USA) before being transferred to liquid nitrogen for long term storage.

2.2 Clone Selection

PC-9 human non-small cell lung cancer cells were plated in each of ten 10 cm dishes (1 x 10^6 per plate) and treated with AZD6738 (1 μM) in complete culture medium. Six weeks later, a resistant colony emerged (SO25) as the single observable colony on the plate and was isolated

and cultured in 1 μM AZD6738. The SO45 and SO46 clones were isolated in a separate experiment using cloning rings. The media was aspirated from the 10 cm plate, the cells were washed with PBS, a cloning ring was placed over the clone to be isolated, and 0.25% trypsin/EDTA was added for three to seven minutes to the area within the cloning ring. The detached cells were then removed in the trypsin with a pipette and transferred to a 25 cm^2 tissue culture flask (Corning Incorporated; Corning, NY, USA) and incubated in a standard humidified incubator at 37 °C and 7.5% CO_2. SO45 was cultured in 2 μM AZD6738 and SO46 in 1 μM AZD6738.

2.3 Drug Treatments

Stock solutions of AZD2281, AZD6738, AZD7762, (AstraZeneca; Macclesfield, UK), camptothecin, docetaxel, gefitinib, MK-1775, NU7441, VE-821, VE-822 (Selleck Chemicals; Houston, TX, USA), gemcitabine (LC Laboratories; Woburn, MA, USA), KU55933 (TOCRIS Bioscience; Bristol, UK), and MLN-4924, (AdooQ® Bioscience; Irvine, CA, USA) were prepared in 100% DMSO at a concentration of 10 mM. Cisplatin (Sigma-Aldrich) was prepared at 3.3 mM in 0.9% sterile saline solution. All stock solutions were aliquoted and stored at -20 °C until use, and dilutions of the drugs for treatment of cells were made using DMSO and/or complete culture media.

2.4 Cell Viability Assay

Resazurin-based cell viability assays were carried out to assess the impact of DNA damage response inhibitors and chemotherapeutic drugs on cell proliferation and viability (O'Brien *et al*, 2000). Cells were seeded in 100 μL complete culture medium in triplicate in 96-well plates (Costar®, flat bottom; Corning Incorporated) at a density of 500 cells/well and incubated overnight to allow for re-attachment. Drugs and inhibitors were then added in 100 μL complete

culture medium at the required concentrations and dilutions, and plates were returned to the incubator for four days. On the fourth day after treatment, 10 µL of resazurin solution (0.125 mg/mL in dH_2O; Sigma-Aldrich) per 100 µL media was added to each well, including media-only "blank" wells, and plates were returned to the incubator for 1.5 h. In metabolically active cells, resazurin is reduced to highly fluorescent resorufin and this fluorescent signal is proportional to the number of viable cells. Fluorescence intensity was measured with a POLARstar Omega plate reader (BMG Labtech GmbH; Ortenberg, Germany) with excitation at 544 nm, emission at 590 nm, and gain 1000. The average of the values of the triplicate "blank" wells were subtracted from all other wells, and normalized to the average of the vehicle-treated wells (in the case of single treatments) or to cells treated with the fixed-concentration combination agent and vehicle (in the case of combination treatments). Origin® 2016 Graphing & Analysis software (OriginLab® Corporation, Northampton, MA, USA) was used to determine the half-maximal inhibitory concentration (IC_{50}) from at least three independent experiments, unless otherwise noted. For viability assays involving the SO25, SO45, and SO46 cell lines in combination with AZD6738, VE-821, VE-822, and AZD7762, IC_{50} values were not able to be calculated due to the shape of the curve, with maximal viability at an intermediate concentration that could not be curve-fitted in the Origin software. As a result, for these experiments, and for siRNA transfection experiments involving PC-9 cells, the cell viability at 1.11 or 0.123 µM is reported.

2.5 PicoGreen Cell Proliferation Assay

The PicoGreen assay is a sensitive and specific assay for dsDNA. The PicoGreen cell proliferation assay was used to measure cell growth (determined by increased dsDNA content) over a period of eight days. Cells were seeded in 100 µL complete culture medium in triplicate in 96- well plates (Costar®, flat bottom; Corning Incorporated) at a density of 500 cells/well

and incubated overnight to allow for re-attachment. The following day, the medium in the first column for "day 1" was aspirated and 100 µL of DNA lysis buffer (see Table 2.2 for composition) per well was added. AZD6738 or 0.01% DMSO (vehicle control) were added in 100 µL complete culture medium to the appropriate remaining wells to reach a final concentration of 1 µM, and the plates were returned to the incubator. Every 24 hours for eight days, the medium was aspirated in the column corresponding to the appropriate day and 100 µL of DNA lysis buffer was added to each well. After DNA lysis buffer was added to the final wells, Quant-iT™ PicoGreen® dsDNA reagent (Life Technologies) was diluted 1:200 in sterile PBS (Lonza; Basel, Switzerland) in the hood with the light off. 100 µL of this PicoGreen® solution was then added to each well, the plates were wrapped in foil, and then placed in the incubator at 37 °C for 20 min. Fluorescence intensity was measured with a POLARstar Omega plate reader (BMG Labtech GmbH) with excitation at 480 nm, emission at 520 nm, and gain 1000. The average of the values of the triplicate "blank" wells (just DNA lysis buffer, no cells) were subtracted from all other wells, and normalized to the average of the wells from "day 1".

Table 2.2: DNA lysis buffer composition.

The following solutions were prepared in the tissue culture hood and then filter sterilised with a 0.45 nm filter (Sartorius Stedim Biotech; Goettingen, Germany). The DNA lysis buffer solution was then stored at 4 °C.

Component	Amount	Final Concentration
0.5M EDTA, pH8.0 [a]	2.5 mL	25 mM
Triton X-100 [b]	50 µL	0.1 %
dH_2O	47.45 mL	

[a] AccuGENE, Lonza
[b] VWR International; Randor, PA, USA

2.6 Protein Detection by Western Blotting (Immunoblotting)

2.6.1 Preparation of cell extracts, gel electrophoresis, and transfer

Cells were seeded in 6-well plates (Corning Incorporated) and grown until they reached approximately 70% confluency. They were then treated for 24 h before cell lysis. For lysis, cells were washed twice in ice-cold (4 °C) 1x PBS (Sigma-Aldrich) on ice. 80-100 µL of lysis buffer (see Table 2.3 for composition) supplemented with 1 mM sodium orthovanadate (Na_3VO_4; Sigma-Aldrich) and cOmplete protease inhibitor cocktail (Roche; Basel, Switzerland) was added to each plate on ice for 10 min. Cells were then scraped and homogenised by brief sonication (Bioruptor® Plus; Diagenode Inc.; Liege, Belgium), and then centrifuged for 15 min at 4 °C at 16,100 x g.

Protein concentrations were determined using a NanoDrop 1000 spectrophotometer (Thermo Scientific), and then diluted in lysis buffer stock and 2x Laemmli sample loading buffer (Sigma-Aldrich) to equal protein concentrations. The samples were then incubated at 95 °C for seven to ten min in a dry heating block (AccuBlock™ Digital Dry Bath; Labnet International, Inc.; Edison, NJ, USA). 30 – 50 µg of protein per lane was loaded onto a precast 4-15% or 4-20% gradient Mini-PROTEAN® TGX™ gel (BioRad; Hercules, CA, USA) alongside a Precision Plus Protein™ Dual Color ladder (BioRad). The gel was then run at 250 V for approximately 25 min with Tris/Glycine/SDS running buffer (BioRad). When assessing the siRNA transfection lysates, a Criterion™ TGX™ gel (BioRad) was used and run at 150 V for approximately 75 min. Proteins were then transferred to nitrocellulose membranes (0.45 µm pore size Trans-Blot®; BioRad) in cold 1x Tris/Glycine buffer (BioRad) with 20% methanol (v/v; Sigma-Aldrich) for 1 h at 150 V (or 90 V for larger gels) with an ice pack cooler and magnetic stirrer.

Table 2.3: Lysis buffer stock components for western blot cell extract collection.
This stock lysis buffer solution was aliquoted and stored at 4 °C.

Component	Amount	Final Concentration
1 M Tris-HCl, pH 7.6 [a]	1.25 mL	50 mM
NaCl [b]	200 mg	137 mM
(v/v) glycerol [b]	2.5 mL	10%
(v/v) Igepal [c]	25 µL	0.1%
10% (v/v) SDS [d]	250 µL	0.1%
2% sodium fluoride (NaF) [c]	2.626 mL	50 mM
dH_2O	16.1 mL	

[a] Promega; Madison, WI, USA
[b] VWR
[c] Sigma-Aldrich
[d] AppliChem GmbH; Darmstadt, Germany

2.6.2 Immunoblotting and chemiluminescent detections

Following transfer, the nitrocellulose membranes were stained with Ponceau S solution (Sigma-Aldrich), cut where necessary, and washed twice with PBS-T or TBS-T (see Table 2.4). Membranes were then incubated in blocking buffer for 1 h at room temperature (RT) on a roller (Stuart® roller mixer SRT9D; Bibby Scientific; Staffordshire, UK) to block non-specific binding of antibodies to the membrane. The membranes were then exposed to the primary antibodies (listed in Table 2.5), diluted in 1° antibody incubation buffer, overnight at 4 °C on a roller, with the exception of pCHK1 antibodies which were incubated for 48 h. Following primary antibody incubation, membranes were washed three times 5 min in PBS-T or TBS-T, and then incubated with the appropriate horseradish peroxidase (HRP)-conjugated secondary antibodies (listed in Table 2.6) for 1 h at RT on a roller, diluted in 2° antibody incubation buffer. Membranes were then washed three times 5 min in PBS-T or TBS-T, followed by 2 x 5 min washes in PBS or TBS. Detection was carried out by chemoluminescence

and visualisation with a ChemiDoc™ MP Imaging System (BioRad). The membranes were covered with either Pierce® ECL Western Blotting Substrate (Thermo Scientific) for 2 min or WesternSure™ PREMIUM Chemiluminescent Substrate (LI-COR; Lincoln, NE, USA) for 5 min depending on the strength of the signal. Bands were quantified using ImageLab 5.2.1 (BioRad).

Table 2.4: Buffers and solutions used in immunoblotting.

Buffer	Composition
1x phosphate buffered saline (PBS)	5x PBS tablets [a] dissolved in 1 litre dH_2O
PBS-T	1x PBS, 0.1% (v/v) Tween-20 [a]
1x Tris-buffered saline (TBS)	1x pack OmniPur® TBS 20x Ready Pack Powder [b] dissolved in 20 litres dH_2O
TBS-T	1x TBS, 0.1% (v/v) Tween-20
blocking buffer	5% (w/v) non-fat skimmed milk powder [a] in 1x PBS or TBS
1°/2° antibody incubation buffer	5% (w/v) non-fat skimmed milk powder in 1x PBS-T or TBS-T

[a] Sigma-Aldrich
[b] Calbiochem; Darmstadt, Germany

Table 2.5: Primary antibodies used for immunoblot analysis.

Specification (Name)	Species/clonality	Dilution (solution)	Manufacturer *catalogue number*
total ATM	Rabbit monoclonal	1:500 (PBS)	Abcam *#ab32420*
phospho-ATM Ser1981	Rabbit monoclonal	1:10,000 (PBS)	Epitomics Inc. [b] *#2152-1*
ATR	Goat polyclonal	1:500 (PBS)	Santa Cruz Biotechnology [c] *#sc-1887*
β-actin	Mouse monoclonal	1:5,000 (PBS)	Sigma-Aldrich *#A1978*

CDC25A	Mouse monoclonal	1:500 (TBS)	Santa Cruz Biotechnology *#sc-7389*
CDC25C	Rabbit polyclonal	1:500 (PBS)	Santa Cruz Biotechnology *#sc-327*
phospho-CDK1/2/3/5 Tyr15	Rabbit monoclonal	1:2,000 (PBS)	Abcam *#ab133463*
CDT1	Rabbit monoclonal	1:1,000 (PBS)	Cell Signaling Technology Inc. [d] *#8064*
total CHK1	Mouse monoclonal	1:1,000 (PBS)	Santa Cruz Biotechnology *#sc-8408*
phospho-CHK1 Ser296	Rabbit polyclonal	1:1,000 (PBS)	Cell Signaling *#2349*
phospho-CHK1 Ser317	Rabbit polyclonal	1:1,000 (TBS)	Cell Signaling *#2344*
phospho-CHK1 Ser345	Rabbit polyclonal	1:500 (PBS)	Cell Signaling *#2341*
phospho-CHK2 Thr68	Rabbit polyclonal	1:1,000 (PBS)	Cell Signaling *#2661*
Cyclin A2	Mouse monoclonal	1:1,000 (PBS)	Abcam *#ab16726*
Cyclin D1	Rabbit monoclonal	1:10,000 (PBS)	Abcam *#ab134175*
Cyclin E1	Rabbit polyclonal	1:1,000 (PBS)	Santa Cruz Biotechnology *#sc-481*
Geminin	Rabbit polyclonal	1:1,000 (PBS)	Thermo Scientific [e] *#PA5-30612*
phospho-H2AX Ser139	Mouse monoclonal	1:1,000 (PBS)	Merck Millipore [f] *#05-636*
phospho-histone H3 Ser10	Rabbit polyclonal	1:2,000 (PBS)	Merck Millipore *#06-570*
total KAP1	Rabbit polyclonal	1:10,000 (PBS)	Bethyl Laboratories [g] *#A300-274A*
phospho-KAP1 Ser824	Rabbit polyclonal	1:2,000 (PBS)	Bethyl Laboratories *#A300-767A*

p21	Rabbit polyclonal	1:1,000 (TBS)	Santa Cruz Biotechnology *#sc-397*
total p53	Mouse monoclonal	1:500 (TBS)	Santa Cruz Biotechnology *#sc-126*
phospho-p53 Ser15	Rabbit polyclonal	1:1,000 (TBS)	Cell Signaling *#9284*
PPIB (Cyclophilin B)	Rabbit polyclonal	1:2,000 (PBS)	Abcam *#ab16045*
RPA32	Mouse monoclonal	1:500 (PBS)	Abcam *#ab2175*

[a] Cambridge, UK
[b] Burlingame, CA, USA
[c] Dallas, TX, USA
[d] Danvers, MA, USA
[e] Waltham, MA, USA
[f] Billerica, MA, USA
[g] Montgomery, TX, USA

Table 2.6: Secondary antibodies used for immunoblot analysis.

Specification (Name)	Species	Dilution	Manufacturer *catalogue number*
Anti-goat-HRP	donkey	1:5,000	Jackson ImmunoResearch Laboratories, Inc. [a] *#705-035-147*
Anti-mouse-HRP	goat	1:5,000	Thermo Scientific *#31430*
Anti-rabbit-HRP	goat	1:5,000	Thermo Scientific *#31460*

[a] West Grove, PA, USA

2.6.3 Two-colour detection with infrared fluorescence

When using the two-colour detection system, the same procedures were followed as in Section 2.6.2, except that membranes were blocked in a 1:1 solution of PBS or TBS and Odyssey® Blocking Buffer (LI-COR). The primary and secondary antibody incubation was also carried

out in a 1:1 solution of PBS-T or TBS-T and Odyssey® Blocking Buffer. The secondary antibodies used are show in Table 2.7. Following the final wash with PBS or TBS, the membranes were placed on the Odyssey® scanner (LI-COR) for detection.

Table 2.7: Secondary antibodies used for two-colour detection with infrared fluorescence.

Specification (Name)	Species/clonality	Dilution	Manufacturer *catalogue number*
IRDye® 800CW	goat polyclonal	1:5,000	LI-COR *#926-32211*
IRDye® 680RD	goat polyclonal	1:5,000	LI-COR *#926-68070*

2.7 Live Cell Imaging

Cells were seeded in 100 µL complete medium in 96-well plates (Costar®, flat bottom; Corning Incorporated) at a density of 4,000 cells/well (PC-9) or 8,000 cells/well (SO25, SO45, SO46). Cells were then incubated overnight at 37 °C before imaging. Cells were imaged on a TE2000-E Eclipse Nikon microscope (Nikon UK Limited, Kingston Upon Thames, UK) equipped to provide a humidified atmosphere at 37 °C and 5% CO_2 within an environmental chamber (Solent Scientific Ltd.; Segensworth, UK). Images were taken at a 100x magnification (10x objective) using the NIS-Elements Advanced Research software 3.2 (Nikon UK Limited). The well positions were set, and initial pictures were taken before taking the plate to the tissue culture hood to add either AZD6738 or VE-822 to a final concentration of 1 µM. The plate was then returned to the incubator setup in the microscope and left for 30-60 min before imaging the same positions again. Pictures were taken of the cells treated with AZD6738 in bright field, while those treated with VE-822 had pictures taken with bright field illumination or fluorescence using DAPI or CFP filter cubes (Nikon UK Limited) to visualise drug up-take.

Previous work in the laboratory has shown that VE-822, (but not VE-821 or AZD6738) is highly fluorescent at ex365nm/em455nm and ex430nm/em480nm (A Ryan, unpublished).

2.8 Clonogenics

2.8.1 Clonogenic survival assay

The clonogenic survival assay assesses the relative abilities of single cells to form a colony of ≥50 cells following control or inhibitor treatment. Cells were plated in triplicate in 6-well plates (Corning Incorporated) at a density of 250 cells/well (PC-9) or 5,000 cells/well (SO25). These cells were plated in either 0.1, 0.3, 1.0, 3.0, or 10.0 μM AZD6738 or 0.01% DMSO (vehicle control) diluted in complete culture medium. The medium was then aspirated, wells were washed with 1x PBS, and fresh medium without the presence of inhibitor was added at either 24 or 48 h. Once colonies reached a size of 50 or more cells (7-11 days later), cells were fixed and stained with 0.5% (w/v) crystal violet (Merck, Darmstadt, Germany) / 75% (v/v) methanol solution for 30 min at RT and air dried. As SO25 was unable to form distinct colonies, pictures were then taken of the PC-9 and SO25 stained plates with a Gelcount™ (Oxford Optronix Ltd.; Abingdon, UK).

2.8.2 Colony forming assay

Unlike the clonogenic survival assay (Section 2.8.1), the colony forming assay assesses the abilities of single cells to form a colony of at least 50 cells while *continuously* in the presence of an inhibitor. Cells were plated in triplicate in 6-well plates at a density of 500 cells/well (PC-9) or 1,000 cells/well (SO25) and incubated overnight to re-attach. The medium was then aspirated and replaced with medium containing either 0.1, 0.3, 1.0, 3.0, or 10 μM AZD6738, VE-821, or VE-822, or 0.01% DMSO (vehicle control) and placed back in the incubator. Inhibitors were replaced in fresh medium after 1 week. Once colonies reached a size of a least

50 cells, they were fixed and stained with the crystal violet solution for 30 min at RT and air dried before colony counting. The colony forming plating efficiency (PE) for each cell line was calculated using the following equation:

$$PE\ (\%) = \frac{number\ of\ colonies\ counted}{number\ of\ cells\ seeded} \times 100$$

2.9 TP53 Gene Sequencing

In order to validate the presence of a TP53 point mutation in SO25 cells that is present in PC-9 cells, Sanger sequencing was performed. PC-9 and SO25 cells were plated in 10 cm dishes until 85% confluent. At this point, cells were trypsinised and pelleted, and then DNA was purified using the MasterPure™ DNA Purification Kit (Epicentre, Madison, WI, USA), following the manufacturer's instructions. Samples were then stored at -20 °C until polymerase chain reaction (PCR) was used to amplify the region of interest, TP53 exon 7.

The primers (Sigma-Aldrich) used were:

Exon 7: Forward: 5'-AGGCGCACTGGCCTCATCTT-3'

Reverse: 5'-TGTGCAGGGTGGCAAGTGGC-3'

PCR reactions were carried out on a MiniOpticon™ Real-Time PCR System/MJ Mini™ Personal Thermo Cycler (BioRad). The amplification was performed in 25 µL reactions (see Table 2.8).

Table 2.8: PCR reaction components.

The components are listed in the order they were added.

Reaction component	Amount
dH_2O	5.9 µL
20 µM forward primer	0.8 µL
20 µM reverse primer	0.8 µL
SYBR® Green PCR Master Mix [a]	12.5 µL
genomic DNA	5 µL

[a] Life Technologies

The following conditions were used:

Activation (hotstart)	95 °C	10 min	
Denaturation	94°C	30 secs	40x
Annealing	60°C	45 secs	
Extension	72°C	1 min	
Melting curve	65-95 °C, 0.5 increments		

The PCR products were then purified using the MinElute® PCR Purification Kit (Qiagen; Hilden, Germany), following the manufacturer's instructions. Sanger sequencing of the purified PCR products was commercially performed by SourceBioscience (Oxford, UK) and the resulting reads were analysed for the presence of the R2248Q point mutation.

2.10 RNA-Sequencing

PC-9 and SO25 cells were plated in 10 cm dishes, with conditions shown in Table 2.9. 48 h after plating, RNA was extracted using the RNeasy® Plus Mini Kit (Qiagen), following the

Table 2.9: Plating conditions for RNA-sequencing.

	Cell Line	Condition	Density (cells/mL)
1	PC-9	complete medium	33,000
2	PC-9	complete medium	33,000
3	PC-9	plated continuously in 0.01% DMSO	33,000
4	SO25	plated continuously in 0.01% DMSO	32,500
5	SO25	plated continuously in 1 μM AZD6738	32,500
6	SO25	plated continuously in 0.3 μM VE-822	32,500

manufacturer's instructions. Samples were stored at -80 °C until RNA-sequencing was carried out by a commercial provider (SourceBioscience, Oxford, UK) using the HiSeq 2000 platform (Illumina). Data analysis was performed by SourceBioscience according to published methods (Trapnell *et al*, 2012). Briefly, sequencing reads were mapped to their genomic location using Bowtie version 2.02 (Langmead *et al*, 2009) and splice junctions were identified using Tophat version 2.0.9 (Kim *et al*, 2013). Cufflinks version 2.1.1 (Trapnell *et al*, 2012) was used to perform transcript assembly, abundance estimation, and differential expression and regulation for samples. Visualisation of differential expression results used CummeRbund (http://compbio.mit.edu/cummeRbund/, accessed 4 Oct 2016) or Integrative Genomics Viewer (IGV; Thorvaldsdóttir *et al*, 2013) and RNA-Seq alignment metrics were generated using Picard (http://broadinstitute.github.io/picard/, accessed 4 Oct 2016). A schematic outlining the method is shown below (Figure 2.1). MetaCore™ Key Pathway Advisor (Thomson Reuters; New York, NY, USA; http://ipscience.thomsonreuters.com/product/metacore, accessed 4 Oct 2016) was used to explore pathway enrichment.

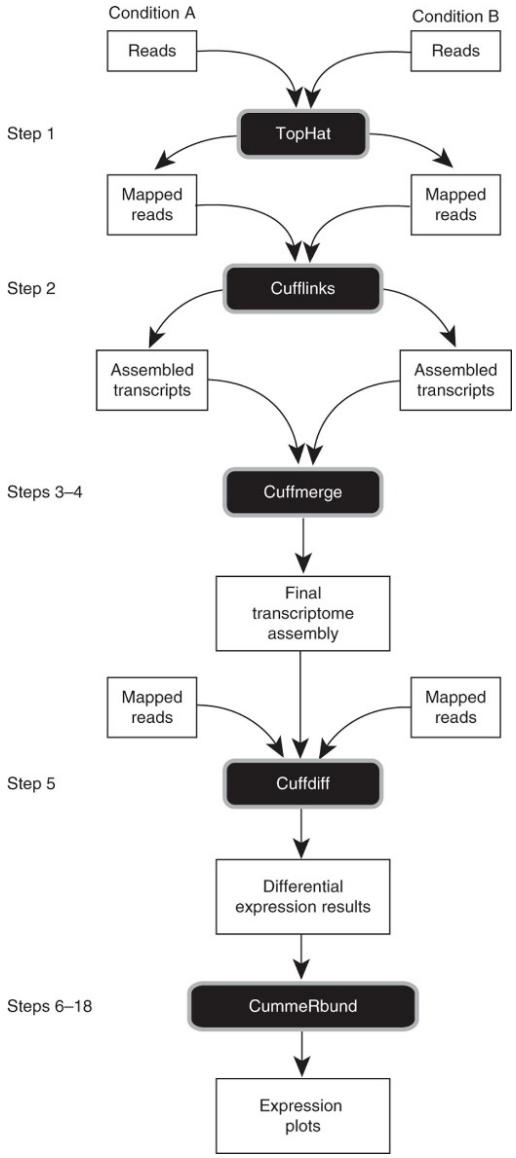


Figure 2.1: Outline of method for analysis of RNA-sequencing data.
Reproduced from Trapnell *et al*, 2012.

2.11 Flow Cytometry

2.11.1 DNA content analysis/cell cycle analysis

In order to analyze DNA content by flow cytometry, cells were first seeded in 10 cm dishes and grown until they were approximately 65% confluent. Cells were then treated with either 1 μM AZD6738 or 0.01% DMSO (vehicle control) for 24 h. Floating/detached cells were

retained while attached cells were trypsinised. Both floating and attached cells were then combined and collected by centrifugation (225 x g, 4 min). The supernatant was discarded and the cell pellets were fixed by the drop-wise addition of 1.5 mL ice-cold 70% ethanol (Sigma-Aldrich) while vortexing. Pellets were then stored at -20 °C until preparation to run the samples. At this point, pellets were washed with 2 mL 1x PBS, resuspended, and rehydrated for 2 min. Cells were then centrifuged at 225 x g for 5 min and then incubated in a 1:200 dilution of RNase A (100 μg/mL stock; Qiagen) in 1x PBS for 30 min at 37 °C. Propidium iodide (PI; Calbiochem) was then added at a final concentration of 20 μg/mL. PI stains DNA stoichiometrically, and thus the amount of fluorescent signal is directly proportional to the DNA content. The DNA content of cells was measured using a FACScan Flow Cytometer (BD Biosciences; San Jose, CA, USA) and BD CellQuest™ Pro software. ModFit LT software (Verity Software House; Topsham, ME, USA) was utilised to determine the proportion of cells in G1, S, or G2/M cell cycle phases.

2.11.2 BrdU chase assay

Bromodeoxyuridine (BrdU) labelling was used to follow cells through the cell cycle. BrdU substitutes for thymidine in replicating DNA and thus newly synthesised DNA can be detected with anti-BrdU antibodies. S-phase populations of asynchronous cells were pulse labelled with 20 μM 5-bromo-2'-deoxyuridine (BrdU; Sigma-Aldrich) for 20 min at 37 °C, protected from light. Cells were then washed with PBS, complete culture medium containing either 1 μM AZD6738 or 0.01% DMSO (vehicle control) was added, and cells were incubated at 37 °C for the time indicated. Floating cells were collected and attached cells were trypsinised and then collected by centrifugation (225 x g, 4 min). The supernatant was discarded and the cell pellets were fixed by the drop-wise addition of 1.5 mL 4°C 70% ethanol while vortexing. Cells were then resuspended in 2 M HCl (Fisher Scientific) and 0.1 mg/mL pepsin (Sigma-Aldrich) and

incubated for 30 min at RT. Following centrifugation (455 x g, 5 min), cells were washed with PBS and then centrifuged again (455 x g, 5 min). The cell pellets were then resuspended in PBS + 2% FBS and incubated for 30 min at RT. These cells were then centrifuged at 455 x g for 5 min, and then resuspended in 100 µL of PBS + 2% FBS containing a 1:100 dilution of mouse anti-BrdU antibody (#347580; BD Biosciences) and incubated overnight at 4°C. This was followed by a wash with PBS + 2% FBS and then incubation in 100 µL of 1:200 dilution of Alexa fluor® 488 goat anti-mouse secondary antibody (Life Technologies) in PBS + 2% FBS for 1 h RT in the dark, vortexing every 20 min. The cell pellets were then washed in PBS, centrifuged (445 x g, 5 min), and resuspended in 500 µL PBS with 20 µg/mL of PI. Both DNA content and BrdU incorporation were assessed with a FACSCalibur Flow Cytometer (BD Biosciences) and BD CellQuest™ Pro software. The analysis of the data was carried out with FlowJo software (FlowJo, LLC; Ashland, OR, USA).

2.12 Immunofluorescence

Cells were seeded in 100 µL complete culture medium in triplicate in 96-well plates at a density of either 4,000 cells/well (PC-9, A549), 6,000 cells/well (Calu-6, H1975, H23), or 8,000 cells/well (NBE1, SO25, SO45, SO46) and left overnight at 37 °C to attach. Wells were then treated with 100 µL of complete culture medium to bring the final concentration to 1 µM AZD6738 or 0.01% DMSO (vehicle control) for 24 h. Cells were then fixed with 100 µL/well of 3% paraformaldehyde (PFA; VWR) in PBS (pH adjusted to 7.4 with 5 M NaOH; VWR) for 30 min at RT. For cells that were to be stained for RPA32 foci, some wells were treated to a final concentration of 10 µM camptothecin for 2 h as a positive control. Following fixation, wells were washed three times with PBS, and then permeabilised and blocked with 100 µL of 0.1% Trition X-100, 1% albumin bovine serum (BSA; Thermo Scientific), and 1% normal goat serum (NGS; Millipore) in PBS for at least 1 h at RT. The cells were then incubated overnight

at 4 °C in 50 µL of primary antibody (see Table 2.10) in 1% BSA and 1% NGS in PBS. After washing three times with PBS, cells were incubated with 50 µL of goat anti-rabbit Alexa fluor® 555 or Alexa fluor® 488 goat anti-mouse secondary antibodies (Life Technologies) diluted 1:1,200 in 1% BSA and 1% NGS in PBS for 1 h at RT in the dark. Hoechst 33258 (10 mg/mL; Sigma-Aldrich) was added to the secondary antibody solution in a 1:1,000 dilution as a nuclear counterstain. Wells were then washed three times with PBS and stored in 200 µL PBS until imaging. The plates were then visualised using the IN Cell Analyzer 1000 automated epifluorescence microscope (GE Healthcare UK Ltd.; Amersham, UK).

Table 2.10: Primary antibodies used in immunofluorescence.

Specification (Name)	Species/clonality	Dilution	Manufacturer *catalogue number*
53BP1	Rabbit polyclonal	1:800	Cell Signaling *#4937*
cyclin A2	Mouse monoclonal	1:250	Abcam *#ab16726*
cyclin E1	Rabbit polyclonal	1:250	Santa Cruz Biotechnology *#sc-481*
phospho-H2AX Ser139	Mouse monoclonal	1:1,500	Merck Millipore *#05-636*
RPA32	Mouse monoclonal	1:250	Abcam *#ab2175*

2.12.1 Quantitative γH2AX, 53BP1, and RPA32 foci staining

The IN Cell Analyzer 1000 Cellular Imaging and Analysis System (GE Healthcare UK) was used to analyse the images. Any mitotic cells (with Hoechst-bright nuclei) and cells on the border of an image were excluded from analyses, while the rest were analysed for γH2AX,

53BP1, and RPA32 foci. Those cells stained for γH2AX were also analysed for pan-nuclear γH2AX staining.

2.12.2 Quantitative cyclin A2 and cyclin E1 staining

The IN Cell Analyzer 1000 Cellular Imaging and Analysis System (GE Healthcare UK) was used to analyse the images. Mitotic cells with bright nuclei and cells on the border of an image were excluded from analyses, while the rest were analysed for positive nuclear staining for cyclin A2 or cyclin E1.

2.13 DNA Fibre Assay

2.13.1 Labelling and spreading fibres

In order to investigate DNA replication, both qualitatively and quantitatively, at the single molecule level, the DNA fibre assay was utilised. The protocol was modified from Foskolou *et al*, 2016. In short, cells were seeded in 10 cm dishes (at a density allowing the cells to reach approximately 65% confluency the following day) in complete culture medium and left to re-attach overnight at 37 °C. The following day, frozen 2.5 mM 5-chloro-2'-deoxyuridine (CldU; Sigma-Aldrich) and 5-iodo-2'-deoxyuridine (IdU; Sigma-Aldrich) stock solutions covered in foil were placed in 37 °C and 52 °C water baths, respectively to thaw. Working solutions were created by diluting the CldU stock 1:100 to 25 μM, and diluting the IdU stock 1:10 to 250 μM in complete culture medium. The medium on the seeded cells was then removed and replaced with complete culture medium containing the appropriate concentration of AZD6738 or 0.01% DMSO (vehicle control) and incubated at 37 °C for 1 h. This medium was then removed and 10 mL of the 25 μM CldU working solution was added and the plates were incubated in the dark at 37 °C for 20 min. Following a wash with complete culture medium that does not contain any thymidine analogues, 10 mL of the 250 μM IdU working solution was added and the plates

were incubated in the dark at 37 °C for another 20 min. The plates were then washed twice with 1x PBS and then trypsinised, spun at 950 x g for 6 min, resuspended in PBS at a concentration of 5 x 10^5 cells/mL, and placed on ice.

The cells were then lysed and spread on Menzel Gläser Superfrost® slides (76 x 26 x 1 mm, #12382098; Thermo Scientific) three slides at a time using a P20 pipette. 2 µL of cell suspension (approximately 2,000 cells) was added on the top of each slide. After 5 min, or once the drop began to flatten, 7 µL of spreading buffer (see Table 2.11) was added and mixed in a circle, not up and down. After two minutes, the slide was tilted 30-40 ° to allow the drop to run down the slide. The slides were allowed to air dry before fixing in 75% methanol / 25% acetic acid (VWR) for 10 min and then stored at 4 °C until staining.

Table 2.11: Spreading buffer components for DNA fibre assay.
The spreading buffer was adjusted to pH 7.4 and can be stored at RT up to 6 months.

Component	Amount	Final Concentration
Tris-HCl	1.5756 g	200 mM
0.5 M EDTA	5 mL	50 mM
10% SDS	2.5 mL	0.5%
dH_2O	up to 50 mL	

2.13.2 Staining

Slides were washed twice with dH_2O for 5 min at RT, followed by incubation with 2.5 M HCl for 5 and then 80 min at RT. Following two washes with 1x PBS, slides were then washed twice with blocking buffer (1% BSA and 0.1% Tween-20 in 1x PBS) for 5 min and incubated in blocking buffer for 1 h at RT. 200 µL of primary antibodies (see Table 2.12) diluted in blocking buffer was then added to each slide, covered with a coverslip (Menzel Gläser 22 x 50 mm; Fisher Scientific UK Ltd.), and incubated, covered, at 37 °C for 1 h. Coverslips were then

removed, slides were washed three times with PBS for 5 min each, and then incubated with 4% PFA for 10 min. Slides were washed 3 x 5 min with PBS then incubated with blocking buffer for 1, 5, and then 25 min. 200 µL of secondary antibodies (see Table 2.13) diluted in blocking buffer were then added to each slide, and a coverslip was placed on top. Slides were incubated, covered, at 37 °C for 1 h, and then the coverslip was removed. Slides were washed two times with PBS, incubated for 1, 5, and then 25 min in blocking buffer, and then rinsed 2x with PBS. Slides were then mounted with Fluoromount (Sigma-Aldrich), without nuclear dye, and covered with a coverslip. Slides were kept at 4 °C before imaging and sealing the coverslip with nail varnish.

Table 2.12: Primary antibodies used in the DNA fibre assay.

Specification (Name)	Species/clonality	Dilution	Manufacturer *catalogue number*
anti-BrdU (labels CldU)	Rat monoclonal	1:500	BioRad *#OBT0030*
anti-BrdU (labels IdU)	Mouse monoclonal	1:500	BD Biosciences *#347580*

Table 2.13: Secondary antibodies used in the DNA fibre assay.

Specification (Name)	Species	Dilution	Manufacturer *catalogue number*
Alexa fluor® 488	goat anti-mouse	1:500	Life Technologies *#A-11017*
Alexa fluor® 555	goat anti-rat	1:500	Life Technologies *#A-21434*

2.13.3 Imaging

The fibres were imaged with a Zeiss LSM780 confocal microscope (Carl Zeiss Microscopy GmbH; Jena, Germany) with a 63x oil objective, using Immersol™ 518 F oil (Carl Zeiss

Microscopy GmbH). While imaging, the fibres were focused on the green label, and fields were picked that had well-separated fibres. As many viable pictures as possible were taken for each condition. Images were collected with ZEN 2.1 (black) imaging software (Carl Zeiss Microscopy GmbH), and files were exported as TIFFs for analysis.

2.13.4 Analysis

The fibre images were imported to ImageJ (National Institutes of Health; Bethesda, MD, USA) for analysis. For quantitative analysis, the length of at least 200 ongoing (incorporated both CldU/red and IdU/green labels) fibre tracts were measured. The following equation (where *x* =length of IdU/green label) was used to determine the replication rates:

$$V_{\text{IdU kb/min}} = \frac{(x * 0.132\ \mu\text{m})(2.59\ \text{kb}/\mu\text{m})}{t\ (\text{min})}$$

2.14 siRNA Transfections

In order to downregulate cyclin A2 and cyclin E1 expression, SMARTpool: ON-TARGETplus human CCNA2[4] and CCNE1[5] siRNA (GE Healthcare Dharmacon Inc.; Lafayette, CO, USA), respectively, were used. ON-TARGETplus Control Pool non-targeting pool[6] siRNA (GE Healthcare Dharmacon Inc.) served as a control. One day before transfection, PC-9 cells were seeded in complete culture medium in 6-well plates for western blot analysis at densities of 150,000 cells/well for collection 24 h post-transfection and 50,000 cells/well for collection 102 h post-transfection, or 96-well plates for proliferation assays at a density of 500 cells/well. After incubating overnight at 37 °C to allow for re-attachment, cells were transfected with 25

[4] #L-003205-00-0005
[5] #L-003213-00-0005
[6] #D-001810-10-05

nM siRNA using the DharmaFECT 2 transfection reagent (GE Healthcare Dharmacon Inc.) according to the manufacturer's instructions.

First, separate mixtures of DharmaFECT 2 with serum-free Opti-MEM® (Life Technologies), and the siRNAs with serum-free Opti-MEM® were prepared and incubated for 5 min at RT. The two solutions were then combined 1:1, mixed, and incubated for 20 min at RT. The mixture was then added to the 96- and 6-well plates, so that the final siRNA concentration was 25 nM. Treatments were made with CCNA2 siRNA, CCNE1 siRNA, non-target siRNA, while there were also wells treated only with transfection reagent and DNase/RNase-free water (Zymo Research; Irvine, CA, USA), and wells left untreated. In order to reduce cytotoxicity to the cells, the medium in all wells was aspirated and replaced with fresh complete culture medium 6 h after transfection. Complete culture medium alone was added to the 6-well plates, while the 96-well plates were treated with dilutions of AZD6738. The first 6-well plates were harvested 24 h post-transfection, while the second 6-well plates were harvested 102 h post-transfection, and all were processed for western blot analysis (see Section 2.6). Before harvesting the cells at 102 h post-transfection, bright-field images were taken of the 6-well plates with a FLoid Cell Imaging Station (Life Technologies) at 460x magnification (20x objective). The 96-well plates for cell viability were assessed by quantification of resazurin metabolism four days after treatment with AZD6738 (102 h post-transfection; see Section 2.4).

2.15 Data Analysis and Statistics

GraphPad Prism® 7 (GraphPad Software, Inc.; La Jolla, CA, USA) was used for all statistical analysis, and all values are expressed as the mean ± standard error of the mean (SEM) of at least three independent experiments unless otherwise stated. For data comparison between two groups, such as inhibitor treated vs. vehicle control treated, two-sided Student's t-test was used. Inhibitor dose responses were compared by analysis of variance (ANOVA) with cell line or

treatment and dose as factors, in order to detect statically significant differences between parental PC-9 and ATR inhibitor resistant (SO25, SO45, SO46) cell lines. Differences with p values <0.05 were considered significant.

CHAPTER 3

3 ATR Resistant Clones

3.1 Isolation of ATR inhibitor resistant clones

The selective ATR kinase inhibitor AZD6738 is currently in phase 1 clinical development and it is likely that resistance will emerge in patients, as has been reported for other kinase inhibitors in cancer therapy (O'Hare *et al*, 2007; Wheeler *et al*, 2010; Barouch-bentov, 2012; Lovly & Pao, 2012; Hartsough *et al*, 2014). It is thus in the interest of patients and physicians to understand potential mechanisms of ATR resistance in order to identify rational strategies to prevent or delay the emergence of resistance in the clinic. In order to identify potential mechanisms of resistance to ATR inhibitors, we used an *in vitro* assay system. However, since ATR function is essential to cell viability (Brown & Baltimore, 2000; De Klein *et al*, 2000; Liu

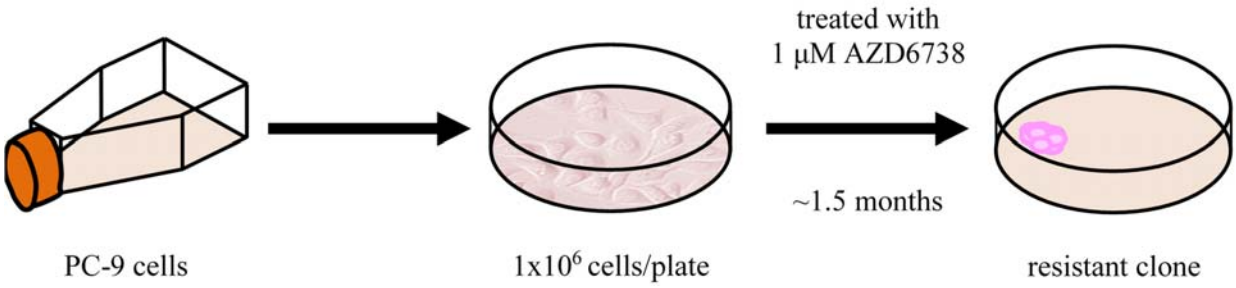


Figure 3.1: Generation of AZD6738 resistant PC-9 clones.

PC-9 human non-small cell lung cancer cells were plated in each of ten 10 cm dishes ($1x10^6$ per plate) and treated with AZD6738 (1 μM). Six weeks later, distinct resistant clones had emerged, which were isolated (using cloning rings for SO45 and SO46), and expanded in culture in the presence of AZD6738 (1 μM for SO25 and SO46, or 2 μM for SO45).

et al, 2000), it was unclear whether the isolation of resistant clones would be possible. PC-9 human non-small cell lung cancer cells were treated with 1 μM AZD6738 for 6 weeks (Figure 3.1), at which point an AZD6738 resistant cell colony emerged (SO25) and was isolated from a plate with only a single observable colony and then cultured in 1 μM AZD6738.

This process was repeated in an independent experiment and two further independent colonies/clones, SO45 and SO46, were isolated from plates containing 1 – 9 distinct colonies/plate using cloning rings and transferred to culture. Approximately 4.9 colonies arose per million cells plated. SO45 was selected and cultured in 2 μM AZD6738, while SO46 was selected and cultured in 1 μM AZD6738, similar to SO25. Throughout this study, the SO25 cells were the principle resistant cells investigated and compared with the parental PC-9 cells. PC-9 NSCLC cells were used to generate the resistant clones because previous work in the lab had established that these p53 mutant cells were rather sensitive to ATR inhibitors, with an AZD6738 mean IC_{50} value of 0.5 μM, range 0.5 - 0.52 (data from Weber, 2015). Using a similar method, we also attempted to isolate resistant clones from H23 cells (AZD6738 mean IC_{50} 0.5 μM, range 0.47 - 0.52, data from Weber, 2015), which harbour a homozygous ATM mutation (p.Q1919P), but no resistant colonies were obtained.

Of note, the resistant clones (SO25, SO45, and SO46) had a distinct morphological phenotype when compared with the parental PC-9 cells (Figure 3.2). Compared with parental PC-9, cells from AZD6738-resistant clones were generally larger in size, irregularly shaped, had occasional cells with multiple nuclei, and cytoplasmic vesicles were visible in many cells.

3.2 Response to ATR inhibitors

Cells from each of the resistant clones showed a similar response to increasing concentrations of AZD6738 (Figure 3.3). Parental PC-9 cells exhibit the expected decrease in relative cell viability with increasing ATR inhibitor concentrations. The resistant clones, however, have a distinct dose-response, showing increased viability at intermediate concentrations (0.1 – 1.0 μM) of AZD6738. Curve-fitting software (Origin®) could not calculate accurate IC_{50} values for this shape of (non-sigmoidal) survival curve, therefore the percent relative cell viability at an AZD6738 concentration of 1.11 μM is reported (Table 3.1), as this approximates the AZD6738

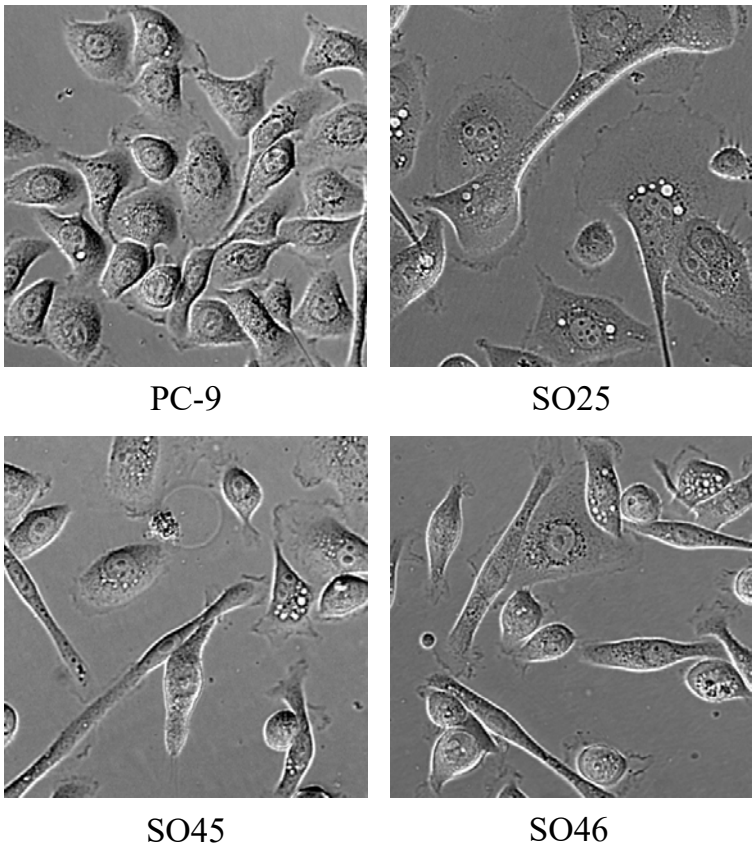


Figure 3.2: Appearance of parental PC-9 and SO25, SO45, and SO46 resistant clones.

Bright field images of AZD6738-resistant cells lines (100x magnification, 10x objective).

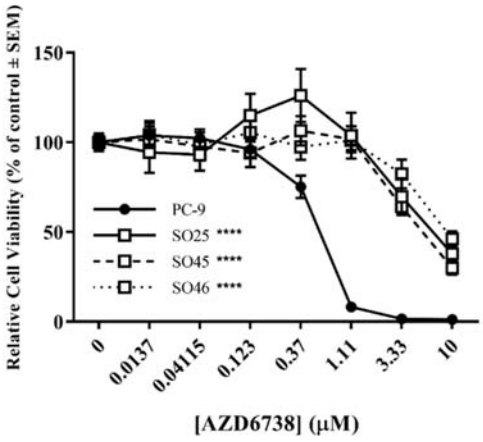


Figure 3.3: Response of PC-9 cells and SO25, SO45, and SO46 resistant clones to increasing concentrations of AZD6738.

PC-9 cells and resistant clones (SO25, SO45, SO46) were incubated for 4 days with AZD6738. Relative cell viability was assessed using the resazurin proliferation assay, and normalised to DMSO treated controls. Each point represents the mean of three independent experiments, each performed in triplicate with error bars = SEM. **** indicates $p<0.0001$ compared with the parental PC-9 cell line (ANOVA).

Table 3.1: Percent relative cell viability at 1.11 µM AZD6738.

Values represent the mean and SEM of three independent experiments, each performed in triplicate. **** indicates p<0.0001 compared with the parental PC-9 cell line (t-test).

Cell Line	AZD6738 % Relative cell viability at 1.11 µM (± SEM)
PC-9	8.15 ± 0.94
SO25	103.75 ± 13.55 ****
SO45	101.70 ± 7.72 ****
SO46	101.02 ± 5.68 ****

concentration used to select the resistant cells. PC-9 cells have a relative cell viability of 8.15% ± 0.94 at 1.11 µM AZD6738, while SO25 cells have a significantly increased relative cell viability of 103.75% ± 13.55.

Cells from resistant clones were then treated with increasing concentrations of ATR inhibitors (VE8-821 and VE-822) that were chemically unrelated to AZD6738. A dose-dependent decrease in relative cell viability was observed for PC-9 cells, while the AZD6738-resistant cells exhibited increased viability at intermediate concentrations of each compound (~0.1 – 1.0 µM for VE-821 and ~0.01-0.1 µM for the more potent compound, VE-822) (Figure 3.4). The greatest relative resistance (69-fold) was apparent for VE-822; 32.46% ± 4.22 vs 0.47% ± 0.17 relative cell viability at 1.11 µM in SO25 and PC-9, respectively (Table 3.2). These data demonstrate that cells from AZD6738-resistant SO25, SO45, and SO46 clones were cross-resistant to chemically unrelated ATR inhibitors (Table 1.1). In addition, the ATR-inhibitor resistant cells grow better at intermediate concentrations of ATR inhibitors.

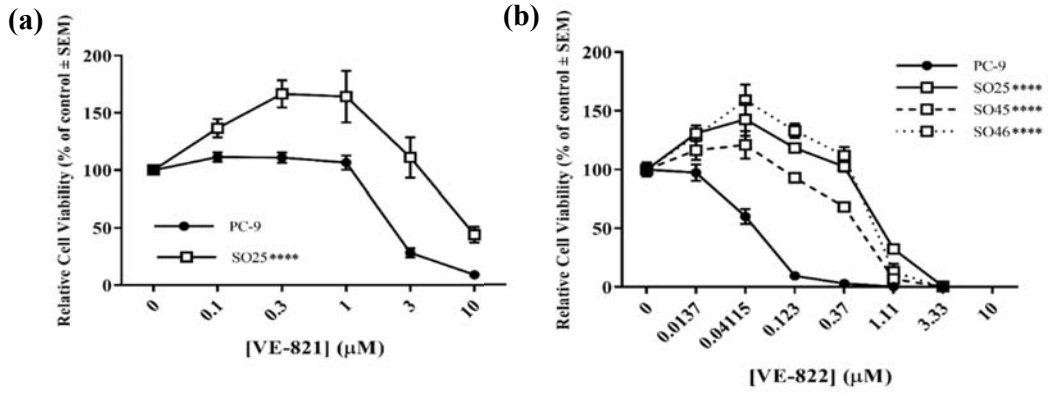


Figure 3.4: Reponses of PC-9, SO25, SO45, and SO46 cells to ATR inhibition by VE-821 and VE-822.

Cells were incubated for 4 days with increasing concentrations of **(a)** VE-821 and **(b)** VE-822. Relative cell viability was assessed using the resazurin proliferation assay, and normalised to DMSO treated controls. Each point represents the mean of three independent experiments, each performed in triplicate with error bars = SEM. Asterisks indicate statistical significance compared with the PC-9 cell line by **** = $p<0.0001$ (ANOVA).

Table 3.2: Percent relative cell viability at 1 μM VE-821 and 1.11 μM VE-822.

Values represent the mean and SEM of three independent experiments, each performed in triplicate. Asterisks indicate statistical significance compared with the parental PC-9 cell line; **** = $p<0.0001$, * = $p<0.05$ (t-test). ND, not done.

Cell Line	VE-821	VE-822
	% Relative cell viability at 1 μM (± SEM)	% Relative cell viability at 1.11 μM (± SEM)
PC-9	106.65 ± 6.69	0.47 ± 0.17
SO25	164.21 ± 23.91 *	32.46 ± 4.22 ****
SO45	ND	6.99 ± 2.70 *
SO46	ND	13.04 ± 7.11

Given the resistance observed across the ATR inhibitors, we wanted to confirm that the compounds were being taken up into the cells. As VE-822 is strongly fluorescent (A Ryan, unpublished data), we treated cells with VE-822 and visualised up-take of the compound. PC-9 cells and the ATR inhibitor resistant clones were imaged before and after the addition of VE-

822 (1 μM). On addition of VE-822, fluorescence was detectable in both the parental and ATR-inhibitor resistant cells suggesting that the ATR resistance is not due to poor uptake of ATR inhibitor in the resistant clones (Figure 3.5). Of note, the VE-822 fluorescence signal was strongest in the cytoplasm rather than the nucleus, and appeared to be associated with cytoplasmic vesicles.

3.3 Proliferation of ATR inhibitor resistant clones

The proliferation rates of the ATR-inhibitor resistant cells lines were low compared with the parental PC-9 cells. PC-9 cells are fast growing, with an estimated doubling time of 28.5 ± 3.3 h, while SO25 cells (cultured in 1 μM AZD6738) grew at almost half the rate, with an estimated doubling time of 50.0 ± 5.7 h (Table 3.3).

Table 3.3: Doubling time of PC-9 and SO25 cells.

Doubling times were estimated from the linear portion of the log growth curve from the PicoGreen cell proliferation assay. Values are calculated from three independent experiments, each in triplicate.

Cell Line	Doubling Time (± SEM) hours
PC-9	28.5 ± 3.3
SO25 (in 1 μM AZD6738)	50.0 ± 5.7

To further assess the growth rate of ATR-inhibitor resistant clones and parental PC-9 cells in the presence and absence of 1 μM AZD6738, a PicoGreen cell proliferation assay (measuring dsDNA as a surrogate of cell number) was performed over 7 days. In the absence of AZD6738, PC-9 cells had the fastest growth rate, while in the presence of AZD6738, cell growth did not increase beyond day 3 (Figure 3.6). In contrast, the ATR-inhibitor resistant clones continued to grow in the presence of 1 μM AZD6738, and by day 7, grew better in the presence of AZD6738 compared with controls.

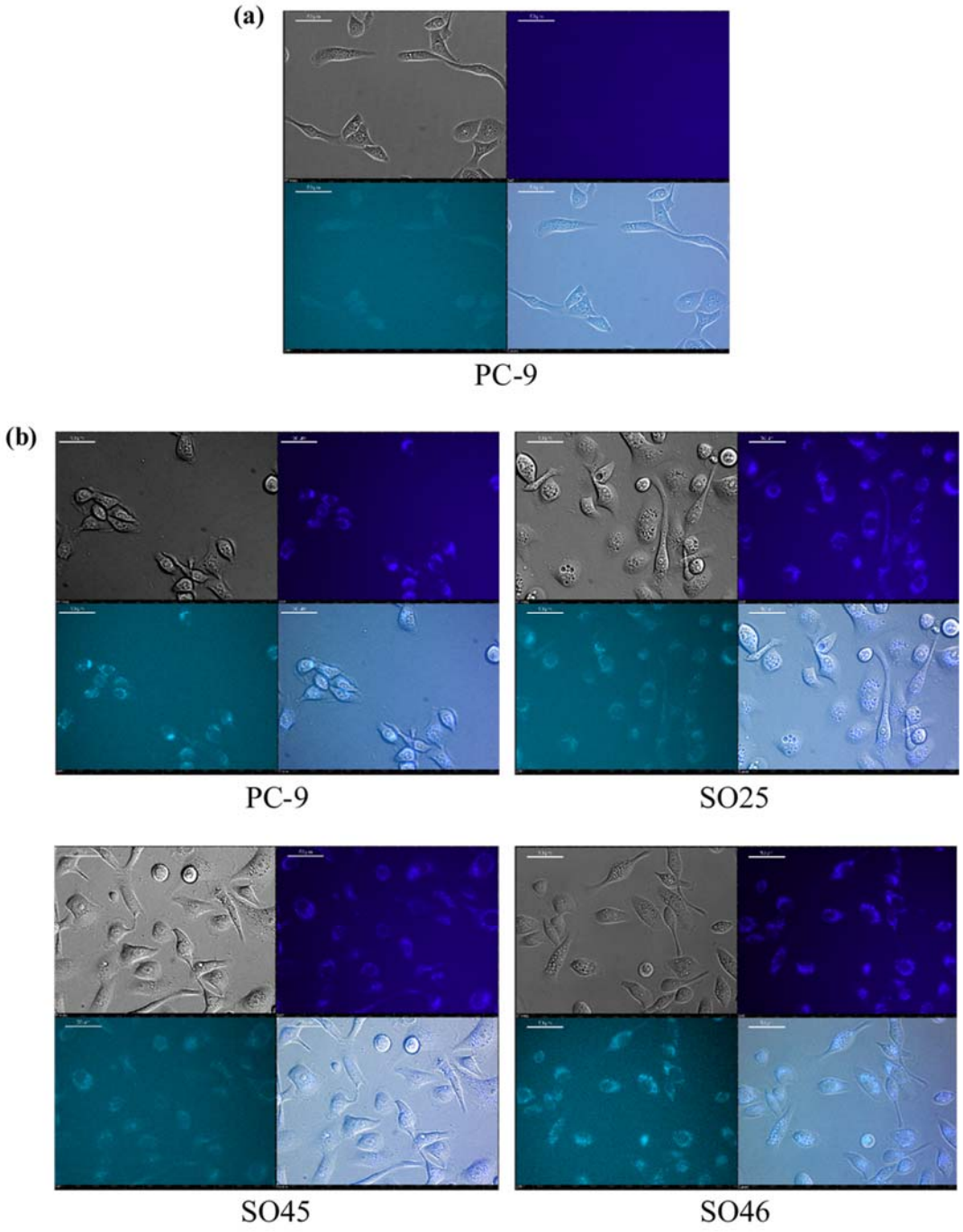


Figure 3.5: Visualisation of the up-take of VE-822 into PC-9 and resistant cells.

PC-9, SO25, SO45, and SO46 cells were plated in 96-well plates and visualised at 100x magnification **(a)** before and **(b)** after the addition of approximately 1 μM VE-822 for 30 mins to 1 h. These are representative images of PC-9, SO25, SO45, and SO46 cells with bright field, DAPI, merge, and CFP going clockwise from the top left.

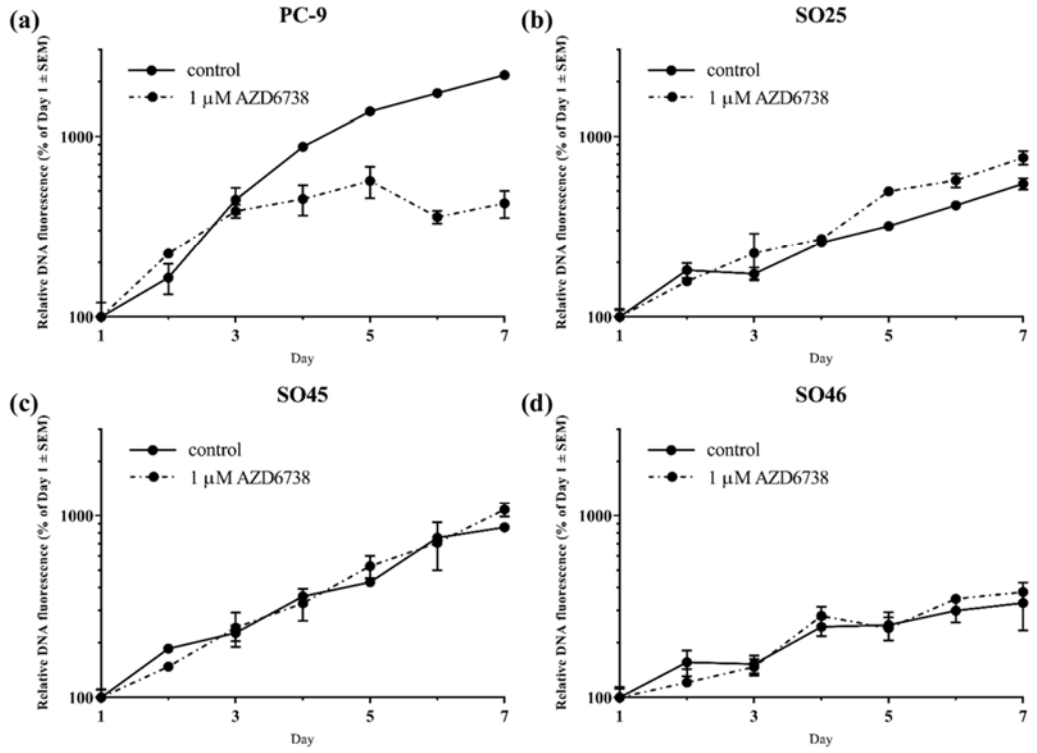


Figure 3.6: Relative growth of PC-9 and ATR resistant cells.

(a) PC9, **(b)** SO25, **(c)** SO45, and **(d)** SO46 cells were treated with either 1 μM AZD6738 or DMSO control and changes in dsDNA content assessed for up to 7 days. DNA content was assessed by PicoGreen and samples were normalised to values from day 1. Graphs represent the mean of three independent experiments done in triplicate (± SEM).

3.4 Colony forming ability of ATR inhibitor resistant cells

As the resistant clones appeared to growth better in the presence of AZD6738, we were interested in determining the plating efficiency of these cells in different concentrations of ATR inhibitors. We assessed plating efficiency using a colony forming assay to determine the ability of single cells to form a colony of at least 50 cells. Unlike a standard clonogenic survival assay, cells were grown *continuously* in the presence of either AZD6738, VE-821, or VE-822. PC-9 cells have a dose-dependent decrease in plating efficiency for all the ATR inhibitors (Figure 3.7). Interestingly, the SO25 cells did not grow and form colonies without the addition of ATR

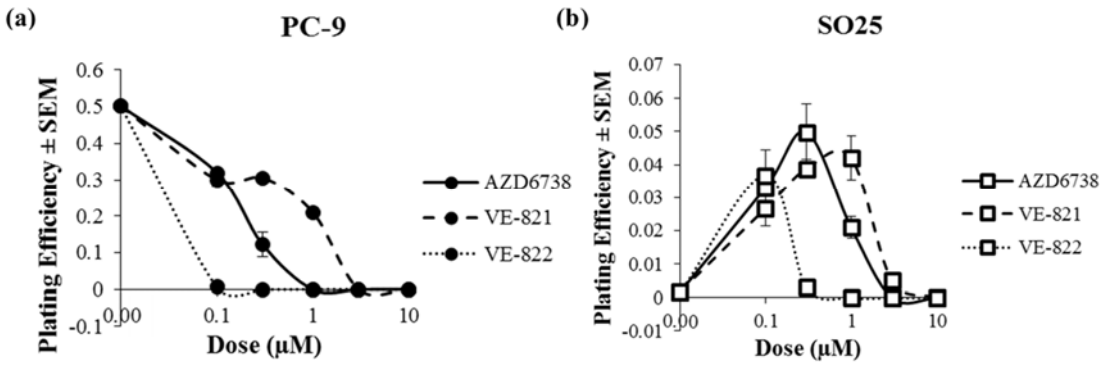


Figure 3.7: Plating efficiency of PC-9 and SO25 cells in the presence of ATR inhibitors.

PC-9 and SO25 cells were plated and then treated with the indicated concentrations of AZD6738, VE-821, and VE-822 or 0.01% DMSO after approximately 24 h. After colonies of about 50 cells had formed, plated were stained with CV and colonies were counted to determine plating efficiency. The experiment was in triplicate and error bars = SEM.

inhibitors. SO25 had the greatest plating efficiencies at 0.3 μM AZD6738, 1 μM VE-821, and 0.1 μM VE-822, while PC-9 cells had the greatest plating efficiency at 0 μM for all three inhibitors. Overall, the maximal observed plating efficiency for SO25 (~5% in 0.3 μM AZD6738) was 10-fold less than that of the parental PC-9 cells (~50% in 0 μM ATR inhibitor). We conclude that the resistant clones appear to be partially dependent on the presence of ATR inhibitors as they have both a greater proliferation and plating efficiency in the presence of these inhibitors.

However, the PicoGreen cell proliferation assay demonstrated that the ATR inhibitor resistant cells grew similarly in the presence or absence of AZD6738, whereas the plating efficiency assay suggests that ATR inhibition is necessary for efficient cell plating and growth. This discrepancy is potentially due to differences in cell density at plating, with sparsely plated resistant cells more sensitive to the absence of ATR inhibitors in the medium, whereas denser cells seem to tolerate the lack of ATR inhibition better. Further work is required in order to confirm this relationship.

3.5 Clonogenic survival of ATR inhibitor resistant clones in the presence of increasing concentrations of AZD6738

Following the colony forming assay, we determined whether SO25 cells were able to form colonies of at least 50 cells after treatment with AZD6738 for 24 h in a standard clonogenic survival assay. While PC-9 cells formed clear, discernible colonies and responded in a dose-dependent manner to AZD6738, SO25 was unable to form clear colonies at low concentrations of AZD6738 (Figure 3.8). Although SO25 cells did not form distinct colonies, the cells

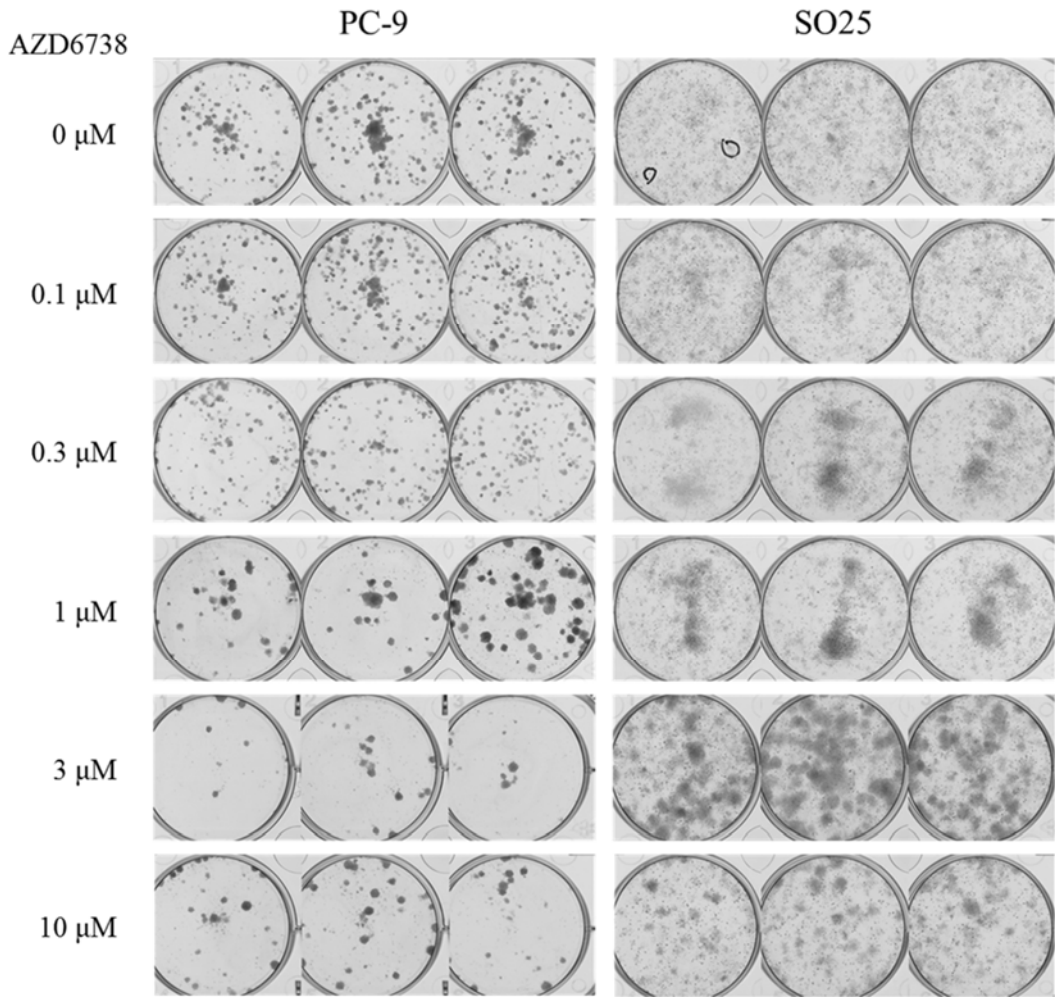


Figure 3.8: Clonogenic survival assay with increasing concentrations of AZD6738.

Cells were plated directly in AZD6738 for 24 h before the cells were washed and replaced with normal culture medium. Once colonies reached the size of at least 50 cells, plated were fixed and stained with CV. Images were taken with a Gelcount™ from a single experiment.

appeared to grow better after treatment with AZD6738 at 3 μM, with cell density decreased at both higher and lower concentrations.

3.6 Cross-resistance of ATR inhibitor resistance cells to other classes of DNA damage response modulators

To better understand the potential pathways involved in ATR resistance, we treated cells with different classes of DNA damage response (DDR) modulators. ATR inhibitor resistant cells were significantly ($p<0.0001$) more resistant to MK-1775, a selective WEE1 inhibitor (Figure 3.9d). PC-9 cells have an IC_{50} of 0.08 μM ± 0.01, compared to SO25 cells with an IC_{50} of 0.34 μM ± 0.12 (Table 3.4). WEE1 plays an important role in the G2/M checkpoint by inhibiting CDK1 and plays a role in regulating firing of DNA replication origins (Domínguez-Kelly *et al*, 2011). Notably, ATR inhibitor resistant cells were also significantly more resistant ($p<0.0001$) to AZD7762, a CHK1/2 inhibitor (Figure 3.9b). CHK1 is a crucial target of ATR, and the dose response curve had a similar profile to resistant cells treated with ATR inhibitors, with intermediate concentrations of AZD7762 stimulating proliferation of ATR inhibitor resistant cells. PC-9 and SO25 cells had relative cell viabilities at 0.123 μM AZD7762 of 25.37% ± 3.34 and 100.52% ± 5.57, respectively (Table 3.5).

Although the response was quite variable, compared to PC-9 cells, SO25 cells were significantly ($p<0.05$) more sensitive to MLN4924, a neddylation inhibitor that inhibits the Nedd8-activating enzyme (NAE) which has implications in cell cycle progression and prevention of re-initiation and replication of DNA (Figure 3.9e, Lin *et al*, 2010). Responses to AZD2281, a PARP inhibitor, NU7441, a DNA-PK inhibitor, and KU55933, an ATM inhibitor, were similar between PC-9 and SO25 cells (Figure 3.9a, c, f).

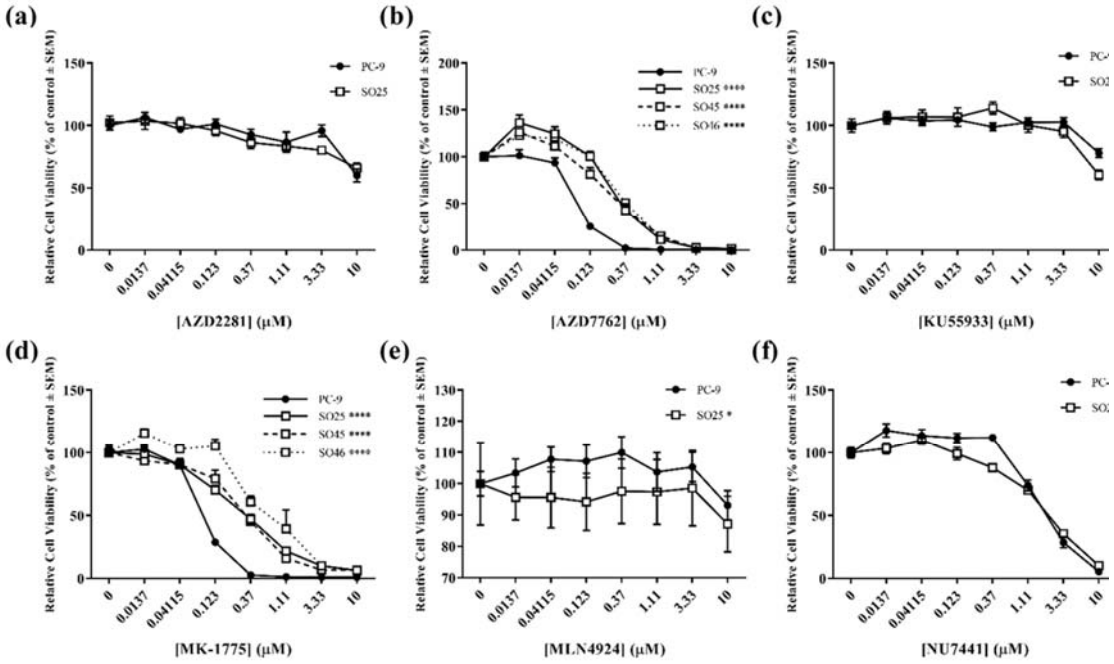


Figure 3.9: Responses of PC-9 and resistant clones to different classes of DNA damage response modulators.

PC-9 cells and ATR inhibitor resistant clones were incubated for 4 days with increasing concentrations of **(a)** AZD2281, **(b)** AZD7762, **(c)** KU55933, **(d)**, MK-1775, **(e)** MLN4924, and **(f)** NU7441. Relative cell viability was assessed using the resazurin proliferation assay, and normalised to DMSO treated controls. Each point represents the mean of three independent experiments, each performed in triplicate with error bars = SEM. Asterisks indicate statistical significance compared with the PC-9 cell line **** = $p<0.0001$ and * = $p<0.05$ (ANOVA).

Table 3.4: Sensitivity of PC-9 and resistant cells to MK-1775.

IC_{50} values are presented as a mean and SEM from three independent experiments, each performed in triplicate.

Cell Line	mean IC_{50} (μM ± SEM)
PC-9	0.08 ± 0.01
SO25	0.34 ± 0.12
SO45	0.32 ± 0.09
SO46	0.40 ± 0.10

Table 3.5: Sensitivity of PC-9 and ATR inhibitor resistant cells to AZD7762.

Values represent the mean and SEM from three independent experiments, each performed in triplicate.

Cell Line	Relative cell viability at 0.123 μM AZD7762 (% ± SEM)
PC-9	25.37 ± 3.34
SO25	100.52 ± 5.57
SO45	81.44 ± 7.41
SO46	100.52 ± 4.11

3.7 Sensitivity to standard cancer chemotherapies

Based on their proposed mechanism of action, ATR inhibitors are likely to be used in combination with chemotherapy and/or radiation therapy in the clinic. Therefore, we investigated whether ATR inhibitor resistant cells had altered sensitivity to common chemotherapies used in lung cancer. We found that ATR inhibitor resistant cells SO25, SO45, and SO46 were also resistant to single-agent gemcitabine, docetaxel, and cisplatin (Table 3.6). As gemcitabine and cisplatin target S-phase, and docetaxel acts in mitosis, this resistance may reflect the slower growth of the ATR inhibitor resistant cells. In combination with AZD6738, parental PC-9 cells and ATR inhibitor resistant cells were more sensitive to gemcitabine and cisplatin, compared with cells treated with chemotherapy alone. Although parental PC-9 cells were *less* sensitive to docetaxel when combined with AZD6738, the resistant cell lines were more sensitive in combination (Table 3.6).

PC-9 cells have an epidermal growth factor receptor (EGFR) activating mutation (E746_A750 in-frame deletion), and are sensitive to EGFR tyrosine kinase inhibitors such as gefitinib or erlotinib. To confirm that the resistant cells had indeed maintained this sensitivity we treated

Table 3.6: Sensitivity of PC-9 and ATR inhibitor resistant cells to chemotherapy agents alone and in combination with AZD6738.

Values from the resazurin assay represent IC50 and SEM from three independent experiments, each performed in triplicate.

Cell Line	Gemcitabine (nM)		Docetaxel (nM)		Cisplatin (μM)	
	DMSO	1 μM AZD6738	DMSO	1 μM AZD6738	DMSO	1 μM AZD6738
PC-9	3.05 ± 0.68	1.11 ± 0.20	0.01 ± 0.01	1.49 ± 1.22	0.39 ± 0.19	0.04 ± 0.02
SO25	15.77 ± 6.67	4.75 ± 0.73	1.63 ± 1.76	0.10 ± 0.06	2.64 ± 0.64	0.33 ± 0.14
SO45	10.94 ± 1.68	4.37 ± 1.04	0.07 ± 0.01	0.05 ± 0.04	1.43 ± 0.26	0.37 ± 0.11
SO46	31.42 ± 6.83	7.94 ± 1.03	0.20 ± 0.18	0.13 ± 0.11	3.23 ± 1.09	0.65 ± 0.22

the cells with increasing doses of gefitinib. SO25, SO45, and SO46 cells did not show any difference in response to gefitinib compared to PC-9 cells, and showed no interaction when treated in combination with AZD6738 (Figure 3.10).

3.8 TP53 mutation status of resistant clones

TP53 status is a major determinant of ATR sensitivity (Nghiem *et al*, 2001; Kaelin, 2005; Gabrielli *et al*, 2012) so we investigated whether resistant cells could have regained a G1 checkpoint due to reversion of TP53 mutation. We showed by Sanger sequencing that both parental PC-9 cells and ATR inhibitor resistant SO25 cells have a homozygous R248Q point mutation in exon 7 of the TP53 gene (Figure 3.11), and confirmed this by examining RNA-sequencing reads (Section 3.9, 100% of reads encoding an R248Q missense mutation), and furthermore, p21 expression, a downstream target of p53 and a mediator of p53-dependent cell cycle arrest, was not detectable by western blotting (data not shown).

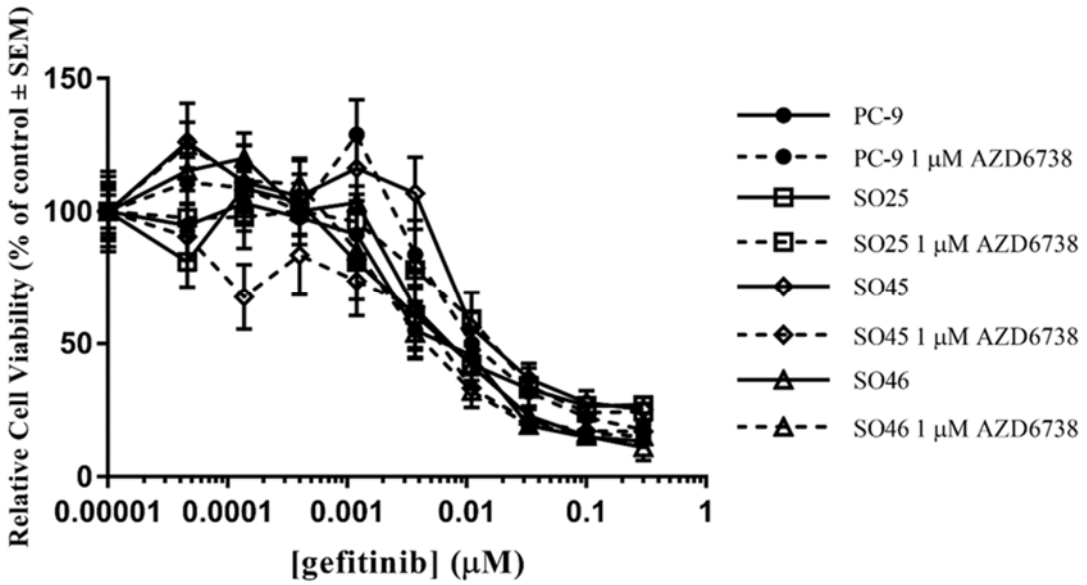


Figure 3.10: Sensitivity of PC-9 and ATR inhibitor resistant cells to increasing doses of gefitinib.

PC-9, SO25, SO45, and SO46 were treated with increasing doses of gefitinib in combination with either 0.01% DMSO or 1 μM AZD6738 for 4 days. Relative cell viability was assessed using the resazurin proliferation assay, and normalised to DMSO treated or AZD6738 treated controls. Each point represents the mean of three independent experiments, each performed in triplicate with error bars = SEM.

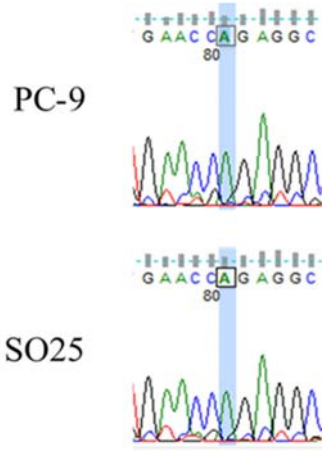


Figure 3.11: SO25 cells express mutant TP53.

DNA Sanger sequencing results demonstrating the presence of a homozygous R248Q G>A point mutation in exon 7 of the TP53 gene in PC-9 and SO25 cell lines. The blue-highlighting indicates the position of the mutation.

3.9 Key pathway analysis

RNA-sequencing analysis was carried out on 6 samples (Table 3.7), using the Illumina HiSeq 2000 platform. An average of 57605546 paired end reads were mapped per sample. There was no significant difference in gene expression within PC-9 samples or ATR inhibitor treated samples (Table 3.8). Biological replicates (#1, #2) showed no differences, nor did the presence of DMSO (#1, #3). Importantly, adding AZD6738 or VE-822 to SO25 cells did not affect gene expression (#4, #5 and #5, #6). Compared with parental PC-9, AZD6738 and VE-822 had significant changes in the expression of 5815 and 6055 genes, respectively. The top 200 differentially expressed genes are shown in Supplementary Table 1. The top 1000 genes with the most significant differences (based on Q value) in gene expression between PC9 (sample #1) and SO25 (sample #4) were entered into Metacore™ Key Pathway Advisor (Thomson Reuters; http://ipscience.thomsonreuters.com/product/metacore), a software package that interprets the consequences of expression changes defining which cellular processes are affected by the differentially expressed genes. Supplementary Table 2 shows the pathways identified, with key pathways affecting cell cycle and ATM/ATR regulation of the G1/S checkpoint featuring prominently. A KPA pathway map showing the cell cycle (Figure 3.12) indicates that mRNA expression from genes, including cyclins and CDK1, which encode proteins critically required for cell cycle progression are markedly downregulated in SO25 cells compared with parental PC-9 cells.

Table 3.7: Samples for RNA-sequencing.

Sample	Cell Line	Condition
#1	PC-9	complete medium
#2	PC-9	complete medium
#3	PC-9	plated continuously in 0.01% DMSO
#4	SO25	plated continuously in 0.01% DMSO
#5	SO25	plated continuously in 1 μM AZD6738
#6	SO25	plated continuously in 0.3 μM VE-822

Table 3.8: Comparisons of RNA-sequencing expression[1]

Comparison	Differentially expressed genes (n)
#1 vs #2	0
#1 vs #3	0
#1 vs #4	5815
#1 vs #6	6055
#4 vs #5	0
#4 vs #6	0
#5 vs #6	0

[1] Q value <0.05

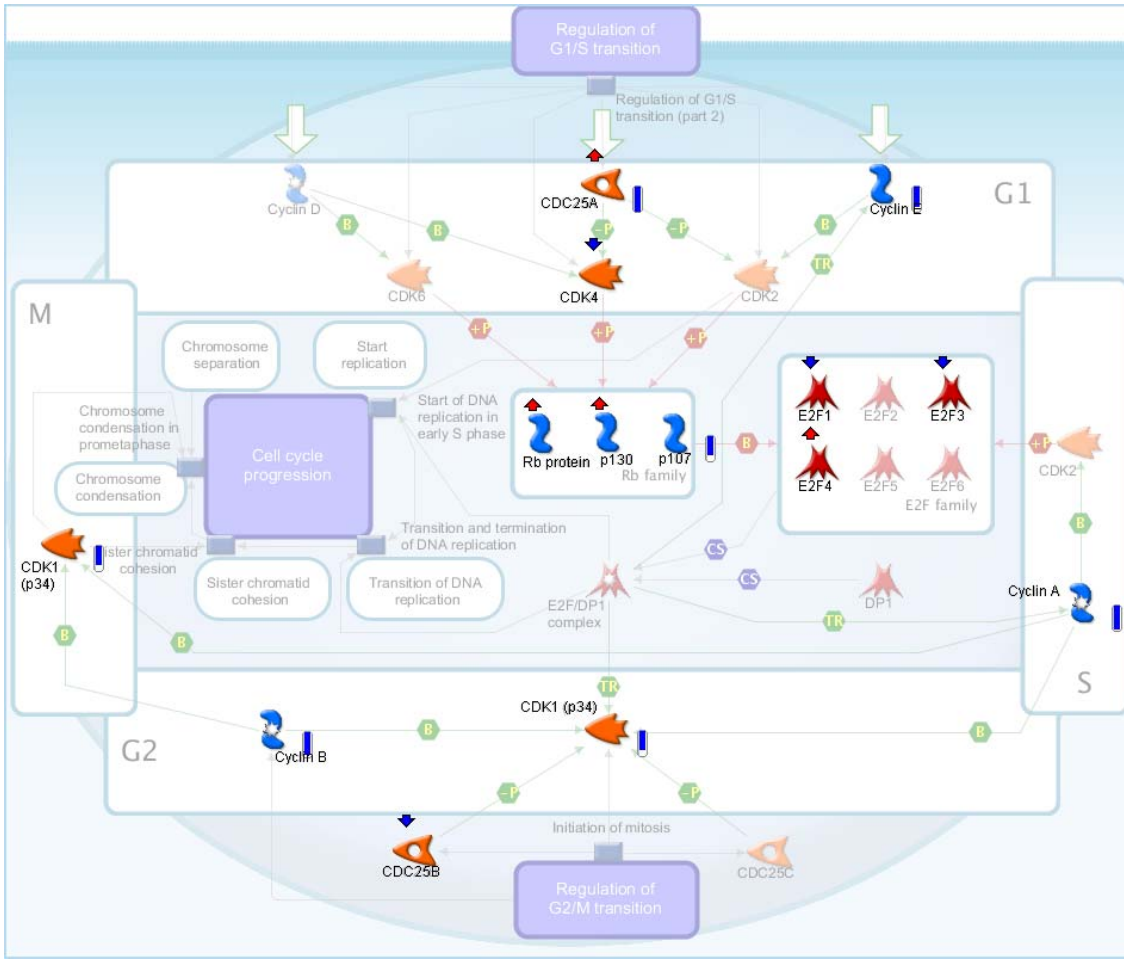


Figure 3.12: Schematic showing Key Pathway Analysis of differential expression of cell cycle regulated in ATR inhibitor resistant SO25 cells and parental PC-9 cells.

The pathway map was produced by inputting the top 1000 most statistically significant differentially expressed genes from RNA-sequencing data into Metacore KPA software. The highlighted proteins are differentially expressed. Blue bars next to proteins indicate that mRNA is down-regulated in SO25 compared with PC-9 cells. Red arrows indicate pathway activation, and blue arrows indicate pathway inhibition. A complete legend for the symbols in this schematic is shown in Supplementary Figure 1.

3.10 Key Findings

We generated independent resistant clones SO25, SO45, and SO46 from human PC-9 NSCLC cells that were resistant to ATR inhibitor AZD6738 and cross-resistant to chemically unrelated ATR inhibitors VE-821 and VE-822. Approximately 4.9 colonies arose per million cells plated, and the selected clones displayed similar phenotypes. Compared with the parental PC-9 cells, the resistant clones were large, irregularly shaped, and many cells had multiple nuclei and/or cytoplasmic vesicles. They were also slow growing, with a doubling time of nearly twice that of PC-9 cells. In addition, the resistance clones' growth was stimulated by the presence of intermediate concentrations of ATR and CHK1/2 inhibitors, and they were partially dependent on the presence of these inhibitors. SO25, SO45, and SO46 were partially resistant to cytotoxic chemotherapy and exhibited cross-resistance to CHK1/2 (AZD7762), and WEE1 (MK-1775), and were (in part) sensitive to neddylation (MLN4924) inhibitors, indicating a common mechanism of resistance associated with the cell cycle. RNA-sequencing data suggested a downregulated expression of critical genes, including cyclins and CDK1, associated with cell cycle progression in the resistant cells, which was consistent with the slower growth rate observed.

CHAPTER 4

4 Mechanism of ATR Resistance

4.1 Cell cycle analysis

As the resistant cells differ from parental PC-9 cells in doubling time, colony forming ability, and response to DDR modulators and chemotherapy agents, we compared their cell cycle profiles in order to determine if potential mechanisms of resistance could emerge from differences in cell cycle distribution. Cells were treated with 1 μM AZD6738 for 24 h before collecting for flow cytometry. An early S-phase arrest was apparent in PC-9 cells when treated with the ATR kinase inhibitor (Figure 4.1a). PC-9 cells have a homozygous p53 mutation and thus do not have a functioning G1 checkpoint, but, as cells empty from G1 but not G2, they do appear to have a functioning G2 checkpoint possibly activated by ATM in the absence of ATR (Murga *et al*, 2009; Dungrawala *et al*, 2015; Kwok *et al*, 2016). The resistant cells had a larger G2 population when compared to parental PC-9 cells without treatment, and there were slight differences in cell cycle profiles between the different resistant clones (Figure 4.1b). The resistant cells, however, do not exhibit an early S-phase arrest when treated with AZD6738. In particular, SO25 cells become more similar to untreated parental PC-9 cells, with lower G2/M and S and greater G0/G1 proportionate cell populations compared to their untreated counterparts. The resistant clones also had a greater aneuploid population in the absence of AZD6738 than in its presence (Figure 4.1c).

To confirm the differences between PC-9 cells and resistant clones in AZD6738-mediated cell cycle effects, BrdU pulse labelling was performed to follow the cell populations through the cell cycle. PC-9 and SO25 cells were pulse labelled with BrdU followed by treatment with 1 μM AZD6738 for 24 h. SO25 cells were also treated for 48 h post-BrdU labelling (data not

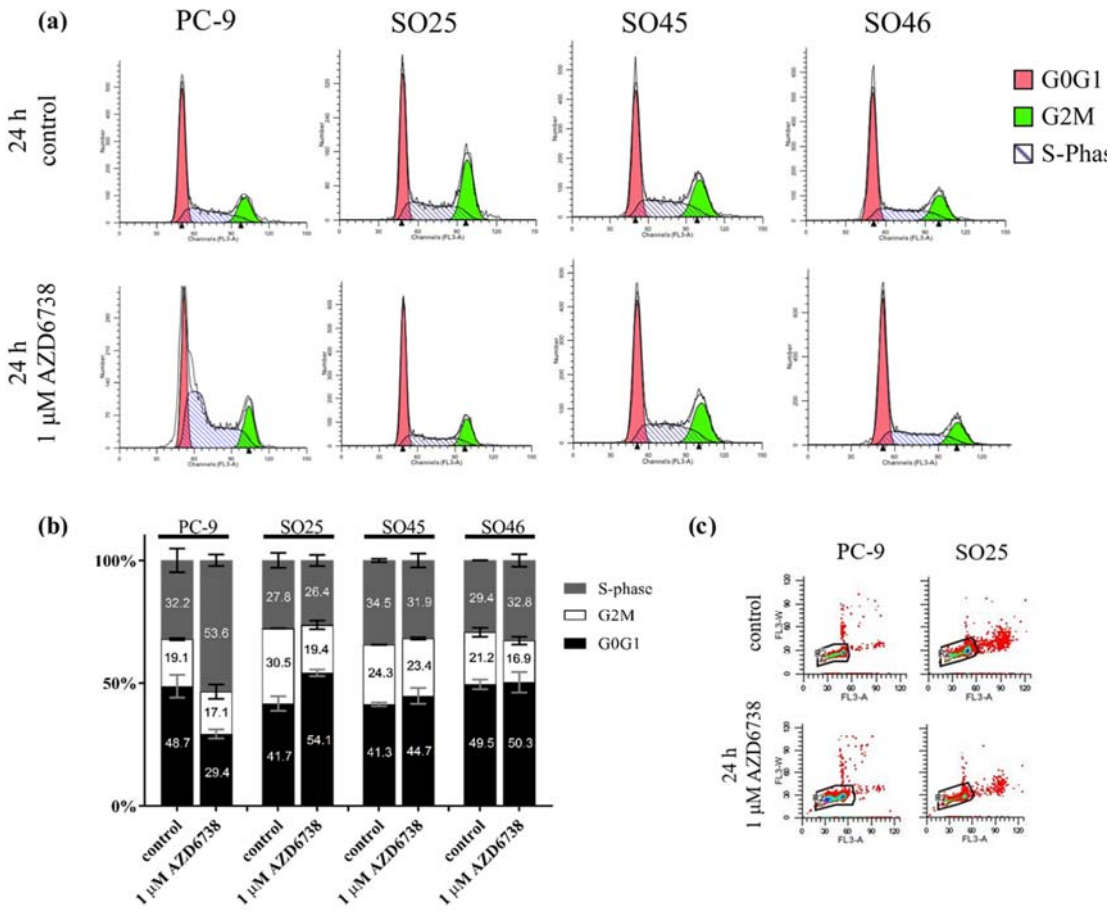


Figure 4.1: AZD6738 leads to early S-phase arrest in PC-9 cells.

PC-9, SO25, SO45, and SO46 cells were treated with 1 μM AZD6738 for 24 h before harvested for assessment of cell cycle distribution by propidium iodide staining and FACS analysis. **(a)** shows representative images of n = 3 (PC-9 and SO25) or n = 2 (SO45 and SO46) independent experiments. **(b)** shows quantification of G0/G1, S, and G2/M cell populations, calculated from the diploid cell population (with the exclusion of aneuploidy cells), and expressed as the average of n =3 (PC-9 and SO25) or n =2 (SO45 and SO46) experiments. Error bars represent SEM (PC-9 and SO25) or standard deviation (SO45 and SO46). **(c)** shows pulse area (FL3-A) vs. pulse width (FL3-W), with aneuploidy cells to the right of the gated population.

shown) as we expected these cells would take longer to progress from one S-phase to the next. Compared with the vehicle-treated controls, a distinct early S-phase sub-population of BrdU labelled cells was apparent in AZD6738 treated PC-9 cells, but not in AZD6738-treated SO25 cells (Figure 4.2), consistent with the early S-phase arrest suggested by the PI staining (Figure 4.1).

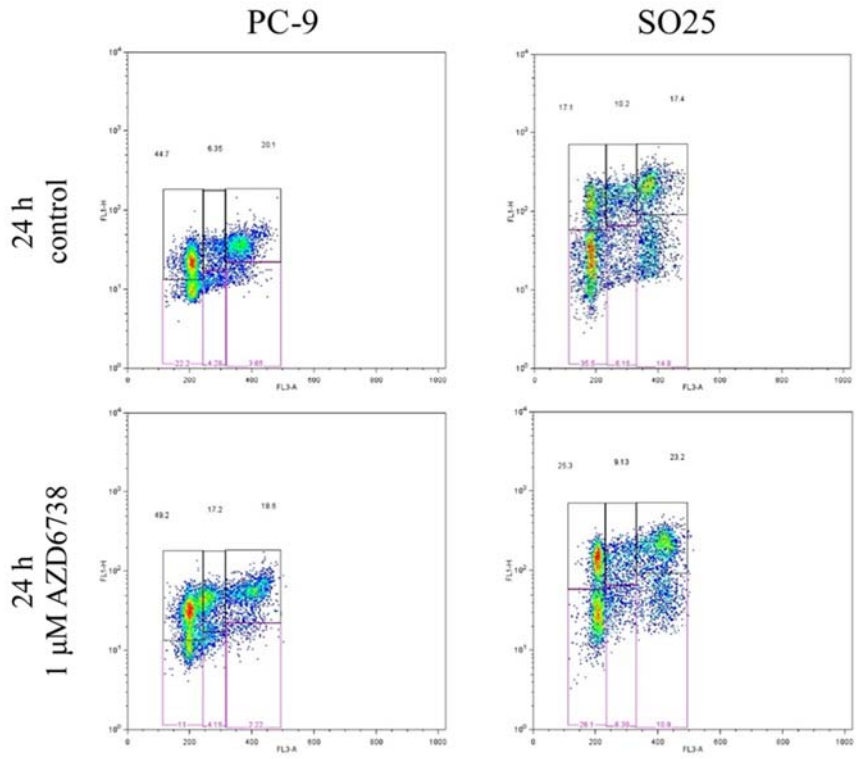


Figure 4.2: Treatment with AZD6738 for 24 h causes more S-phase incorporation of BrdU in SO25 cells.

PC-9 and SO25 cells were pulse labelled with BrdU for 20 mins before treatment with 1 μM AZD6738 or 0.01% DMSO (vehicle control) for 24 h Cells were then harvested, fixed, and stained with PI and anti-BrdU antibody for flow cytometry analysis. Diagrams are representative of three independent experiments. The gates represent BrdU-labelled cell populations (black) and non-BrdU-labelled cell populations (pink), and from left to right represent G1/early S-phase, intra-S-phase, and late S-/G2/M phase.

4.2 DNA fibre analysis

To more fully explore the S phase dynamics of these cells, we carried out DNA fibre analysis to examine DNA replication. This technique measures replicating DNA through the incorporation of halogenated base analogues that can be detected by immunofluorescence in order to calculate DNA synthesis tract lengths and replication fork speeds. PC-9 and SO25 cells were treated for 60 mins with 0.01% DMSO, 0.3 μM AZD6738, or 1 μM AZD6738 while SO45 and SO46 cells were only treated with 0.01% DMSO. The cells were sequentially labelled with 5-chlorodeoxyuridine (CldU) and then 5-iododeoxyuridine (IdU) for 20 mins each. After staining and imaging, the CldU tract lengths were measured.

With increasing AZD6738 concentration, PC-9 tract lengths became significantly shorter (Table 4.1 and Figure 4.3) indicating a decreased replication fork speed, which is consistent with the increased proportion of cells in S phase and the S-phase arrest seen in FACS analysis in response to ATR inhibitor treatment. SO25 cells had decreased CldU tract lengths with increasing AZD6738 concentration, but at each concentration, had longer mean tract lengths than PC-9 cells. At lower concentrations of ATR inhibitor, SO25 cells had a wider distribution of tract lengths compared to PC-9 cells, which had tract lengths clustered at the shorter end. Interestingly, the distribution of SO25 tract lengths at 1 μM AZD6738 was similar to that of PC-9 cells treated with DMSO. This is consistent with 'normalised' DNA replication speed at 1 μM AZD6738 and reflects the observation that certain concentrations of the ATR inhibitor improve the growth rate of SO25 cells. All three resistant clones had longer endogenous tract lengths when treated with DMSO than parental PC-9 cells. PC-9 had a mean tract length with DMSO of 4.83 ± 0.10 μm, while SO25, SO45, and SO46 resistant cells had mean tract lengths of 7.36 ± 0.21 μm, 6.66 ± 0.14 μm, and 9.27 ± 0.20 μm, respectively.

Table 4.1: Mean CldU fibre tract lengths in PC-9 and resistant cells.

PC-9, SO25, SO45, and SO46 cells were treated with the indicated concentration of AZD6738 or DMSO for 60 mins and subsequently labelled with CldU and IdU for 20 mins each. The fibres were then spread, labelled, and imaged, and CldU tract lengths were measured. Values represent the mean (μm) ± SD from two independent experiments, with a total of 229 – 400 fibres measured per condition.

Cell Lines	0.01% DMSO (μm)	0.3 μM AZD6738 (μm)	1 μM AZD6738 (μm)
PC-9	4.83 ± 0.10	2.86 ± 0.11	3.00 ± 0.09
SO25	7.36 ± 0.21	5.49 ± 0.14	5.13 ± 0.15
SO45	6.66 ± 0.14	-----	-----
SO46	9.27 ± 0.20	-----	-----

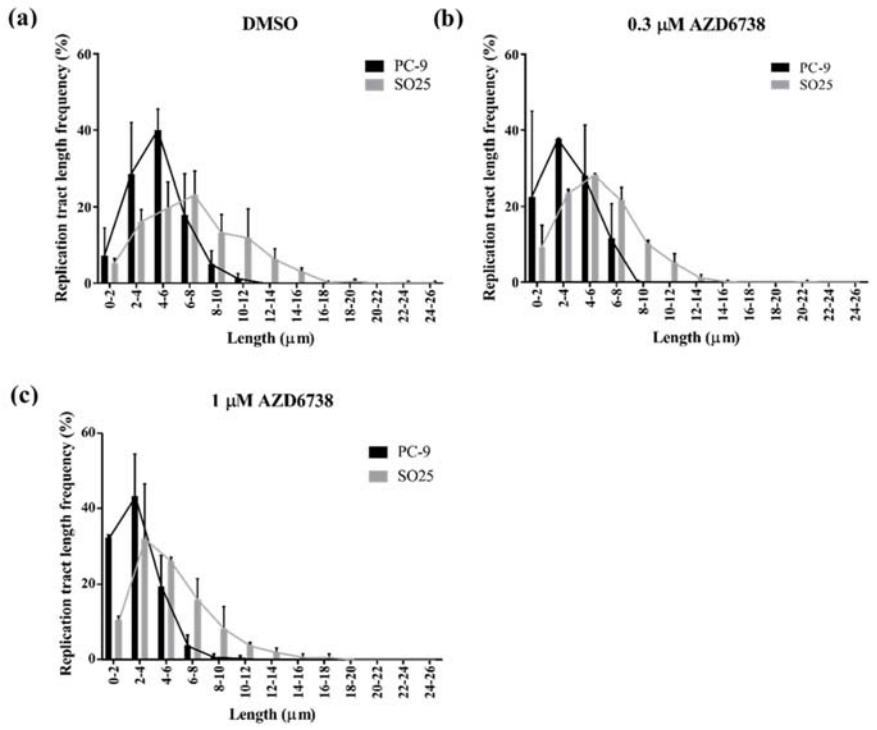


Figure 4.3: CldU tract length distribution in PC-9 and SO25 cells following treatment with AZD6738.

PC-9 and SO25 cells were treated with AZD6738 or DMSO for 60s mins and sequentially labelled with CldU and IdU for 20 mins each. The fibres were then spread, labelled, and imaged, and CldU tract lengths were measured. Values represent the mean of the percentage of fibres of each length taken from two independent experiments, with a total of 229 – 400 fibres measured per condition, and error bars = SEM.

4.3 Analysis of RPA32 and γH2AX

Due to the differences in tract length and replication fork speed between the parental PC-9 cells and the resistant clones, we investigated the levels of replication stress present in the presence and absence of AZD6738 by measuring RPA nuclear foci. Replication protein A (RPA) binds to single-stranded DNA and is considered a marker of replication stress (Zeman & Cimprich, 2014). The average number of RPA32 foci/cell was determined in cells treated with either 1 μM AZD6738 or DMSO (vehicle control). The ATR inhibitor resistant cell lines had higher levels of RPA32 foci/cell compared to untreated PC-9 cells, indicating higher levels of endogenous replication stress (Figure 4.4a). Upon treatment with 1 μM AZD6738, PC-9 cells

had a greater than two-fold increase in RPA32 foci/cell, whereas the levels of RPA foci in the ATR resistant cells were unaffected (Figure 4.4a, b), suggesting that replication stress is only increased upon treatment with AZD6738 in the parental PC-9 cells.

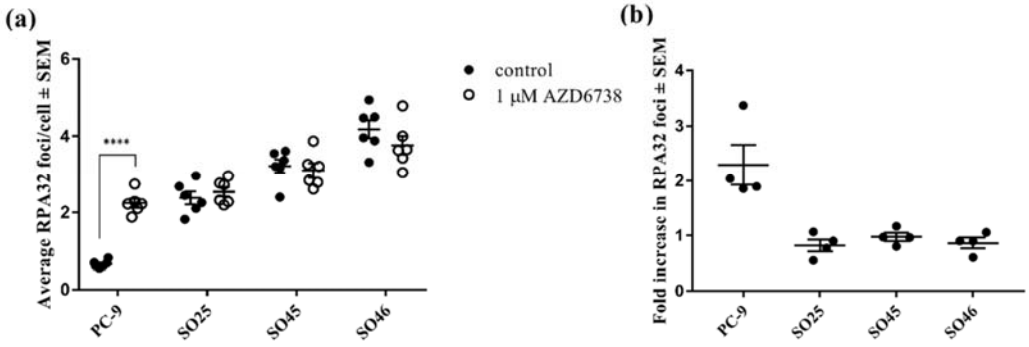


Figure 4.4: Average RPA32 per cell foci upon treatment with AZD6738.

PC-9, SO25, SO45, and SO46 cells were treated with either 0.01% DMSO or 1 μM AZD6738 for 24 h before fixing and staining for RPA32. RPA32 foci were quantified using the IN Cell Analyzer 1000 Cellular Imaging and Analysis System, and average RPA foci/cell in treated and control treated cells was calculated. **(a)** Representative data containing 6 replicate values from one of four independent experiments. Means with SEM are shown; **** = $p<0.0001$. **(b)** Fold increase in average RPA32 foci/cell in treated versus control treated cells. Values are shown from each of four independent experiments, each with 3 – 6 replicates. Error bars = SEM.

We also looked at levels of γH2AX foci/cell, (an indirect indicator of DNA double strand breaks) in cells treated with either 1 μM AZD6738 or DMSO (vehicle control). There was little difference in γH2AX foci/cell in parental PC-9 cells regardless of treatment, although in ATR resistant cells there was a trend towards lower levels of γH2AX foci following treatment with AZD6738, which reached statistical significance only in SO25 cells (Figure 4.5a). However, when looking at percentage of cells exhibiting pan-nuclear γH2AX, another potential marker of DNA replication stress (Toledo *et al*, 2011), there was a significant increase in PC-9 cells upon treatment with 1 μM AZD6738, while the resistant cells exhibited a significant decrease (Figure 4.5b). We had also stained for 53BP1, regarded as a more specific marker of DNA damage response than γH2AX, but the staining was not very effective. However, we were able to show that in cases where we were able to detect the staining, 53BP1 foci co-localised with

γH2AX foci (Figure 4.6). There were also instances where γH2AX foci were visible, but we were unable to detect clear 53BP1 foci.

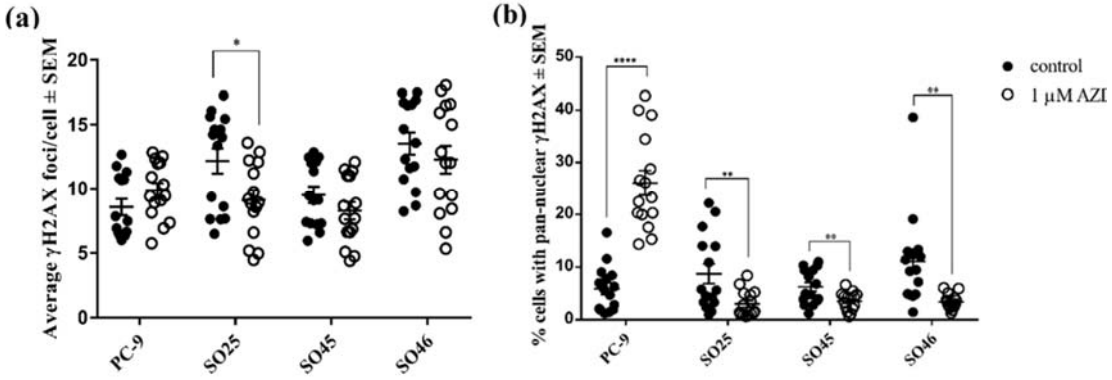


Figure 4.5: Average γH2AX foci per cell and pan-nuclear γH2AX upon treatment with AZD6738.

PC-9, SO25, SO45, and SO46 cells were treated with either 0.01% DMSO or 1 μM AZD6738 for 24 h before fixing and staining for γH2AX. **(a)** γH2AX foci were quantified using the IN Cell Analyzer 1000 Cellular Imaging and Analysis System, and average γH2AX foci/cell in treated and control treated cells was calculated. Values are shown from each of four independent experiments, each with 3 – 6 replicates. Error bars = SEM; * = $p<0.05$. **(b)** The percent of cells positive for pan-nuclear γH2AX was determined with the IN Cell Analyzer. Values are shown from each of four independent experiments, each with 3 – 6 replicates. Asterisks indicate the level of significance with ** = $p<0.01$ and **** = $p<0.0001$.

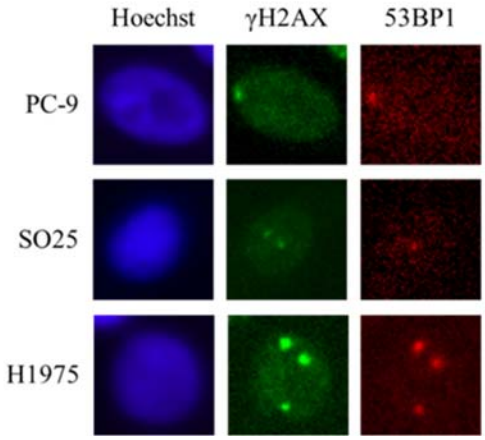


Figure 4.6: Co-localisation of 53BP1 and γH2AX foci.

Cells were stained with Hoechst, γH2AX, and 53BP1 and imaged on a TE2000-E Eclipse Nikon microscope at 100x magnification.

4.4 Effect of endogenous replication stress on sensitivity to ATR inhibitors

To determine if the effects of replication stress on sensitivity to ATR inhibitors are specific to PC-9 cells, we investigated a number of lung derived human cell lines with a range of known IC_{50} values for AZD6738, with PC-9 the most sensitive and A549 as the least sensitive (Table 4.2).

Table 4.2: Sensitivity of various cell lines to AZD6738.
Data taken from Weber, 2015.

Cell Line	Histological subtype	p53 expression status	AZD6738 IC_{50} [μM] (Mean ± SEM, range)
A549	Adenocarcinoma	Wild-type	5.2 (5.0-5.5)
H1975	Adenocarcinoma	Homozygous mutant	2.2 (2.1-2.4)
NBE1	Bronchial epithelium	Wild-type	1.4 (1.2-1.5)
Calu-6	Anaplastic carcinoma	Null	0.7 (0.64-0.72)
PC-9	Adenocarcinoma	Homozygous mutant	0.5 (0.5-0.52)

We used FACS to investigate the cell cycle distribution of these cell lines in response to treatment with AZD6738. Cells were treated with 1 μM AZD6738 for 24 h before collecting for flow cytometry. None of the NSCLC cell lines exhibited the marked early S-phase arrest that was observed in PC-9 cells (compare Figure 4.1 and Figure 4.7). In addition, the non-tumour NBE1 cells did not appear to have a substantial change in cell cycle distribution upon treatment with AZD6738.

There was no correlation observed between pre-treatment or AZD6738 treatment induced replication stress (as measured by fold increase in average RPA32 foci/cell upon treatment with

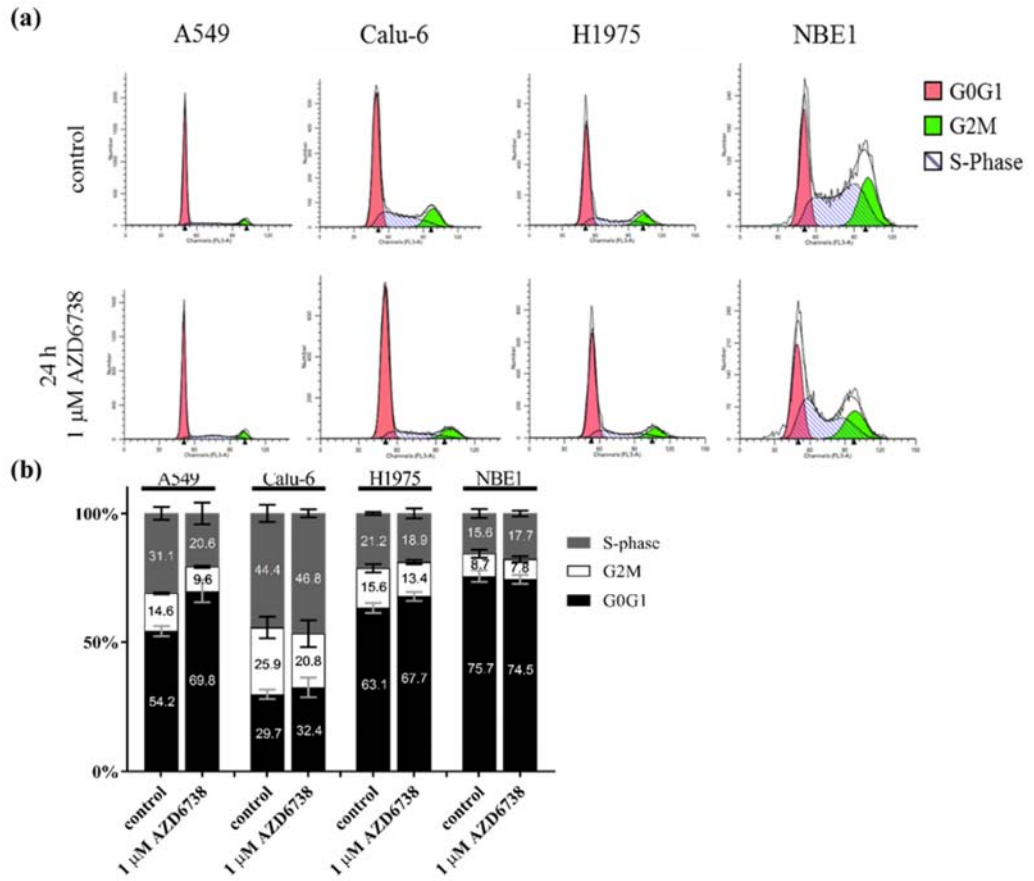


Figure 4.7: A549, Calu-6, H1975, and NBE1 lack an early S-phase arrest following treatment with AZD6738.

A549, Calu-6, H1975, and NBE1 cells were treated with 1 μM AZD6738 for 24 h before harvested for assessment of cell cycle distribution by PI staining and FACS analysis. **(a)** shows representative images of n = 3 independent experiments. **(b)** shows quantification of G0/G1, S, and G2/M cell populations, calculated from the diploid cell population (with the exclusion of aneuploid cells), and expressed as the average of n =3. Error bars represent SEM.

AZD6738) and sensitivity to AZD6738 (data not shown). Nor was there a correlation with γH2AX foci/cell (Figure 4.8a). However, while the pre-treatment levels of pan-nuclear γH2AX pre-treatment did not appear to be a good predictor of sensitivity to AZD6738 (Figure 4.8b), the increase in the proportion of cells with pan-nuclear γH2AX after treatment appeared to be a potential biomarker for sensitivity to the effects of ATR inhibition in these cell lines (Figure 4.8c).

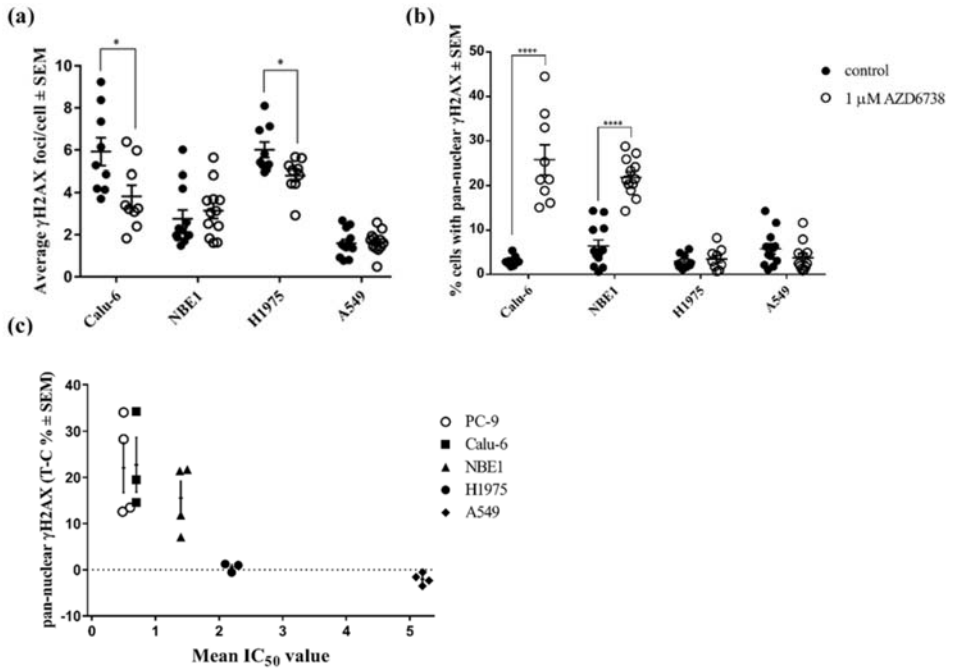


Figure 4.8: Increase in pan-nuclear γH2AX, but not in γH2AX foci, upon treatment with AZD6738 correlates with sensitivity.

Calu-6, NBE1, H1975, and A549 cells were treated with either 0.01% DMSO or 1 μM AZD6738 for 24 h before fixing and staining for γH2AX. **(a)** γH2AX foci were quantified using the IN Cell Analyzer 1000 Cellular Imaging and Analysis System, and average γH2AX foci/cell in treated and control treated cells was calculated. **(b)** The percent of cells positive for pan-nuclear γH2AX was determined with the IN Cell Analyzer. **(c)** The percentage induction of pan-nuclear γH2AX in treated minus control (T-C) cells versus mean IC_{50} value for AZD6738. Cells are listed left to right in order of decreasing sensitivity to AZD6738. Values are shown from each of n = 4 (PC-9, NBE1 and A549) or n = 3 (Calu-6 and H1975) independent experiments, each with 3 - 6 replicates. Error bars = SEM. Asterisks indicate the level of significance with * = $p<0.05$ and **** = $p<0.0001$.

4.5 Further pathway analysis

To further investigate the differential responses to ATR inhibitor treatment in PC-9 and the resistance clones, we carried out western blot analyses. We focused on the ATM and ATR signalling pathways, and cell cycle pathways as a result of the differences in FACS results, growth rate, and replication rate.

There was little difference between PC-9 and resistant cells in regards to ATR signalling (Figure 4.9). As a positive control, PC-9 cells were treated with 50 nM gemcitabine for 24 h in order to induce replication stress and early S-phase arrest. There was activation of downstream

pCHK1 S317 and S345 as expected, although S296 was not detected under these conditions. Following treatment with AZD6738 there was a clear decrease in pCHK1 S317 levels in ATR inhibitor resistant cells compared to controls, indicating that AZD6738 was inhibiting ATR kinase activity in these cells. Similar reductions in pCHK1 S345 were also noted, although the expression levels were low. Surprisingly, PC-9 cells had a marginal up-regulation of pCHK1 S317 when treated for 24 h with AZD6738, suggesting that other PIKK family members (ATM, DNA-PK) may phosphorylate CHK1 under conditions of prolonged replication stress. pCHK296 could only be detected in one cell line (SO45), and expression was not altered by treatment with AZD6738 (Figure 4.9).

Treatment of PC-9 cells with 50 nM gemcitabine activated ATM downstream signalling (Figure 4.10). Notably, ATM signalling (pATM, pKAP1, pCHK2, γH2AX) was strongly activated in PC-9 cells treated with 1 μM AZD6738 for 24 h, while this pathway was not activated in the ATR inhibitor treated resistant cells. Rather, SO25, SO45, and SO46 cells had only baseline levels of pATM, and did not activate downstream pKAP1 S824, pCHK2 T68 or γH2AX S139. This activation of the ATM pathway upon treatment with ATR inhibitor suggests that PC-9 is responding to prolonged DNA replication stress through ATM signalling, and the activation of downstream pCHK2 is consistent with the S-phase arrest through CDK2, as was observed with FACS analysis. The increase in γH2AX in PC-9 treated with AZD6738 by western blotting is consistent with what was observed in the IN Cell Analyzer by immunofluorescence.

Due to the clear differences in cell cycle kinetics between the PC-9 and resistant cells, we then investigated proteins involved in the regulation of the cell cycle. As a control, PC-9 cells were treated with gemcitabine (an inhibitor of DNA synthesis known to induce S-phase arrest) and showed decreases in CDT1 (a DNA replication licensing factor) and phospho-histone H3

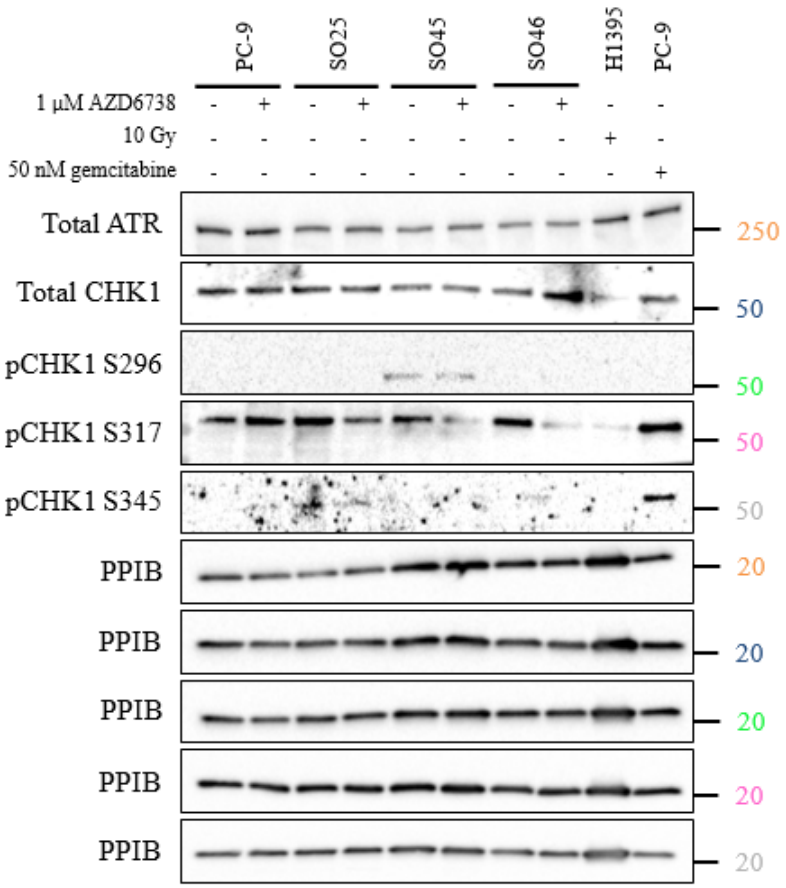


Figure 4.9: ATR signalling in PC-9 and resistant cells.

PC-9, SO25, SO45, and SO46 cells were treated with either 0.01% DMSO or 1 µM AZD6738 for 24 h before lysates were collected. H1395 were irradiated (10 Gy) followed by a 60 min incubation at 37 °C and PC-9 treated with 50 nM gemcitabine for 24 h served as controls for lack of ATM signalling and replication stress, respectively. Protein levels were assessed by western blot analysis. PPIB loading are colour-coded to match their respective protein.

(pHH3, a marker of mitosis) and an upregulation of geminin (a negative regulator of CDT1) and CDK1/2 Y15 (the inhibitory phosphate added by WEE1 kinase) when compared with PC-9 cells treated with DMSO (Figure 4.11). There were no clear AZD6738 treatment-related changes in levels of CDC25C, geminin, RPA32 or phospho-histone H3, although levels of RPA32 were higher in the resistant clones compared with parental PC-9 cells. In addition, levels of phospho-histone H3 were lower than in PC-9 for two of the resistant clones (SO45, SO46), but not for SO25. In all cells there was an up-regulation of CDT1 in response to 24 h

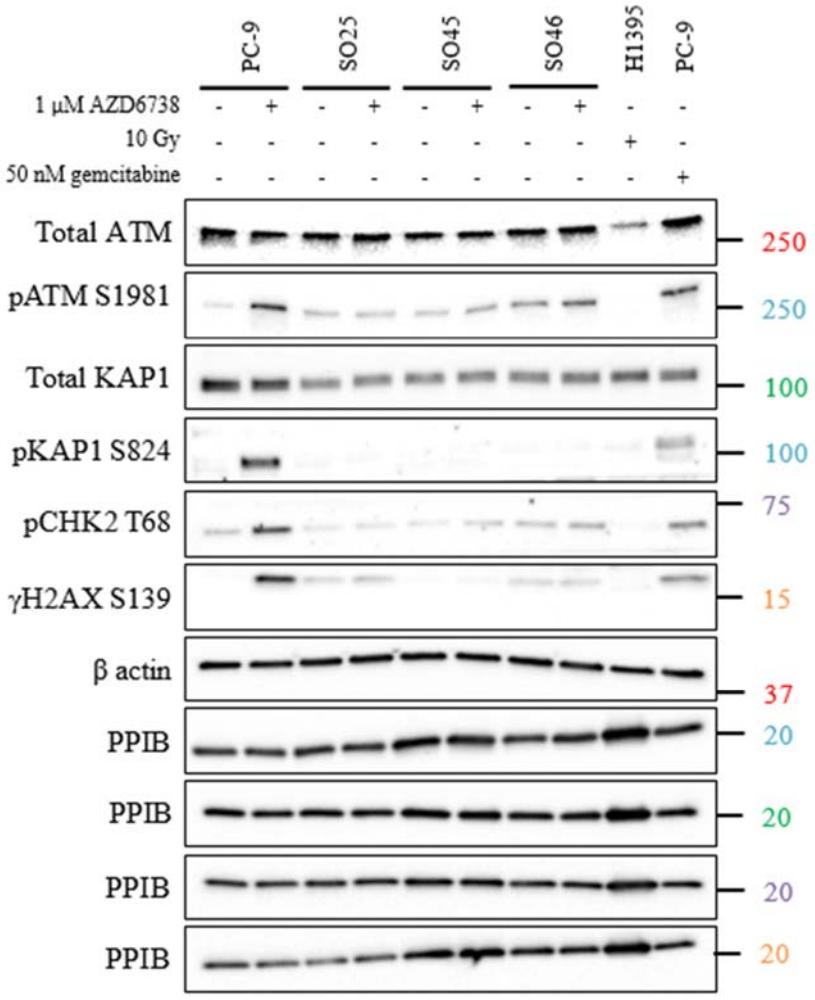


Figure 4.10: ATM signalling is activated in PC-9 cells, but not resistant cells, in response to ATR inhibition.

PC-9, SO25, SO45, and SO46 cells were treated with either 0.01% DMSO or 1 μM AZD6738 for 24 h before lysates were collected. H1395 cells were irradiated (10 Gy) followed by a 60 min incubation at 37 °C and PC-9 treated with 50 nM gemcitabine for 24 h served as controls for lack of ATM signalling and replication stress, respectively. H1395, a human NSCLC adenocarcinoma cell line with a homozygous p.T2666A mutation in ATM, showed decreased total ATM and a lack of pATM S1981 and acted as a control. Protein levels were assessed by western blot analysis. Loading controls β actin and PPIB are colour-coded to match their respective protein.

treatment with 1 μM AZD6738. Levels of CDC25A decreased in PC-9 cells treated with the ATR inhibitor, but remained unchanged in the resistant clones. This is consistent with increased levels of pCHK2 in treated PC-9 cells, as pCHK2 promotes CDC25A degradation (Figure 4.10). There was also a small increase in cyclin D1 levels in the resistant cells upon treatment,

which may be reflect a greater proportion of cells in G1 as shown in the FACS analysis. However, most notable were the differences in cyclin A2 and E1 levels (involved in G2/M and G1/S transitions, respectively) between PC-9 and resistant cells. Both cyclin A2 and E1 were decreased in the resistant cells compared to the parental PC-9 cells. Relative cyclin A2 and E1 levels in DMSO treated SO25 cells were 0.37 and 0.16, respectively, compared with DMSO treated PC-9 cells (which were normalised to 1.0), which was of interest since these proteins were highlighted as differentially regulated in the cell cycle pathway in the RNA-sequencing analysis (see Section 3.9).

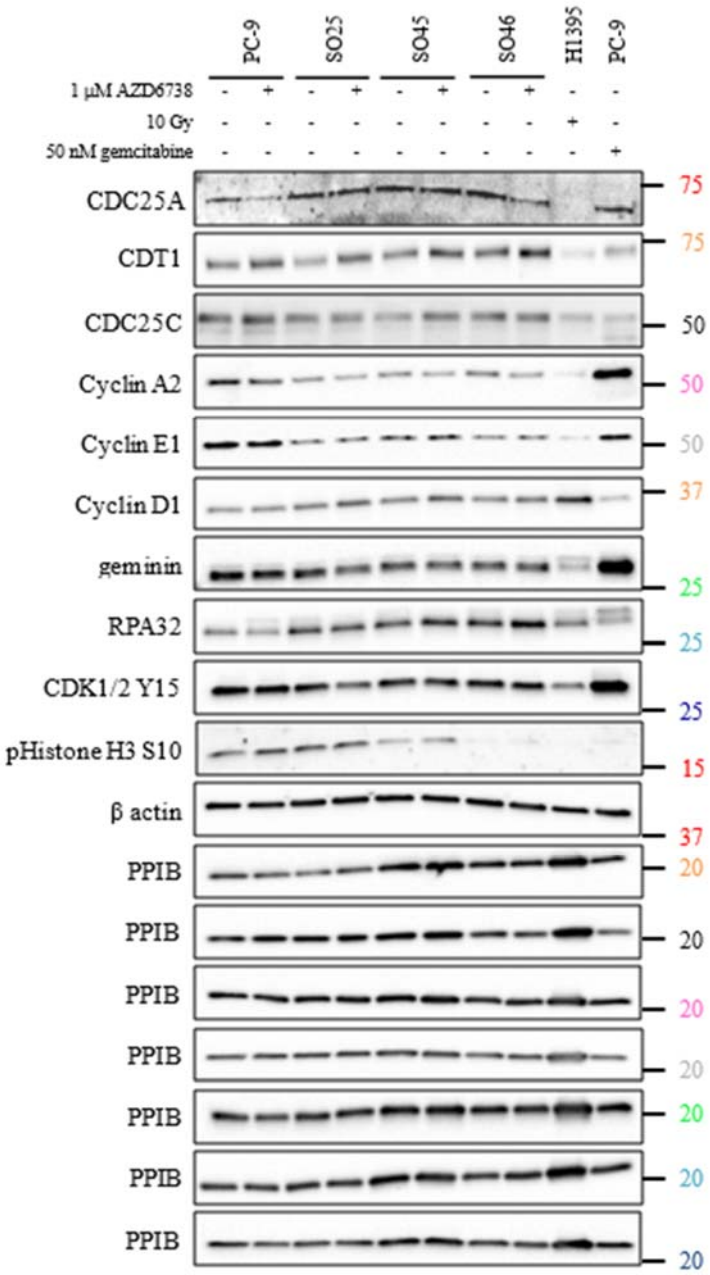


Figure 4.11: Resistant clones have lower levels of cyclin A2 and E1.

PC-9, SO25, SO45, and SO46 cells were treated with either 0.01% DMSO or 1 μM AZD6738 for 24 h before lysates were collected. H1395 irradiated with 10 Gy followed by a 60 min incubation at 37 °C and PC-9 treated with 50 nM gemcitabine for 24 h served as controls for lack of ATM signalling and replication stress, respectively. Protein levels were assessed by western blot analysis. Loading controls β actin and PPIB are colour-coded to match their respective protein.

4.6 Confirmation of cyclin A2 and E1 levels with RNA-sequencing

RNA-sequencing data demonstrated that the resistant cells do indeed have lower levels of cyclin A2 and cyclin E1 transcripts than parental PC-9 cells (Figure 4.12). Fragments Per Kilobase of transcript per Million mapped reads (FPKM) values showed that SO25 cells treated with DMSO had significantly lower levels of both cyclins compared to PC-9 cells treated with DMSO. The mean FPKM value for CCNA2 in PC-9 was 122.33 ± 0.60, while SO25 had a value of 55.97 ± 0.09. For CCNE1, PC-9 had a mean value of 26.66 ± 0.40 and SO25 cells had a mean value of 16.69 ± 0.03. These data reflected the changes in transcript levels and point to these lower cyclin A2 and E1 levels as potential mechanism of resistance to ATR inhibitors.

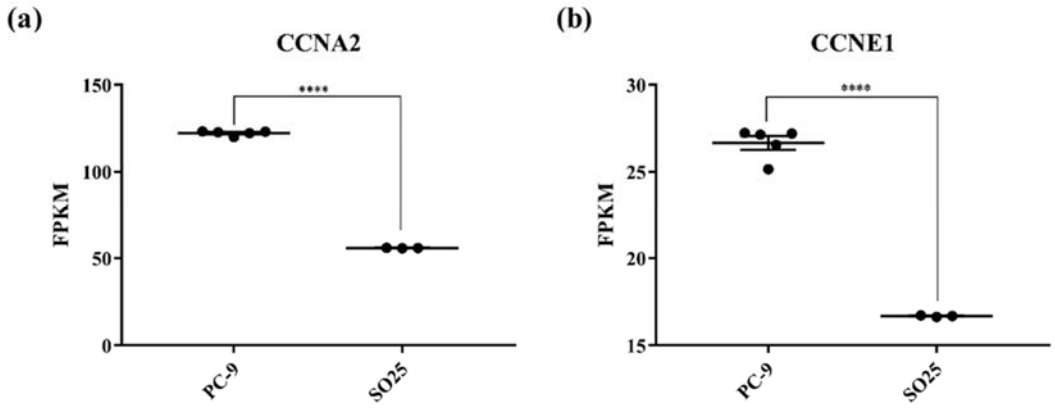


Figure 4.12: RNA-sequencing confirms significantly lower levels of cyclins A2 and E1 in SO25 cells compared to parental PC-9.

PC-9 and SO25 cells treated with 0.01% DMSO are compared by RNA-sequencing analysis. Data points represent 5 (PC-9) or 3 (SO25) Fragments Per Kilobase of transcript per Million mapped reads (FPKM) values, showing mean and SEM. **** = $p<0.0001$.

4.7 Effect of knockdown of cyclins A2 and E1

As there was a difference in cyclins A2 and E1 expression between the parental and resistant cells, we investigated whether this could in part explain the ATR inhibitor-resistance phenotype we observed. We used siRNAs to knockdown cyclin A2 (CCNA2) alone, cyclin E1 (CCNE1) alone, and both cyclins A2 and E1. Cells were also treated with non-target siRNA, transfection

reagent alone, or untreated as controls. Cyclin A2 protein levels were markedly reduced at both 24 h (0.02 relative to 1.0 normalised untreated control) and 102 h (0.18 relative to 1.0 normalised untreated control) post-CCNA2 siRNA transfection, as expected, but cyclin E1 protein levels were not reduced by treatment with CCNE1 siRNA (1.15 and 0.71 relative to 1.0 normalised untreated control at 24 and 102 h, respectively) (Figure 4.13). Treatment with cyclin A2 siRNA led to lower levels of cyclin E1 protein, which may reflect underlying changes in cell cycle distribution following CCNA2 siRNA treatment. Increased pATM S1981 levels

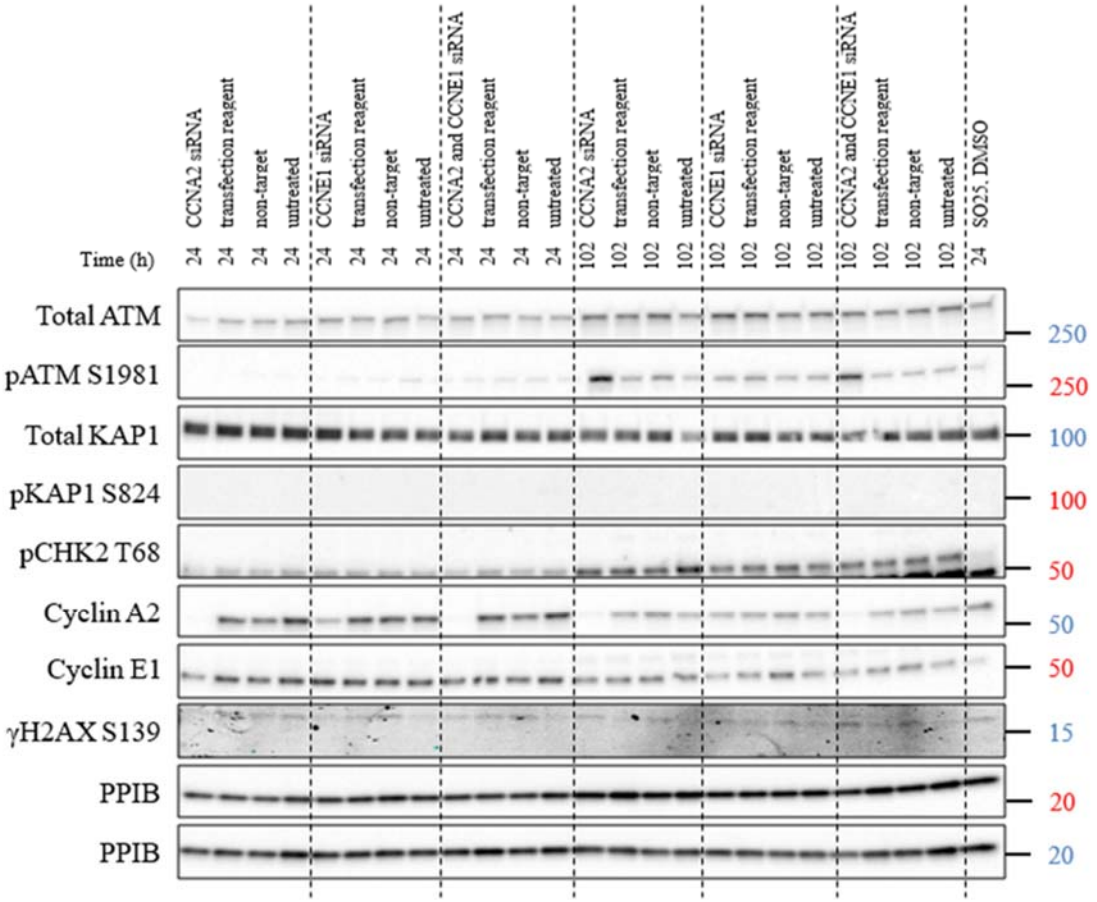


Figure 4.13: Cyclin A2, but not cyclin E1 showed sufficient knockdown with siRNA.

PC-9 cells were transfected with 25 nM CCNA2 (cyclin A2), CCNE1 (cyclin E1), or both siRNAs. Control samples were treated with non-target siRNA, transfection reagent only, or left untreated. Lysates were collected 24 and 102 h post-transfection. SO25 cells treated with DMSO for 24 h is shown for comparison. Protein levels were assessed by western blot analysis. PPIB loading controls are colour-coded to match their respective proteins.

were seen 102 h after transfection with CCNA2 siRNA, but there was no phosphorylation of downstream KAP1 (S824). Increased levels of pATM without phosphorylation of KAP1 was also seen in the ATR-inhibitor resistant clones, perhaps indicating that the cells were responding to stress. Levels of pCHK2 T68 and γH2AX S139 were unchanged in siRNA treated PC-9 cells and controls.

To investigate if treatment with siRNAs to cyclin A2 and E1 conferred resistance to ATR inhibitors, PC-9 cells were incubated with AZD6738, starting 6 h post-transfection until 102 h post-transfection (4 days). The control cells for each condition all exhibited the typical dose response seen previously with PC-9 cells in response to AZD6738 (see Figure 4.14), while those treated with cyclin A2 or E1 siRNAs were significantly more resistant to AZD6738 than the controls, and showed a dose response profile typical of the ATR-inhibitor resistant clones (Figure 4.14). The percent relative cell viability of the control cells at 1.11 μM AZD6738 was similar to that seen previously in untreated PC-9 cells (8.15 % ± 0.94, Table 3.1), while the relative viability was significantly higher in cells treated with cyclin A2 or E1 siRNA (Table 4.3). PC-9 cells treated with CCNA2 siRNA had an increased relative viability at 1.11 μM of 52.58 % ± 12.87, while cells treated with both CCNA2 and CCNE1 siRNA had the highest relative viability of 78.75 % ± 6.22. The relative viability of cells treated with CCNE1 siRNA also increased, but to a lesser extent.

Interestingly, cells treated with CCNA2 siRNA and both CCNA2 and CCNE1 siRNA had a phenotype at 102 h post-transfection that resembled the resistant cells (see Figure 3.2; Figure 4.15). The cells were larger and more spread out than the rounded PC-9 cells treated with non-target siRNA or transfection reagent alone. The cells also contained multiple vesicles with occasional multinucleate cells similar to SO25, SO45, and SO46 ATR-inhibitor resistant cells.

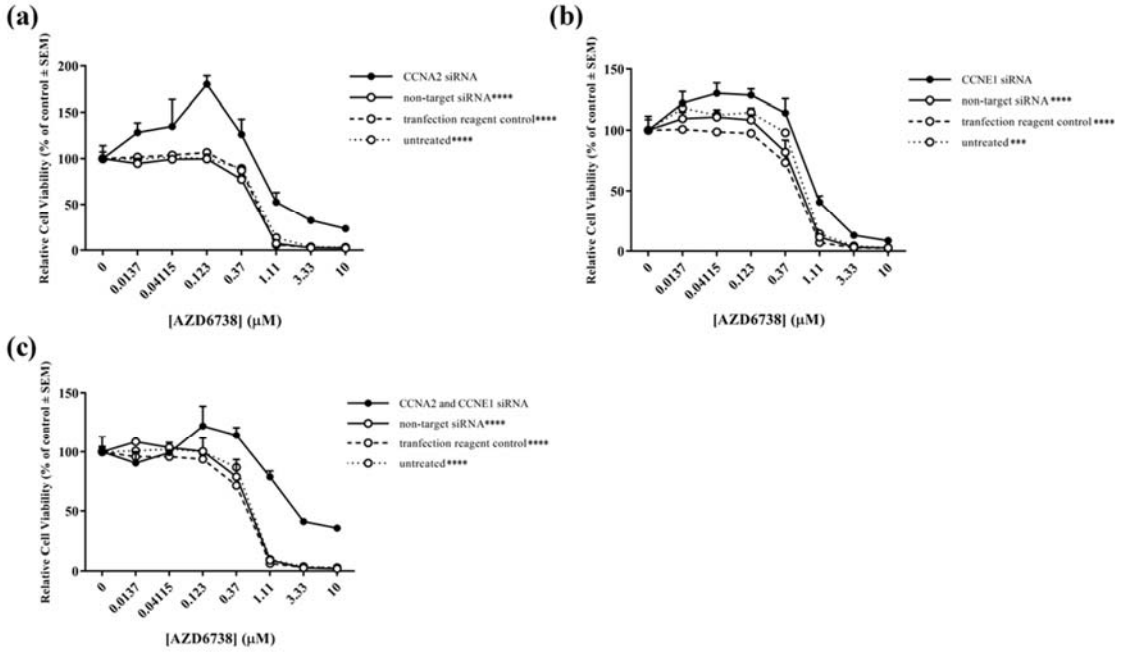


Figure 4.14: Cyclin A2 and E1 knockdown in PC-9 cells confers resistance to AZD6738 treatment.

PC-9 cells were treated with 25 nM siRNA for **(a)** CCNA2, **(b)** CCNE1, or **(c)** both. Control cells were treated with non-target siRNA, transfection reagent only, or untreated. Media was changed 6 h post-transfection, and 24 h post-transfection, cells were incubated for 4 days with AZD6738 (0-10 μM). Relative cell viability was assessed using the resazurin proliferation assay 102 h post-transfection, and normalised to DMSO treated controls. Each point represents the mean n = 1 experiments performed in triplicate with error bars = SEM. All asterisks indicate significance compared with the siRNA-treated cells when compared by two-way ANOVA. **** = $p<0.0001$ and *** = $p<0.001$.

Table 4.3: PC-9 cells treated with cyclin A2 and/or E1 have increased relative cell viability at 1.11 µM AZD6738.

PC-9 cells were treated with 25 nM siRNA for CCNA2, CCNE1, or both. Controls were treated with non-target siRNA, transfection reagent only, or untreated. Media was changed 6 h post-transfection, and 24 h post-transfection, cells were incubated for 4 days with ATR inhibitor (0-10 µM). Relative cell viability was assessed using the resazurin proliferation assay 102 h post-transfection, and normalised to DMSO treated controls. Values represent relative cell viability (% of control ± SEM) at 1.11 µM concentration AZD6738 (n = 1 experiments done in triplicate). * indicates $p<0.05$, ** indicates $p<0.01$, and *** indicates $p<0.001$ compared with non-target siRNA (t-test).

	Cell Viability in 1.11 µM AZD6738 (% DMSO ± SEM)	
	Cyclin siRNA	**non-target siRNA**
A2	52.58 ± 12.87 *	7.34 ± 1.14
E1	40.64 ± 6.39 **	11.54 ± 1.41
A2 and E1	78.75 ± 6.22 ***	9.17 ± 1.46

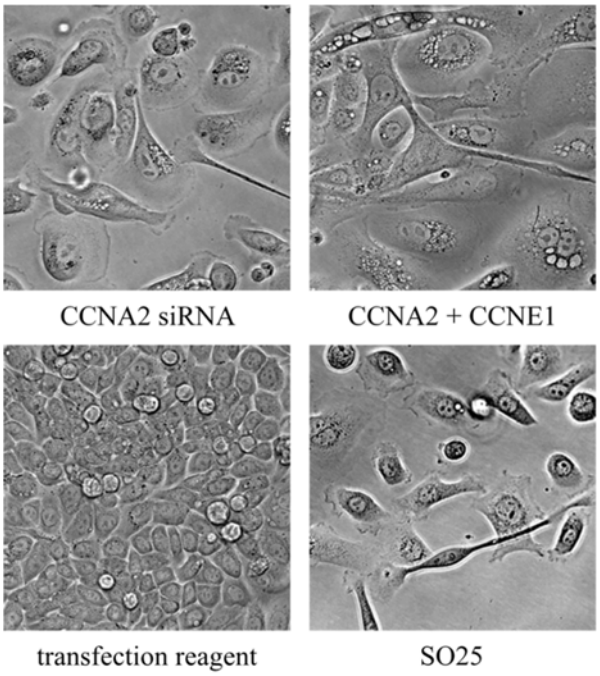


Figure 4.15: Cyclin A2 and E1 – treated PC-9 cells have a similar appearance to resistant cells.

Images show SO25 resistant cells alone and PC-9 cells treated with 25 nM cyclin A2 (CCNA2) siRNA, cyclin A2 and cyclin E1 (CCNE1) siRNA, or transfection reagent alone. Images were taken 102 h post-transfection at 100x magnification.

CHAPTER 5

5 Discussion

To date, there have been no reports of resistance to ATR kinase inhibitors, an attractive target for cancer therapeutics. We generated independent ATR inhibitor-resistant clones from human PC-9 NSCLC cells and investigated potential mechanisms of resistance, for example by measuring cell proliferation, colony forming ability, cell cycle distribution, responses to DDR modulators, DNA replication, and DDR pathway protein levels. We were unable to isolate ATR inhibitor-resistant clones from human H23 NSCLC cells, which harbour homozygous inactivating mutations in both ATM (p.Q1919P) and p53 (p.M246I) (https://portals.broadinstitute.org/ccle/home, accessed 20 Sept 2016), possibly because mutations in these pathways sensitise cells to cell killing by ATR inhibitors (Nghiem *et al*, 2001; Murga *et al*, 2009; Ruzankina *et al*, 2009; Reaper *et al*, 2011; Jacq *et al*, 2012; Guichard *et al*, 2013; Kwok *et al*, 2015, 2016; Vendetti *et al*, 2015).

The ATR inhibitor resistant PC-9 cells (SO25, SO45, and SO46) had a distinct morphology compared to the parental PC-9 cells, with multiple cytoplasmic vesicles and occasional cells containing multiple nuclei. Resistant cells grew poorly in the absence of ATR inhibitors, and in contrast to the parental cell lines, actually grew better in the presence of certain concentrations of ATR inhibitors. Cells selected in AZD6738 were also cross-resistant to chemically unrelated ATR kinase inhibitors (VE-821 and VE-822), suggesting that resistance to AZD6738 is not due to efflux via a drug-specific efflux pump (Gottesman, 2002). VE-822 is fluorescent and we demonstrated, using live cell microscopy, that this compound is taken up to a similar extent in both ATR-resistant and parental PC-9 cells, further suggesting that the differences in ATR-inhibitor sensitivity were not due to differences in drug uptake or efflux. In addition, FACS data revealed that parental PC-9 cells, but not the resistant cells, respond to

AZD6738 treatment with an early S-phase arrest. PC-9 cells (formally known as PC-14) have a homozygous R248Q point mutation in exon 7 of the p53 gene (https://portals.broadinstitute.org/ccle/home, accessed 20 Sept 2016), and since mutations in p53 are reported to confer sensitivity to ATR inhibitors (Nghiem *et al*, 2001; Kaelin, 2005; Murga *et al*, 2009; Ruzankina *et al*, 2009; Reaper *et al*, 2011; Toledo *et al*, 2011; Gabrielli *et al*, 2012; Hall *et al*, 2014; Kwok *et al*, 2015, 2016), it was possible that reversion to wild-type p53 could contribute to ATR inhibitor resistance. However, both Sanger DNA and RNA sequencing confirmed the presence of a homozygous R248Q mutation in p53 in ATR-resistant cells, and therefore genetic reversion of p53 is not responsible for their decreased sensitivity to ATR inhibitors.

Interestingly, the ATR inhibitor resistant cells grew better, with faster doubling times, in the presence of the ATR inhibitors compared to their absence. The best cell growth was at intermediate concentrations of ATR inhibitors, as well as with the CHK1/2 inhibitor AZD7762, producing an unusual shape of dose-response curve. Sanjiv *et al*, 2016 reported potential synthetic lethality between CHK1 and ATR inhibitors that is specific to cancer cells in vivo and in vitro, even though these two proteins act predominantly in the same pathway. However, our ATR inhibitor resistant cells were cross-resistant to AZD7762. Cells were also cross-resistant to WEE1 inhibition (MK-1775), but in this case with a more typical dose-response curve. Mak *et al*, 2014 reported that H1299 and HeLa cell lines have a similar increased cell growth at lower concentrations of WEE1 (MK-1775) or CHK1/2 (AZD7762) inhibitors (Mak *et al*, 2014). It was postulated that limited inhibition of the ATR-CHK1-WEE1 pathway using low-doses of inhibitors disrupts cell cycle control, but does not result in mitotic catastrophe, instead accelerating and shortening the cell cycle. In our studies, FACS data confirmed that the ATR inhibitor resistant PC-9 cells had a smaller number of aneuploid cells and few cells in S phase, which could imply a faster cell cycle progression when treated with AZD6738, enabling

the cells to appear more like parental PC-9 cells. This suggests that the ATR inhibitors may be accelerating the cell cycle and thus stimulating the growth of the resistant cells by a similar mechanism. However, a limitation of this study is that the ATR inhibitor resistant cells arose from a single cell line (PC-9) that is intrinsically sensitive to ATR inhibition. As the reasons for this sensitivity are uncertain, it is not clear whether the S phase arrest seen in parental PC-9 cells treated with ATR inhibitors is a standard response to ATR inhibition. Therefore, further work is required to investigate whether the results of this study are broadly applicable to other cell lines.

Standard treatments for patients with NSCLC include surgery and radiotherapy for early stage disease, and cisplatin-based chemotherapy and molecular targeted therapies against oncogenic driver mutations such as EGFR, ALK, or BRAF. ATR inhibitor resistant cells were also more resistant to S-phase (gemcitabine and cisplatin) and M-phase (docetaxel) selective chemotherapy agents, possibly due to their slower growth rate. The combination of AZD6738 with chemotherapy generally produced strongly additive cytotoxicity in both ATR inhibitor resistant cells and parental PC-9 cells. Of interest, ATR inhibitor treatment antagonised docetaxel in the parental PC-9 cells, presumably because the S phase arrest induced by the ATR inhibitor prevented cells progressing to mitosis. There was no evidence for an interaction between ATR activity and the oncogenic driver mutation. PC-9 cells have an EGFR activating mutation (E746_A750 deletion) which renders them highly dependent on EGFR signalling for growth and survival, and therefore hypersensitive to cell killing by EGFR tyrosine kinase inhibitors such as gefitinib. Both the parental PC-9 and ATR inhibitor resistant cells were similarly highly sensitive to the EGFR inhibitor gefitinib suggesting that the mechanism of resistance to ATR inhibitors does not involve the oncogenic EGFR pathway. Future studies are needed to investigate the response of the ATR resistant cells to radiation in the presence and absence of the ATR inhibitor.

RNA-sequencing analysis suggested differences in the expression of DNA replication and cell cycle related genes between PC-9 and resistant cells. The FACS data showed that SO25, SO45, and SO46 cells did not have the early S phase arrest that characterised parental PC-9 cells in response to AZD6738 treatment. In some respects, the ATR inhibitor resistant cells when treated with AZD6738 appeared more like untreated parental PC-9 cells. For example, DNA fibre analysis showed that SO25 cells treated with AZD6738 had a similar distribution of CldU fibre lengths to parental PC-9 cells treated only with DMSO. Surprisingly, the DNA fibre analysis also revealed that DNA replication appeared to be faster in the ATR inhibitor resistant cells, as indicated by a longer fibre length. Both the PC-9 and SO25 fibre lengths were shortened as the AZD6738 concentration was increased. This may be due to increased replication origin firing that depletes the limited dinucleotide triphosphate (dNTP) pool and thus slows or stalls replication as ssDNA, usually protected by ATR-mediated RPA, increases (Bester *et al*, 2011; Maréchal & Zou, 2013). In conditions of DNA replication stress or DNA damage in S phase, ATR is responsible for the S phase checkpoint that suppresses origin firing and preserves replication fork integrity in order to prevent fork collapse (Luciani *et al*, 2004; Couch *et al*, 2013; Toledo *et al*, 2013). Furthermore, ATR is thought to act to minimise the level of un-replicated DNA that progresses into mitosis. It has been reported that treatment with ATR inhibitors slows DNA replication forks and accelerates entry into a premature mitosis with unreplicated DNA. Under these conditions, the cells have more chromosome bridges at anaphase, increased chromatid gaps and chromosome loss, failed cytokinesis, and increased cell death (Eykelenboom *et al*, 2013). Thus, in the presence of ATR inhibitors, replication forks are prone to failing sooner and progressing more slowly, as shown by shorter tract lengths. This is consistent with what we observed in the PC-9 and resistant cells.

Due to these differences in replication speed, we investigated the levels of replication stress shown by RPA32 foci. Higher levels of endogenous replication stress have been reported as

predictive of sensitivity to ATR inhibitors (Nghiem *et al*, 2001; López-Contreras & Fernandez-Capetillo, 2010; Toledo *et al*, 2011; Middleton *et al*, 2015). However, we found that the ATR inhibitor resistant cells had higher levels of baseline RPA32 foci, and that the parental PC-9 cells had greater induction of replication stress upon treatment with AZD6738. The ATR inhibitor resistant clones did not have any significant induction of RPA32 foci upon treatment, and the fold increase in RPA32 foci in other human lung cancer cell lines did not correlate with sensitivity to ATR inhibitors. As a result, we conclude that RPA32 foci levels are not a reliable marker of intrinsic sensitivity to ATR inhibitors. Nonetheless, we did show that the resistant clones did not induce DNA replication stress (measured by RPA32 foci) upon treatment with the AZD6738 ATR inhibitor.

Similarly, levels of γH2AX foci, an indirect indicator of DNA DSBs, were not a reliable marker for sensitivity to ATR inhibitors. However, the percentage of cells positive for pan-nuclear γH2AX, an alternative marker of DNA replication stress, was found to be predictive (Jacq *et al*, 2012; Guichard *et al*, 2013). In our studies, the induction of pan-nuclear γH2AX negatively correlated with the IC_{50} values in cell lines. Furthermore, upon treatment with 1 μM AZD6738, there was a significant increase in the percentage of parental PC-9 cells positive for pan-nuclear γH2AX, but a significant decrease in pan-nuclear γH2AX in ATR inhibitor resistant cells. Previously, it was reported that pan-nuclear γH2AX levels increased in ATR inhibitor- and hydroxyurea (HU)-treated cells and that this was linked to aberrant replication fork processing and subsequent collapse that occurs when ATR is unable to regulate SMARCAL1, a genome maintenance protein (Couch *et al*, 2013). Bansbach *et al*, 2009 also observed that pan-nuclear γH2AX increased with cells that overexpressed SMARCAL1 as well as in cells where RPA gene expression was silenced. SMARCAL1 is also increased after transfection of human cells with DNA fragments, in S-phase of UV-treated cells, and in response to hypotonic treatment (Marti *et al*, 2006; Baure *et al*, 2009; Quanz *et al*, 2009). Pan-nuclear γH2AX has also been

reported to be dependent on DNA-PK in cells that are deficient in ATR, perhaps due to collapse or inhibition of replication forks that have initiated during drug treatment (Dungrawala *et al*, 2015). Meyer *et al*, 2013 also proposed that pan-nuclear γH2AX was mediated by DNA-PK, which also phosphorylates γH2AX at DSBs. In addition, Quanz *et al*, 2009 reported that pan nuclear γH2AX may result from hyper-activation of DNA-PK associated DNA repair, though γH2AX levels were not to be associated with cell survival (Baure *et al*, 2009). Accordingly, cells that are more sensitive to ATR inhibitors may be responding to replication stress by signalling DNA damage responses through DNA-PK. Future studies should investigate DNA fibre tract lengths in the presence and absence of ATR inhibitors in a broader range of tumour and non-tumour cell lines than was used in this study to better determine if there is any correlation with ATR inhibitor sensitivity.

Western blot analysis showed that parental PC-9 cells treated with AZD6738 activated ATM signalling (evidenced by increased levels of pATM, pKAP1, pCHK2 and γH2AX), as has been previously demonstrated (Murga *et al*, 2009; Dungrawala *et al*, 2015; Kwok *et al*, 2016). However, the ATR-inhibitor resistant cells did not activate ATM signalling after treatment with AZD6738, although the baseline levels of pATM (but not pKAP1 or pCHK2) were higher in the resistant cells compared with parental PC-9. This could indicate activation of non-nuclear ATM (e.g. associated with peroxisomes or mitochondria) in the resistant cells, potentially as a response to increased reactive oxygen species (Alexander & Walker, 2010), although this was not examined in this study. Levels of RPA32 protein were higher in the ATR inhibitor resistant cells, as suggested by the RPA32 foci data. In order to better determine the role of ATM signalling in the response to ATR resistance, future studies should investigate whether it is possible to generate ATR inhibitor resistant clones in isogenic cell lines, with or without loss of ATM signalling. Alternatively, an ATM kinase inhibitor could also be used to suppress ATM signalling together with ATR inhibitor (e.g. AZD6738) to determine if resistant clones

can be generated from PC-9 cells under these conditions. Furthermore, the ATM signalling pathway should be investigated in the other cells lines used in this study (NBE1, Calu-6, H1975, and A549) in order to observe whether there is any link between ATM pathway activation and sensitivity to ATR inhibitors.

In Western blots, pCHK1 S317, a marker of ATR activity, was detected in PC-9 cells 24 hours after treatment with AZD6738. However, this marker has been shown to be only specific for ATR at early time points (Gatei *et al*, 2003; Dai & Grant, 2010; Dungrawala *et al*, 2015). In cells treated with an ATR inhibitor and HU, it was demonstrated that pCHK1 S317 levels are only reduced for the first 3 h after treatment with ATR inhibitor, and it then increases, regardless of whether or not ATR inhibitor is added again. CHK1 S317 phosphorylation may be carried out by ATM or DNA-PK (Dungrawala *et al*, 2015). DNA-PK may play a role as it maintains the CHK1-Claspin complex stability and so facilitates the ATR-CHK1 pathway in response to replication stress (Lin *et al*, 2014). Levels of pCHK1 S296, which is a DNA damage-induced autophosphorylation site (Okita *et al*, 2012), were low, although SO45 cells had higher baseline levels, but the significance of this is uncertain. pCHK1 S345, a more ATR-specific marker of replication stress showed the highest levels in the control PC-9 cells treated with gemcitabine, a known inhibitor of DNA replication which induces S-phase arrest, as expected. pCHK1 S317 levels were decreased in ATR inhibitor resistant cells following treatment with AZD6738, but were increased in parental PC-9 cells. CDT1, a DNA licensing factor regulated in part by geminin, was increased upon treatment with ATR inhibitor in both parental and resistant cell lines, and may reflect altered DNA replication licensing or CDT1 degradation when ATR kinase is inhibited due to replication stress (Sakaguchi *et al*, 2012). Interestingly, CDC25A is overexpressed in human cancers and it was reported that cells deficient in CDC25A are more tolerant of higher doses of ATR inhibitor (Ray & Kiyokawa, 2008; Ruiz *et al*, 2016). However, in our studies, the ATR inhibitor resistant cells did have

lower levels of CDC25A compared with the parental PC-9 cells, and treated PC-9 cells had the lowest levels. This suggest that the mechanism of acquired resistance in our studies is not a result of low levels of CDC25A preventing premature entry into mitosis.

There were, however, lower levels of both cyclin E1 and cyclin A2 protein in the resistant cells compared to PC-9 cells. This was also confirmed at the mRNA level in the RNA-sequencing data, and knockdown of cyclin A2 and cyclin E1 expression by siRNA was able to recapitulate the phenotype seen in the resistant cells SO25, SO45, and SO46. Cyclin E1 accumulates at the G1/S border and is degraded as cells progress through S phase (Dulić *et al*, 1992). It is responsible for DNA replication licensing and its downregulation generally indicates a slowing of the cell cycle and a delay in entering S phase. Cyclin E has also been found to be commonly overexpressed in cancer cells, including NSCLC, because it interferes with replication (Mishina *et al*, 2000; Hwang & Clurman, 2005; Bartkova *et al*, 2006; Neelsen *et al*, 2013). Deregulation of cyclin E expression interferes with pre-replication complex assembly, initiation of replication, and fork movement, and leads to chromosome instability (Spruck *et al*, 1999; Ekholm-Reed *et al*, 2004). ATR inhibitors have been reported to be synthetically lethal with replication stress caused by cyclin E overexpression (Toledo *et al*, 2011). This was also confirmed in a study that showed ATR inhibitors induced ssDNA, γH2AX, and replication catastrophe more efficiently in cells overexpressing cyclin E compared to the control cells (Buisson *et al*, 2015). Surprisingly, the only report of cyclin E with regards to resistance is in $HER2^+$ breast cancer. In these cells, it was demonstrated that overexpression of cyclin E was the mechanism of resistance to trastuzumab, and that knockdown of cyclin E lead to decreased proliferation and enhanced apoptosis (Scaltriti *et al*, 2011).

Cyclin A2 is also known to be increased in cancer due to high copy number, and is linked to poor outcomes in NSCLC (Volm *et al*, 1997). Cyclin A associates with CDK2 in S-phase and

is necessary for S-phase entry as well as the onset of DNA replication (Girard *et al*, 1991; Resnitzky *et al*, 1995). Cyclin A also plays a role in G2 in association with CDC2 (Pagano *et al*, 1992). There has been a report of a correlation between cyclin A gene expression and drug resistance in acute leukaemia (Ma *et al*, 2003) where they found that lower levels of cyclin A lowered the vulnerability of these patients to chemotherapies due to the slow cycling of their cells.

It seems plausible that the lower levels of cyclin A2 and cyclin E1 seen in resistant cells in our study are a key factor associated with the slower progression of these cells through the cell cycle. Eykelenboom *et al*, 2013 showed that ATR inhibition could be rescued with a CDK1 (a mitotic regulator) inhibitor that prolonged the cell cycle providing more time for DNA replication such that mitosis and cell division could complete with more fully replicated DNA. It has been suggested that unreplicated DNA is only detrimental when cells prematurely enter mitosis due to the loss of mitotic checkpoints that are regulated by ATR. It was suggested that ATR regulates a checkpoint that enforces a minimum threshold of replication before the onset of mitosis. It allows cell cycle progression when there are small amount of un-replicated DNA that can then be dealt with in the next cycle or in mitosis by dissolution (Lukas *et al*, 2011; Eykelenboom *et al*, 2013). A similar mechanism may in part be responsible for the resistance of SO25, SO45, and SO46 cells to ATR inhibitors. The resistant cells also have an appearance that suggests there may be residual DNA damage from potentially under-replicated DNA that is still able to complete the cell cycle, as seen in their morphology and in the increased aneuploidy seen in FACS. Future studies should further investigate cyclin E1 and A2 siRNA-treated cells to see if they have similar cell cycle kinetics, DNA fibre tract lengths, activation of signalling pathways, and cross resistance to CHK1/2 inhibitors compared to the resistant SO25, SO45, and SO46 cells. Furthermore, in order to more robustly define the role of cyclins A2 and E1 in ATR resistance, these cyclins should be overexpressed in the resistant clones

using an siRNA-resistant cDNA in order to see whether this re-sensitises the cells to ATR inhibitors.

In conclusion, we generated human NSCLC cells resistant to ATR inhibitors, which are cross-resistant to CHK1/2 and WEE1 inhibitors, and also cross-resistant to standard chemotherapies used in the treatment of NSCLC. Surprisingly, the cells grow best at intermediate doses of ATR and CHK1/2 inhibitors, suggesting partial inhibition of ATR activity has become beneficial to the growth of these cell lines. We have identified downregulation of cyclin A2 and cyclin E1 expression as a potential mechanism of resistance to ATR inhibitors. As phase I trials are currently recruiting patients for treatment with ATR inhibitors (VE-822 and AZD6738) in combination with chemotherapy and/or radiotherapy to assess tolerability, and it is anticipated that these inhibitors will be developed in a wide range of cancer types, including NSCLC. A common feature of the use of kinase inhibitors in cancer therapy is the emergence of drug resistance. Our data provide a first step in understanding potential mechanisms of acquired resistance to ATR kinase inhibitors, although the clinical relevance will only be apparent as these agents progress through phase II and phase III studies.

6 References

Alexander A, Walker CL (2010) Differential localization of ATM is correlated with activation of distinct downstream signaling pathways. *Cell Cycle* **9**: 3685–3686, doi:10.4161/cc.9.18.13253.

Bansbach CE, Bétous R, Lovejoy CA, Glick GG, Cortez D (2009) The annealing helicase SMARCAL1 maintains genome integrity at stalled replication forks. *Genes Dev* **23**: 2405–2414, doi:10.1101/gad.1839909.

Bao S, Wu Q, McLendon RE, Hao Y, Shi Q, Hjelmeland AB, Dewhirst MW, Bigner DD, Rich JN (2006) Glioma stem cells promote radioresistance by preferential activation of the DNA damage response. *Nature* **444**: 756–760, doi:10.1038/nature05236.

Barnes DE, Lindahl T (2004) Repair and genetic consequences of endogenous DNA base damage in mammalian cells. *Annu Rev Genet* **38**: 445–476, doi:10.1146/annurev.genet.38.072902.092448.

Barouch-bentov R (2012) Mechanisms of Drug-Resistance in Kinases. *Expert Opin Investig Drugs* **20**: 153–208, doi:10.1517/13543784.2011.546344.Mechanisms.

Bartek J, Lukas J (2003) Chk1 and Chk2 kinases in checkpoint control and cancer. *Cancer Cell* **3**: 421–429.

Bartkova J, Rezaei N, Liontos M, Karakaidos P, Kletsas D, Issaeva N, Vassiliou L-VF, Kolettas E, Niforou K, Zoumpourlis VC, Takaoka M, Nakagawa H, Tort F, Fugger K, Johansson F, Sehested M, Andersen CL, Dyrskjot L, Ørntoft T, Lukas J, Kittas C, Helleday T, Halazonetis TD, Bartek J, Gorgoulis VG (2006) Oncogene-induced senescence is part of the tumorigenesis barrier imposed by DNA damage checkpoints. *Nature* **444**: 633–637, doi:10.1038/nature05268.

Baure J, Izadi A, Suarez V, Giedzinski E, Cleaver JE, Fike JR, Limoli CL (2009) Histone H2AX phosphorylation in response to changes in chromatin structure induced by altered osmolarity. *Mutagenesis* **24**: 161–167, doi:10.1093/mutage/gen064.

Bentley NJ, Holtzman DA, Flaggs G, Keegan KS, DeMaggio A, Ford JC, Hoekstra M, Carr AM (1996) The Schizosaccharomyces pombe rad3 checkpoint gene. *EMBO J* **15**: 6641–6651.

Bester AC, Roniger M, Oren YS, Im MM, Sarni D, Chaoat M, Bensimon A, Zamir G, Shewach DS, Kerem B (2011) Nucleotide deficiency promotes genomic instability in early stages of cancer development. *Cell* **145**: 435–446, doi:10.1016/j.cell.2011.03.044.

Blasina A, Price BD, Turenne GA, McGowan CH (1999) Caffeine inhibits the checkpoint kinase ATM. *Curr Biol* **9**: 1135–1138, doi:10.1016/S0960-9822(99)80486-2.

De Bont R, van Larebeke N (2004) Endogenous DNA damage in humans: A review of quantitative data. *Mutagenesis* **19**: 169–185, doi:10.1093/mutage/geh025.

Bouwman P, Jonkers J (2012) The effects of deregulated DNA damage signalling on cancer chemotherapy response and resistance. *Nat Rev Cancer* **12**: 587–598, doi:10.1038/nrc3342.

Brown EJ, Baltimore D (2000) ATR disruption leads to chromosomal fragmentation and early embryonic lethality. *Genes Dev* **14**: 397–402, doi:10.1101/gad.14.4.397.

Buisson R, Boisvert JL, Benes CH, Zou L (2015) Distinct but Concerted Roles of ATR, DNA-PK, and Chk1 in Countering Replication Stress during S Phase. *Mol Cell* **59**: 1011–1024, doi:10.1016/j.molcel.2015.07.029.

Casper AM, Nghiem P, Arlt MF, Glover TW (2002) ATR regulates fragile site stability. *Cell* **111**: 779–789, doi:10.1016/S0092-8674(02)01113-3.

Cha RS, Kleckner N (2002) ATR Homolog Mec1 Promotes Fork Progression, Thus Averting Breaks in Replication Slow Zones. *Science (80-)* **297**: 602–606, doi:10.1126/science.1071398.

Charrier JD, Durrant SJ, Golec JMC, Kay DP, Knegtel RM a, MacCormick S, Mortimore M, O'Donnell ME, Pinder JL, Reaper PM, Rutherford AP, Wang PSH, Young SC, Pollard JR (2011) Discovery of Potent and Selective Inhibitors of Ataxia Telangiectasia Mutated and Rad3 Related (ATR) Protein Kinase as Potential Anticancer Agents. *J Med Chem* **54**: 2320–2330.

Ciccia A, Elledge SJ (2010) The DNA Damage Response: Making It Safe to Play with Knives. *Mol Cell* **40**: 179–204, doi:10.1016/j.molcel.2010.09.019.

Cimprich K a, Cortez D (2008) ATR: an essential regulator of genome integrity. *Nat Rev Mol Cell Biol* **9**: 616–627, doi:10.1038/nrm2450.

Cimprich KA, Shin TB, Keith CT, Schreiber SL (1996) cDNA cloning and gene mapping of a candidate human cell cycle checkpoint protein. *Proc Natl Acad Sci U S A* **93**: 2850–2855, doi:10.1073/pnas.93.7.2850.

Cortez D, Guntuku S, Qin J, Elledge SJ (2001) ATR and ATRIP: partners in checkpoint signaling. *Science (80-)* **294**: 1713–1716, doi:10.1126/science.1065521.

Couch FB, Bansbach CE, Driscoll R, Luzwick JW, Glick GG, Bétous R, Carroll CM, Jung SY, Qin J, Cimprich KA, Cortez D (2013) ATR phosphorylates SMARCAL1 to prevent replication fork collapse. *Genes Dev* **27**: 1610–1623, doi:10.1101/gad.214080.113.

Dai Y, Grant S (2010) New insights into checkpoint kinase 1 in the DNA damage response signaling network. *Clin Cancer Res* **16**: 376–383, doi:10.1158/1078-0432.CCR-09-1029.

Delacroix S, Wagner JM, Kobayashi M, Yamamoto KI, Karnitz LM (2007) The Rad9-Hus1-Rad1 (9-1-1) clamp activates checkpoint signaling via TopBP1. *Genes Dev* **21**: 1472–1477, doi:10.1101/gad.1547007.

Domínguez-Kelly R, Martín Y, Koundrioukoff S, Tanenbaum ME, Smits VAJ, Medema RH, Debatisse M, Freire R (2011) Wee1 controls genomic stability during replication by regulating the Mus81-Eme1 endonuclease. *J Cell Biol* **194**: 567–579, doi:10.1083/jcb.201101047.

Donzelli M, Draetta GF (2003) Regulating mammalian checkpoints through Cdc25 inactivation. *EMBO Rep* **4**: 671–677, doi:10.1038/sj.embor.embor887.

Dulić V, Lees E, Reed SI (1992) Association of human cyclin E with a periodic G1-S phase protein kinase. *Science (80-)* **257**: 1958–1961, doi:10.1126/science.1329201.

Dungrawala H, Rose KL, Bhat KP, Mohni KN, Glick GG, Couch FB, Cortez D (2015) The Replication Checkpoint Prevents Two Types of Fork Collapse without Regulating Replisome Stability. *Mol Cell* **59**: 998–1010, doi:10.1016/j.molcel.2015.07.030.

Ekholm-Reed S, Méndez J, Tedesco D, Zetterberg A, Stillman B, Reed SI (2004) Deregulation of cyclin E in human cells interferes with prereplication complex assembly. *J Cell Biol* **165**: 789–800, doi:10.1083/jcb.200404092.

Ellison V, Stillman B (2003) Biochemical characterization of DNA damage checkpoint complexes: Clamp loader and clamp complexes with specificity for 5' recessed DNA. *PLoS Biol* **1**: 231–243, doi:10.1371/journal.pbio.0000033.

Errico A, Costanzo V (2012) Mechanisms of replication fork protection: a safeguard for genome stability. *Crit Rev Biochem Mol Biol* **47**: 222–235, doi:10.3109/10409238.2012.655374.

Eykelenboom J, Harte E, Canavan L, Pastor-Peidro A, Calvo-Asensio I, Llorens-Agost M, Lowndes NF (2013) ATR Activates the S-M Checkpoint during Unperturbed Growth to Ensure Sufficient Replication Prior to Mitotic Onset. *Cell Rep* **5**: 1095–1107, doi:10.1016/j.celrep.2013.10.027.

Flynn RL, Cox KE, Jeitany M, Wakimoto H, Bryll AR, Ganem NJ, Bersani F, Pineda JR, Suvá ML, Benes CH, Haber DA, Boussin FD, Zou L (2015) Alternative lengthening of telomeres renders cancers hypersensitive to ATR inhibitors. *Science (80-)* **347**: 273–277.

Fokas E, Prevo R, Pollard JR, Reaper PM, Charlton PA, Cornelissen B, Vallis KA, Hammond EM, Olcina MM, Gillies McKenna W, Muschel RJ, Brunner TB (2012) Targeting ATR in vivo using the novel inhibitor VE-822 results in selective sensitization of pancreatic tumors to radiation. *Cell Death Dis* **3**: e441, doi:10.1038/cddis.2012.181.

Foote KM, Blades K, Cronin A, Fillery S, Guichard SS, Hassall L, Hickson I, Jacq X, Jewsbury PJ, Mcguire TM, Nissink JWM, Odedra R, Page K, Perkins P, Suleman A, Tam K, Thommes P, Broadhurst R, Wood C (2013) Discovery of 4-{4-[(3R)-3-Methylmorpholin-4-yl]-6-[1-(methylsulfonyl)cyclopropyl]pyrimidin-2-yl}-1H-indole (AZ20): A Potent and Selective Inhibitor of ATR Protein Kinase with Monotherapy in Vivo Antitumor Activity. *J Med Chem* **56**: 2125–2138, doi:10.1021/jm301859s.

Foskolou IP, Biasoli D, Olcina MM, Hammond EM (2016) Measuring DNA Replication in Hypoxic Conditions. In Tumor Microenvironment: Study Protocols, C. Koumenis, M.L. Coussens, A. Giaccia, and E. Hammond, eds. (Cham: Springer International Publishing), pp. 11–25.

Gabrielli B, Brooks K, Pavey S (2012) Defective cell cycle checkpoints as targets for anti-cancer therapies. *Front Pharmacol* **3 FEB**: 1–6, doi:10.3389/fphar.2012.00009.

Garraway LA, Jänne PA (2012) Circumventing cancer drug resistance in the era of personalized medicine. *Cancer Discov* **2**: 214–226, doi:10.1158/2159-8290.CD-12-0012.

Garrett MD, Collins I (2011) Anticancer therapy with checkpoint inhibitors: What, where and when? *Trends Pharmacol Sci* **32**: 308–316, doi:10.1016/j.tips.2011.02.014.

Gatei M, Sloper K, Sørensen C, Sylju??sen R, Falck J, Hobson K, Savage K, Lukas J, Zhou BB, Bartek J, Khanna KK (2003) Ataxia-telangiectasia-mutated (ATM) and NBS1-dependent phosphorylation of Chk1 on Ser-317 in response to ionizing radiation. *J Biol Chem* **278**: 14806–14811, doi:10.1074/jbc.M210862200.

Girard F, Strausfeld U, Fernandez a, Lamb NJ (1991) Cyclin A is required for the onset of DNA replication in mammalian fibroblasts. *Cell* **67**: 1169–1179, doi:10.1016/0962-8924(92)90073-V.

Glover TW, Arlt MF, Casper AM, Durkin SG (2005) Mechanisms of common fragile site instability. *Hum Mol Genet* **14**: 197–205, doi:10.1093/hmg/ddi265.

Gottesman MM (2002) Mechanisms of cancer drug resistance. *Annu Rev Med* **53**: 615–627.

Gray LH, Conger AD, Ebert M, Hornsey S, Scott OC (1953) The concentration of oxygen dissolved in tissues at the time of irradiation as a factor in radiotherapy. *Br J Radiol* **26**: 638–648, doi:10.1259/0007-1285-26-312-638.

Guichard SM, Brown E, Odedra R, Hughes A, Heathcote D, Barnes J, Lau A, Powell S, Jones CD, Nissik W, Foote KM, Jewsbury PJ, Pass M (2013) The pre-clinical in vitro and in vivo activity of AZD6738: A potent and selective inhibitor of ATR kinase. In Proceedings of the 104th Annual Meeting of the American Association for Cancer Research; 2013 Apr 6-10; Washington, DC., (Philadelphia (PA)), p.

Hall AB, Newsome D, Wang Y, Boucher DM, Eustace B, Gu Y, Hare B, Johnson M a, Milton S, Murphy CE, Takemoto D, Tolman C, Wood M, Charlton P, Charrier J-D, Furey B, Golec J, Reaper PM, Pollard JR (2014) Potentiation of tumor responses to DNA damaging therapy by the selective ATR inhibitor VX-970. *Oncotarget* **5**: 5674–5685, doi:10.18632/oncotarget.2158.

Hall-Jackson C a, Cross D a, Morrice N, Smythe C (1999) ATR is a caffeine-sensitive, DNA-activated protein kinase with a substrate specificity distinct from DNA-PK. *Oncogene* **18**: 6707–6713, doi:10.1038/sj.onc.1203077.

Hartsough E, Shao Y, Aplin AE (2014) Resistance to RAF inhibitors revisited. *J Invest Dermatol* **134**: 319–325, doi:10.1038/jid.2013.358.

Helleday T, Eshtad S, Nik-Zainal S (2014) Mechanisms underlying mutational signatures in human cancers. *Nat Rev Genet* **15**: 585–598, doi:10.1038/nrg3729.

Hoeijmakers JH (2009) DNA damage, aging, and cancer. *N Engl J Med* **361**: 1475–1485, doi:361/15/1475 [pii]10.1056/NEJMra0804615.

Hwang HC, Clurman BE (2005) Cyclin E in normal and neoplastic cell cycles. *Oncogene* **24**: 2776–2786, doi:10.1038/sj.onc.1208613.

Jackson SP, Bartek J (2010) The DNA-damage response in human biology and disease. *Nature* **461**: 1071–1078, doi:10.1038/nature08467.The.

Jacq X, Smith L, Brown E, Hughes A, Odedra R, Heathcote D, Barnes J, Powell S, Maguire S, Pearson V, Boros J, Caie P, Thommes PA, Nissink W, Foote K, Jewsbury PJ, Guichard SM (2012) AZ20, a novel potent and selective inhibitor of ATR kinase with in vivo antitumour activity. (abstract). In Proceedings of the 103rd Annual Meeting of the American Association

for Cancer Research; 2012 Mar 31–Apr 4 ;Chicago, IL. Cancer Res 72(8 Suppl.)., (Philadelphia (PA)), p.

Jeong SY, Kumagai A, Lee J, Dunphy WG (2003) Phosphorylated Claspin Interacts with a Phosphate-binding Site in the Kinase Domain of Chk1 during ATR-mediated Activation. *J Biol Chem* **278**: 46782–46788, doi:10.1074/jbc.M304551200.

Jones CD, Blades K, Foote KM, Guichard SM, Jewsbury PJ, McGuire T, Nissik JW, Odedra R, Tam K, Thommes P, Turner P, Wilkinson G, Wood C, Yates JW (2013) Discovery of AZD6738, a potent and selective inhibitor with the potential to test the clinical efficacy of ATR kinase inhibition in cancer patients. In Proceedings of the 104th Annual Meeting of the American Association for Cancer Research; 2013 Apr 6-10; Washington, DC., (Philadelphia (PA)), p.

Jossé R, Martin SE, Guha R, Ormanoglu P, Pfister TD, Reaper PM, Barnes CS, Jones J, Charlton P, Pollard JR, Morris J, Doroshow JH, Pommier Y (2014) ATR inhibitors VE-821 and VX-970 sensitize cancer cells to topoisomerase I inhibitors by disabling DNA replication initiation and fork elongation responses. *Cancer Res* **74**: 6968–6978, doi:10.1158/0008-5472.CAN-13-3369.

Kaelin WG (2005) The concept of synthetic lethality in the context of anticancer therapy. *Nat Rev Cancer* **5**: 689–698, doi:10.1038/nrc1691.

Karnitz LM, Flatten KS, Wagner JM, Loegering D, Hackbarth JS, Arlander SJ, Vroman BT, Thomas MB, Baek YU, Hopkins KM, Lieberman HB, Chen J, Cliby WA, Kaufmann SH (2005) Gemcitabine-induced activation of checkpoint signaling pathways that affect tumor cell survival. *Mol Pharmacol* **68**: 1636–1644, doi:10.1124/mol.105.012716.

Kastan MB, Bartek J (2004) Cell-cycle checkpoints and cancer. *Nature* **432**: 316–323, doi:10.1038/nature03097.

Kemp MG, Akan Z, Yilmaz S, Grillo M, Smith-Roe SL, Kang TH, Cordeiro-Stone M, Kaufmann WK, Abraham RT, Sancar A, Ünsal-Kaçmaz K (2010) Tipin-replication protein A interaction mediates Chk1 phosphorylation by ATR in response to genotoxic stress. *J Biol Chem* **285**: 16562–16571, doi:10.1074/jbc.M110.110304.

Kim D, Pertea G, Trapnell C, Pimentel H, Kelley R, Salzberg SL (2013) TopHat2: accurate alignment of transcriptomes in the presence of insertions, deletions and gene fusions. *Genome Biol* **14**: 1–13, doi:10.1186/gb-2013-14-4-r36.

De Klein A, Muijtjens M, Van Os R, Verhoeven Y, Smit B, Carr AM, Lehmann AR, Hoeijmakers JHJ (2000) Targeted disruption of the cell-cycle checkpoint gene ATR leads to early embryonic lethality in mice. *Curr Biol* **10**: 479–482, doi:10.1016/S0960-9822(00)00447-4.

Kondo T, Wakayama T, Naiki T, Matsumoto K, Sugimoto K (2001) Recruitment of Mec1 and Ddc1 Checkpoint Proteins to Double-Strand Breaks Through Distinct Mechanisms. *Science (80-)* **294**: 867–870, doi:10.1126/science.1063827.

Konstantinidou G, Bey EA, Rabellino A, Schuster K, Maira MS, Gazdar AF, Amici A, Boothman DA, Scaglioni PP (2009) Dual phosphoinositide 3-kinase/mammalian target of

rapamycin blockade is an effective radiosensitizing strategy for the treatment of non-small cell lung cancer harboring K-RAS mutations. *Cancer Res* **69**: 7644–7652, doi:10.1158/0008-5472.CAN-09-0823.

Kumagai A, Dunphy WG (2003) Repeated phosphopeptide motifs in Claspin mediate the regulated binding of Chk1. *Nat Cell Biol* **5**: 161–165, doi:10.1038/ncb921.

Kumagai A, Kim SM, Dunphy WG (2004) Claspin and the activated form of ATR-ATRIP collaborate in the activation of Chk1. *J Biol Chem* **279**: 49599–49608, doi:10.1074/jbc.M408353200.

Kumagai A, Lee J, Yoo HY, Dunphy WG (2006) TopBP1 activates the ATR-ATRIP complex. *Cell* **124**: 943–955, doi:10.1016/j.cell.2005.12.041.

Kwok M, Davies N, Agathanggelou A, Smith E, Oldreive C, Petermann E, Stewart G, Brown J, Lau A, Pratt G, Parry H, Taylor M, Moss P, Hillmen P, Stankovic T (2016) ATR inhibition induces synthetic lethality and overcomes chemoresistance in TP53 or ATM defective chronic lymphocytic leukemia cells. *Blood* **127**: 582–595, doi:10.1182/blood-2015-05-644872.

Kwok M, Davies N, Agathanggelou A, Smith E, Petermann E, Yates E, Brown J, Lau A, Stankovic T (2015) Synthetic lethality in chronic lymphocytic leukaemia with DNA damage response defects by targeting the ATR pathway. In Spring Meeting for Clinician Scientists in Training 2015, p. S58.

Langmead B, Trapnell C, Pop M, Salzberg SL (2009) Ultrafast and memory-efficient alignment of short DNA sequences to the human genome. *Genome Biol* **10**: 1–10, doi:10.1186/gb-2009-10-3-r25.

Lau CC, Pardee AB (1982) Mechanism by which caffeine potentiates lethality of nitrogen mustard. *Proc Natl Acad Sci U S A* **79**: 2942–2946, doi:10.1073/pnas.79.9.2942.

Lee J, Kumagai a, Dunphy WG (2001) Positive regulation of Wee1 by Chk1 and 14-3-3 proteins. *Mol Biol Cell* **12**: 551–563.

Lee J, Kumagai A, Dunphy WG (2003) Claspin, a Chk1-regulatory protein, monitors DNA replication on chromatin independently of RPA, ATR, and Rad17. *Mol Cell* **11**: 329–340, doi:10.1016/S1097-2765(03)00045-5.

Lin JJ, Milhollen MA, Smith PG, Narayanan U, Dutta A (2010) NEDD8 targeting drug MLN4924 elicits DNA re-replication by stabilizing Cdt1 in S Phase, triggering checkpoint activation, apoptosis and senescence in cancer cells. *Cancer Res* **24**: 10310–10320, doi:10.1126/scisignal.2001449.Engineering.

Lin YF, Shih HY, Shang Z, Matsunaga S, Chen BP (2014) DNA-PKcs is required to maintain stability of Chk1 and Claspin for optimal replication stress response. *Nucleic Acids Res* **42**: 4463–4473, doi:10.1093/nar/gku116.

Lindahl T (1993) Instability and decay of the primary structure of DNA. *Nature* **362**: 709–715, doi:10.1038/362709a0.

Lippert TH, Ruoff H-J, Volm M (2011) Current status of methods to assess cancer drug resistance. *Int J Med Sci* **8**: 245–253.

Liu Q, Guntuku S, Cui XS, Matsuoka S, Cortez D, Tamai K, Luo G, Carattini-Rivera S, DeMayo F, Bradley A, Donehower LA, Elledge SJ (2000) Chk1 is an essential kinase that is regulated by Atr and required for the G2/M DNA damage checkpoint. *Genes Dev* **14**: 1448–1459, doi:10.1101/gad.14.12.1448.

Liu Q, Xu C, Kirubakaran S, Zhang X, Hur W, Liu Y, Kwiatkowski NP, Wang J, Westover KD, Gao P, Ercan D, Niepel M, Thoreen CC, Kang SA, Patricelli MP, Wang Y, Tupper T, Altabef A, Kawamura H, Held KD, Chou DM, Elledge SJ, Janne PA, Wong KK, Sabatini DM, Gray NS (2013) Characterization of Torin2, an ATP-competitive inhibitor of mTOR, ATM, and ATR. *Cancer Res* **73**: 2574–2586, doi:10.1158/0008-5472.CAN-12-1702.

López-Contreras AJ, Fernandez-Capetillo O (2010) The ATR barrier to replication-born DNA damage. *DNA Repair (Amst)* **9**: 1249–1255, doi:10.1016/j.dnarep.2010.09.012.

Lovejoy CA, Cortez D (2009) Common mechanisms of PIKK regulation. **8**: 1004–1008, doi:10.1016/j.dnarep.2009.04.006.Common.

Lovly CM, Pao W (2012) Escaping ALK inhibition: mechanisms of and strategies to overcome resistance. *Sci Transl Med* **4**: 120ps2, doi:10.1126/scitranslmed.3003728.

Luciani MG, Oehlmann M, Blow JJ (2004) Characterization of a novel ATR-dependent, Chk1-independent, intra-S-phase checkpoint that suppresses initiation of replication in Xenopus. *J Cell Sci* **117**: 6019–6030, doi:10.1242/jcs.01400.

Lukas C, Savic V, Bekker-Jensen S, Doil C, Neumann B, Pedersen RS, Grøfte M, Chan KL, Hickson ID, Bartek J, Lukas J (2011) 53BP1 nuclear bodies form around DNA lesions generated by mitotic transmission of chromosomes under replication stress. *Nat Cell Biol* **13**: 243–253, doi:10.1038/ncb2201.

Luong K V., Wang L, Roberts BJ, III JKW, Peng A, Luong K V., Wang L, Roberts BJ, Wahl III JK, Peng A (2016) Cell fate determination in cisplatin resistance and chemosensitization. *Oncotarget* **7**: 23383–23394.

Luqmani YA (2005) Mechanisms of drug resistance in cancer chemotherapy. *Med Princ Pract* **14**: 35–48, doi:10.1159/000081921.

Ma J, Xu S, Lai Y, Lu Y (2003) The correlation of cyclin A gene expression with drug resistance in adult acute leukemia patients. *J Huazhong Univ Sci Technol* **23**: 245–248.

Maira S-M, Stauffer F, Brueggen J, Furet P, Schnell C, Fritsch C, Brachmann S, Chène P, De Pover A, Schoemaker K, Fabbro D, Gabriel D, Simonen M, Murphy L, Finan P, Sellers W, García-Echeverría C (2008) Identification and characterization of NVP-BEZ235, a new orally available dual phosphatidylinositol 3-kinase/mammalian target of rapamycin inhibitor with potent in vivo antitumor activity. *Mol Cancer Ther* **7**: 1851–1863, doi:10.1158/1535-7163.MCT-08-0017.

Mak JPY, Man WY, Ma HT, Poon RYC (2014) Pharmacological targeting the ATR-CHK1-WEE1 axis involves balancing cell growth stimulation and apoptosis. *Oncotarget* **5**: 10546–10557, doi:10.18632/oncotarget.2508.

Maréchal A, Zou L (2013) DNA damage sensing by the ATM and ATR kinases. *Cold Spring*

Harb Perspect Biol **5**: doi:10.1101/cshperspect.a012716.

Marti TM, Hefner E, Feeney L, Natale V, Cleaver JE (2006) H2AX phosphorylation within the G1 phase after UV irradiation depends on nucleotide excision repair and not DNA double-strand breaks. *Proc Natl Acad Sci U S A* **103**: 9891–9896, doi:10.1073/pnas.0603779103.

Melo JA, Cohen J, Toczyski DP (2001) Two checkpoint complexes are independently recruited to sites of DNA damage in vivo Two checkpoint complexes are independently recruited to sites of DNA damage in vivo. *Genes Dev* **15**: 2809–2821, doi:10.1101/gad.903501.

Meyer B, Voss KO, Tobias F, Jakob B, Durante M, Taucher-Scholz G (2013) Clustered DNA damage induces pan-nuclear H2AX phosphorylation mediated by ATM and DNA-PK. *Nucleic Acids Res* **41**: 6109–6118, doi:10.1093/nar/gkt304.

Middleton FK, Patterson MJ, Elstob CJ, Fordham S, Herriott A, Wade MA, McCormick A, Edmondson R, May FEB, Allan JM, Pollard JR, Curtin NJ (2015) Common cancer-associated imbalances in the DNA damage response confer sensitivity to single agent ATR inhibition. *Oncotarget* **6**: 32396–32409, doi:10.18632/oncotarget.6136.

Mirkin E V, Mirkin SM (2007) Replication fork stalling at natural impediments. *Microbiol Mol Biol Rev* **71**: 13–35, doi:10.1128/MMBR.00030-06.

Mishina T, Dosaka-akita H, Hommura F, Nishi M, Kojima T, Ogura S, Shimizu M, Katoh H, Kawakami Y (2000) Cyclin E Expression , a Potential Prognostic Marker for Non-Small Cell Lung Cancers. *Clinical* **6**: 11–16.

Mohni KN, Kavanaugh GM, Cortez D (2014) ATR pathway inhibition is synthetically lethal in cancer cells with ercc1 deficiency. *Cancer Res* **74**: 2835–2845, doi:10.1158/0008-5472.CAN-13-3229.

Mordes DA, Glick GG, Zhao R, Cortez D (2008) TopBP1 activates ATR through ATRIP and a PIKK regulatory domain. *Genes Dev* **22**: 1478–1489, doi:10.1101/gad.1666208.

Murga M, Bunting S, Montaña MF, Soria R, Mulero F, Cañamero M, Lee Y, McKinnon PJ, Nussenzweig A, Fernandez-Capetillo O (2009) A mouse model of ATR-Seckel shows embryonic replicative stress and accelerated aging. *Nat Genet* **41**: 891–898, doi:10.1038/ng.420.

Myers K, Gagou ME, Zuazua-Villar P, Rodriguez R, Meuth M (2009) ATR and Chk1 suppress a caspase-3-dependent apoptotic response following DNA replication stress. *PLoS Genet* **5**: doi:10.1371/journal.pgen.1000324.

Neelsen KJ, Zanini IMY, Herrador R, Lopes M (2013) Oncogenes induce genotoxic stress by mitotic processing of unusual replication intermediates. *J Cell Biol* **200**: 699–708, doi:10.1083/jcb.201212058.

Nghiem P, Park PK, Kim Y, Vaziri C, Schreiber SL (2001) ATR inhibition selectively sensitizes G1 checkpoint-deficient cells to lethal premature chromatin condensation. *Proc Natl Acad Sci U S A* **98**: 9092–9097, doi:10.1073/pnas.161281798.

O'Brien J, Wilson I, Orton T, Pognan F (2000) Investigation of the Alamar Blue (resazurin) fluorescent dye for the assessment of mammalian cell cytotoxicity. *Eur J Biochem* **267**: 5421–

5426, doi:10.1046/j.1432-1327.2000.01606.x.

O'Driscoll M, Ruiz-Perez VL, Woods CG, Jeggo PA, Goodship JA (2003) A splicing mutation affecting expression of ataxia-telangiectasia and Rad3-related protein (ATR) results in Seckel syndrome. *Nat Genet* **33**: 497–501, doi:10.1038/ng1129.

O'Flanagan CH, O'Shea S, Lyons A, Fogarty FM, Kennedy RD, O'Connor R (2016) IGF-1R inhibition sensitizes breast cancer cells to ATM-Related Kinase (ATR) inhibitor and cisplatin. *Oncotarget*.

O'Hare T, Eide CA, Deininger MWN (2007) Bcr-Abl kinase domain mutations , drug resistance , and the road to a cure for chronic myeloid leukemia. *Blood* **110**: 2242–2249, doi:10.1182/blood-2007-03-066936.

Okita N, Minato S, Ohmi E, Tanuma SI, Higami Y (2012) DNA damage-induced CHK1 autophosphorylation at Ser296 is regulated by an intramolecular mechanism. *FEBS Lett* **586**: 3974–3979, doi:10.1016/j.febslet.2012.09.048.

Oliver TG, Mercer KL, Sayles LC, Burke JR, Mendus D, Lovejoy KS, Cheng MH, Subramanian A, Mu D, Powers S, Crowley D, Bronson RT, Whittaker CA, Bhutkar A, Lippard SJ, Golub T, Thomale J, Jacks T, Sweet-Cordero EA (2010) Chronic cisplatin treatment promotes enhanced damage repair and tumor progression in a mouse model of lung cancer. *Genes Dev* **24**: 837–852, doi:10.1101/gad.1897010.

Pagano M, Pepperkok R, Verde F, Ansorge W, Draetta G (1992) Cyclin A is required at two points in the human cell cycle. *EMBO J* **11**: 961–971.

Peasland A, Wang L-Z, Rowling E, Kyle S, Chen T, Hopkins A, Cliby W a, Sarkaria J, Beale G, Edmondson RJ, Curtin NJ (2011) Identification and evaluation of a potent novel ATR inhibitor, NU6027, in breast and ovarian cancer cell lines. *Br J Cancer* **105**: 372–381, doi:10.1038/bjc.2011.243.

Peng C, Graves PR, Thoma RS, Wu Z, Shaw AS, Piwnica-worms H (1997) Mitotic and G2 Checkpoint Control: Regulation of 14-3-3 Protein Binding by Phosphorylation of Cdc25C on Serine-216. *Science (80-)* **277**: 1501–1505, doi:10.1126/science.277.5331.1501.

Pinedo HM, Giaccone G (1998) Drug resistance in the treatment of cancer (Cambridge: Cambridge University Press).

Pires IM, Olcina MM, Anbalagan S, Pollard JR, Reaper PM, Charlton P a, McKenna WG, Hammond EM (2012) Targeting radiation-resistant hypoxic tumour cells through ATR inhibition. *Br J Cancer* **107**: 291–299, doi:10.1038/bjc.2012.265.

Prevo R, Fokas E, Reaper PM, Charlton P a., Pollard JR, McKenna WG, Muschel RJ, Brunner TB (2012) The novel ATR inhibitor VE-821 increases sensitivity of pancreatic cancer cells to radiation and chemotherapy. *Cancer Biol Ther* **13**: 1072–1081.

Quanz M, Chassoux D, Berthault N, Agrario C, Sun JS, Dutreix M (2009) Hyperactivation of DNA-PK by double-strand break mimicking molecules disorganizes DNA damage response. *PLoS One* **4**: 1–11, doi:10.1371/journal.pone.0006298.

Ray D, Kiyokawa H (2008) CDC25A phosphatase: A rate-limiting oncogene that determines

genomic stability. *Cancer Res* **68**: 1251–1253, doi:10.1158/0008-5472.CAN-07-5983.

Reaper PM, Griffiths MR, Long JM, Charrier J-D, Maccormick S, Charlton P a, Golec JMC, Pollard JR (2011) Selective killing of ATM- or p53-deficient cancer cells through inhibition of ATR. *Nat Chem Biol* **7**: 428–430, doi:10.1038/nchembio.573.

Resnitzky D, Hengst L, Reed SI (1995) Cyclin A-associated kinase activity is rate limiting for entrance into S phase and is negatively regulated in G1 by p27Kip1. *Mol Cell Biol* **15**: 4347–4352.

Ruiz S, Mayor-Ruiz C, Lafarga V, Murga M, Vega-Sendino M, Ortega S, Fernandez-Capetillo O (2016) A Genome-wide CRISPR Screen Identifies CDC25A as a Determinant of Sensitivity to ATR Inhibitors. *Mol Cell* **62**: 307–313, doi:10.1016/j.molcel.2016.03.006.

Ruzankina Y, Pinzon-Guzman C, Asare A, Ong T, Pontano L, Cotsarelis G, Zediak VP, Velez M, Bhandoola A, Brown EJ (2007) Deletion of the Developmentally Essential Gene ATR in Adult Mice Leads to Age-Related Phenotypes and Stem Cell Loss. *Cell Stem Cell* **1**: 113–126, doi:10.1016/j.stem.2007.03.002.

Ruzankina Y, Schoppy DW, Asare A, Clark CE, Vonderheide RH, Brown EJ (2009) Tissue regenerative delays and synthetic lethality in adult mice after combined deletion of Atr and Trp53. *Nat Genet* **41**: 1144–1149, doi:10.1038/ng.441.

Sakaguchi H, Takami T, Yasutani Y, Maeda T, Morino M, Ishii T, Shiomi Y, Nishitani H (2012) Checkpoint Kinase ATR Phosphorylates Cdt2, a Substrate Receptor of CRL4 Ubiquitin Ligase, and Promotes the Degradation of Cdt1 following UV Irradiation. *PLoS One* **7**: doi:10.1371/journal.pone.0046480.

Sakurikar N, Eastman A (2015) Will targeting Chk1 have a role in the future of cancer therapy? *J Clin Oncol* **33**: 1075–1077, doi:10.1200/JCO.2014.60.0767.

Sanjiv K, Hagenkort A, Calderón-Montaño JM, Koolmeister T, Reaper PM, Mortusewicz O, Jacques SA, Kuiper R V., Schultz N, Scobie M, Charlton PA, Pollard JR, Berglund UW, Altun M, Helleday T (2016) Cancer-Specific Synthetic Lethality between ATR and CHK1 Kinase Activities. *Cell Rep* **14**: 298–309, doi:10.1016/j.celrep.2015.12.032.

Sarkaria JN, Busby EC, Tibbetts RS, Roos P, Taya Y, Karnitz LM, Abraham RT (1999) Inhibition of ATM and ATR kinase activities by the radiosensitizing agent, caffeine. *Cancer Res* **59**: 4375–4382.

Scaltriti M, Eichhorn PJ, Cortés J, Prudkin L, Aura C, Jiménez J, Chandarlapaty S, Serra V, Prat A, Ibrahim YH, Guzmán M, Gili M, Rodríguez O, Rodríguez S, Pérez J, Green SR, Mai S, Rosen N, Hudis C, Baselga J (2011) Cyclin e amplification/overexpression is a mechanism of trastuzumab resistance in HER2+ breast cancer patients. *Breast Dis* **22**: 266–267, doi:10.1016/j.breastdis.2011.06.033.

Sørensen CS, Syljuasen RG, Falck J, Schroeder T, Rönnstrand L, Khanna KK, Zhou BB, Bartek J, Lukas J (2003) Chk1 regulates the S phase checkpoint by coupling the physiological turnover and ionizing radiation-induced accelerated proteolysis of Cdc25A. *Cancer Cell* **3**: 247–258, doi:10.1016/S1535-6108(03)00048-5.

Spruck CH, Won K a, Reed SI (1999) Deregulated cyclin E induces chromosome instability. *Nature* **401**: 297–300, doi:10.1038/45836.

Sultana R, Abdel-Fatah T, Perry C, Moseley P, Albarakti N, Mohan V, Seedhouse C, Chan S, Madhusudan S (2013) Ataxia Telangiectasia Mutated and Rad3 Related (ATR) Protein Kinase Inhibition Is Synthetically Lethal in XRCC1 Deficient Ovarian Cancer Cells. *PLoS One* **8**: e57098, doi:10.1371/journal.pone.0057098.

Thorvaldsdóttir H, Robinson JT, Mesirov JP (2013) Integrative Genomics Viewer (IGV): High-performance genomics data visualization and exploration. *Brief Bioinform* **14**: 178–192, doi:10.1093/bib/bbs017.

Toledo LI, Altmeyer M, Rask M-B, Lukas C, Larsen DH, Povlsen LK, Bekker-Jensen S, Mailand N, Bartek J, Lukas J (2013) ATR prohibits replication catastrophe by preventing global exhaustion of RPA. *Cell* **155**: 1088–1103, doi:10.1016/j.cell.2013.10.043.

Toledo LI, Murga M, Zur R, Soria R, Rodriguez A, Martinez S, Oyarzabal J, Pastor J, Bischoff JR, Fernandez-Capetillo O (2011) A cell-based screen identifies ATR inhibitors with synthetic lethal properties for cancer-associated mutations. *Nat Struct Mol Biol* **18**: 721–727, doi:10.1038/nsmb.2076.

Trapnell C, Roberts A, Goff L, Pertea G, Kim D, Kelley DR, Pimentel H, Salzberg SL, Rinn JL, Pachter L (2012) Differential gene and transcript expression analysis of RNA-seq experiments with TopHat and Cufflinks. *Nat Protoc* **7**: 562–578, doi:10.1016/j.pestbp.2011.02.012.Investigations.

Vendetti FP, Lau A, Schamus S, Conrads TP, O'Connor MJ, Bakkenist CJ (2015) The orally active and bioavailable ATR kinase inhibitor AZD6738 potentiates the anti-tumor effects of cisplatin to resolve ATM-deficient non-small cell lung cancer in vivo. *Oncotarget* **6**: 44289–44305, doi:10.18632/oncotarget.6247.

Volm M, Koomägi R, Mattern J, Stammler G (1997) Cyclin A is associated with an unfavourable outcome in patients with non-small-cell lung carcinomas. *Br J Cancer* **75**: 1774–1778.

Wagner JM, Kaufmann SH (2010) Prospects for the use of ATR inhibitors to treat cancer. *Pharmaceuticals* **3**: 1311–1334, doi:10.3390/ph3051311.

Weber AM (2015) Targeting ATM/ATR signalling in lung cancer. University of Oxford.

Weber AM, Ryan AJ (2015) ATM and ATR as therapeutic targets in cancer. *Pharmacol Ther* **149**: 124–138, doi:10.1016/j.pharmthera.2014.12.001.

Wheeler DL, Dunn EF, Harari PM (2010) Understanding resistance to EGFR inhibitors - impact on future treatment strategies. *Nat Rev Clin Oncol* **7**: 493–507, doi:10.1038/nrclinonc.2010.97.Understanding.

Woods D, Turchi JJ (2013) Chemotherapy induced DNA damage response. *Cancer Biol Ther* **14**: 379–389.

Wouters BG, Brown JM (1997) Cells at intermediate oxygen levels can be more important than the 'hypoxic fraction' in determining tumor response to fractionated radiotherapy. *Radiat Res*

147: 541–550.

Xiao Z, Chen Z, Gunasekera AH, Sowin TJ, Rosenberg SH, Fesik S, Zhang H (2003) Chk1 mediates S and G2 arrests through Cdc25A degradation in response to DNA-damaging agents. *J Biol Chem* **278**: 21767–21773, doi:10.1074/jbc.M300229200.

Zahreddine H, Borden KLB (2013) Mechanisms and insights into drug resistance in cancer. *Front Pharmacol* **4**: doi:10.3389/fphar.2013.00028.

Zeman MK, Cimprich KA (2014) Causes and consequences of replication stress. *Nat Cell Biol* **16**: 2–9, doi:10.1038/ncb2897.

Zhao H, Watkins JL, Piwnica-Worms H (2002) Disruption of the checkpoint kinase 1/cell division cycle 25A pathway abrogates ionizing radiation-induced S and G2 checkpoints. *Proc Natl Acad Sci U S A* **99**: 14795–14800, doi:10.1073/pnas.182557299.

Zou L, Elledge SJ (2003) Sensing DNA damage through ATRIP recognition of RPA-ssDNA complexes. *Science (80-)* **300**: 1542–1548, doi:10.1126/science.1083430.

7 Supplemental Information

Supplementary Table 1: Top 200 differentially expressed genes between conditions #1 (PC-9) and #4 (SO25) ranked on Q value (low to high), p value (low to high) and ABS (test statistic) (high to low).

Gene name	Expression FPKM (PC-9)	Expression FPKM (SO25)	log2 fold change	Test Statistic[1,2]
SNORA31	336.194	86.5947	-1.95694	-73.0138
RNA5-8SP6	1312.68	782.665	-0.74605	-38.2816
AKR1C2	709.881	35.3671	-4.3271	-28.8872
HIST1H2AJ	194.755	52.659	-1.88691	-26.2226
INA	27.7636	3.92469	-2.82254	-24.3549
CST6	27.902	138.595	2.31244	23.2908
EEF1A2	3.61441	41.4895	3.52091	23.0972
HIST1H3H	446.524	144.689	-1.62578	-22.6929
HIST1H4L	525.929	169.264	-1.6356	-22.2632
TACSTD2	128.635	490.737	1.93167	20.9345
G0S2	12.7963	75.9637	2.56958	20.2389
SERINC2	17.5533	70.5465	2.00683	19.5021
HIST2H3D	211.474	82.8175	-1.35247	-19.0642
HIST1H2BB	145.572	52.0814	-1.48289	-18.9321
ISG15	9.0548	45.8976	2.34166	18.8063
HIST1H4D	845.464	341.476	-1.30796	-18.7393
HIST1H3G	678.11	258.86	-1.38934	-18.4374
HLA-B	2.28286	39.5577	4.11504	18.412
HIST1H2BM	52.6794	3.77281	-3.80353	-18.1988
HIST1H4A	313.054	121.851	-1.36129	-17.5312
HIST1H2AH	737.159	301.021	-1.29211	-17.4142
FBXO2	18.0643	77.7942	2.10652	17.393
NCCRP1	7.15316	25.1312	1.81283	17.3879
HIST1H2BI	582.902	209.43	-1.47678	-17.2585
HIST1H3I	290.965	121.747	-1.25695	-17.2159
HIST1H2AB	312.044	129.63	-1.26735	-17.098
FABP5	55.1624	9.1614	-2.59005	-16.9775
HIST1H2BE	344.532	121.406	-1.50479	-16.9276
HIST1H2AL	144.562	51.7472	-1.48214	-16.9013
KYNU	3.83744	25.9064	2.75509	16.2642
KIAA1644	5.0426	0.772446	-2.70666	-16.1847
HIST1H3A	395.209	183.379	-1.10779	-16.0913
HIST1H1B	477.608	148.753	-1.68291	-16.0891
PLAT	30.4097	140.679	2.2098	15.9107
GAS6	4.92414	22.0676	2.16398	15.8721
CKB	16.5802	54.9757	1.72933	15.795
LGALS1	68.903	309.992	2.16959	15.7787
MGP	11.022	54.4856	2.3055	15.7236

SIRPA	8.14956	1.45176	-2.48892	-15.7175
IGFBP3	84.9289	380.967	2.16534	15.6156
SERPINB3	1.46716	18.6758	3.67008	15.5962
HIST1H4B	992.751	459.815	-1.11038	-15.5415
HIST1H3B	1220.21	586.283	-1.05746	-15.3486
GOLGA7B	9.17263	1.69225	-2.43839	-15.2526
CTH	3.1942	26.0376	3.02707	15.2279
WFDC3	7.88906	39.8541	2.3368	15.1614
SPP1	130.474	28.9675	-2.17125	-15.125
ANXA1	68.0352	287.759	2.08051	15.0841
PRSS8	4.90505	27.4846	2.48628	14.9459
PADI4	25.689	3.28904	-2.96541	-14.9207
BLVRA	43.0969	9.20749	-2.2267	-14.8846
ARSA	4.82255	21.8519	2.17989	14.7495
SLCO1B3	3.95025	25.5488	2.69324	14.7159
MFI2	12.6469	62.4469	2.30385	14.7033
CLIC4	19.9186	89.7765	2.17223	14.6831
TMEM45A	3.21386	19.9334	2.63281	14.5926
HIST1H2BL	165.391	65.2681	-1.34143	-14.5716
BIRC3	3.93232	21.9597	2.4814	14.5707
HIST1H4J	297.018	147.047	-1.01427	-14.393
S1PR3	8.98647	2.13898	-2.07083	-14.3079
HIST1H4C	900.718	460.991	-0.96634	-14.3039
GNA15	6.39562	23.2038	1.85921	14.2583
NEDD9	4.76499	24.619	2.36923	14.2393
YPEL3	4.72445	24.5027	2.37472	14.0797
MCAM	10.8074	68.3637	2.66121	13.9276
GAL	42.1986	6.98886	-2.59407	-13.8853
HIST1H2AK	34.9872	11.0733	-1.65975	-13.8393
B2M	321.793	895.626	1.47676	13.8314
SRGN	49.0364	0.482071	-6.66846	-13.8208
HIST1H2AE	364.274	162.831	-1.16165	-13.729
HIST1H2BG	588.664	252.105	-1.22342	-13.6882
CCDC85B	27.9336	61.8588	1.14698	13.6306
HIST1H3C	771.139	394.774	-0.96597	-13.6136
MMP14	1.79779	20.2335	3.49245	13.6024
ARL14	3.90875	19.2685	2.30146	13.397
CHPT1	17.3092	4.77068	-1.85928	-13.3768
HIST1H1E	1133.86	429.876	-1.39925	-13.3469
IL1A	0.389533	9.82318	4.65637	13.3103
LYAR	37.9917	9.6397	-1.97862	-13.2755
HSD3B7	2.01749	9.84099	2.28624	13.1892
CDCA7	46.0195	12.354	-1.89726	-13.1388
ANKRD1	2.47139	12.859	2.37938	13.076
HIST1H2AI	185.882	88.0153	-1.07856	-12.9872
TNFSF9	3.52764	10.6084	1.58843	12.9521

RP11-148B18.4	10.4262	33.363	1.67804	12.9107
PBXIP1	2.54477	14.4394	2.5044	12.8648
FN1	7.63502	65.9353	3.11035	12.8447
KLK10	7.57853	30.2259	1.9958	12.8143
CCDC71L	2.77818	9.37615	1.75486	12.7355
CDA	23.3753	81.5356	1.80245	12.6692
QPRT	24.5552	113.902	2.21369	12.6188
GBP3	5.85656	29.809	2.34763	12.5735
TMEM133	2.05151	8.42967	2.03879	12.4815
SESN2	2.29348	7.28959	1.6683	12.4692
TNFSF15	1.30247	8.96139	2.78247	12.3856
C15orf48	2.99803	35.8437	3.57963	12.2056
RBP1	6.95463	30.4893	2.13226	12.1918
GPR153	0.757752	3.13421	2.0483	12.165
CHPF2	22.8184	58.6281	1.3614	12.1344
TMEM65	11.5422	4.69723	-1.29704	-12.1032
HIST1H2BO	488.827	239.044	-1.03205	-12.0732
IL1RL1	205.379	56.2367	-1.86871	-12.0508
INHBA	2.89409	12.3967	2.09877	11.9769
EDN1	7.70559	24.2821	1.65591	11.9014
ASNS	10.7733	38.9623	1.85462	11.8556
ACSS1	5.11585	0.573625	-3.15679	-11.8393
HIST1H2BF	115.586	48.0761	-1.26558	-11.7622
KRT34	0.359488	9.10574	4.66276	11.7552
TXNIP	50.8394	156.806	1.62496	11.7512
BMP4	5.79442	19.1865	1.72736	11.5622
HIST1H1C	1198.09	523.708	-1.1939	-11.5398
SEZ6L2	5.26569	18.8387	1.83901	11.504
GBA	14.3845	55.6937	1.953	11.4836
RHOB	63.5199	29.1391	-1.12425	-11.4643
HIST1H1A	12.6447	1.32341	-3.2562	-11.442
TIMP4	9.28696	24.04	1.37216	11.4255
RRAS	3.99836	16.7801	2.06928	11.4074
FAM129A	3.60628	13.8335	1.93958	11.3543
CITED4	13.2818	21.9895	0.727365	11.2424
PLA2G16	28.8136	107.967	1.90576	11.1945
AC104389.28	2.71416	37.6549	3.79426	11.1924
POLD4	36.3209	104.193	1.52039	11.141
NMU	7.00105	31.3263	2.16173	11.1399
S100A4	36.1742	93.5198	1.37031	11.1166
WFDC2	35.8075	105.859	1.56381	11.1017
TIMP2	16.7023	41.528	1.31404	11.0928
MSMO1	38.65	110.408	1.5143	11.0915
C11orf68	15.4153	43.6197	1.50062	11.0607
C6orf15	1.37081	7.91157	2.52893	10.9892
PLAU	102.565	303.561	1.56545	10.9677

C1orf116	2.48212	9.78371	1.97881	10.9509
APOBEC3B	18.7093	49.19	1.39461	10.9059
GALNT14	50.9357	9.06127	-2.49089	-10.896
PALD1	7.36908	1.03124	-2.8371	-10.8925
TMEM238	4.82991	10.6893	1.1461	10.875
PCSK9	6.22768	17.4006	1.48237	10.8741
BIK	9.79469	20.9457	1.09658	10.8579
PRPS2	68.0381	24.0618	-1.4996	-10.8539
TMEM125	10.9383	34.6465	1.66332	10.8178
CHPF	34.816	73.2886	1.07384	10.8072
ALPPL2	0.611726	3.90571	2.67463	10.7892
HIST1H1D	320.978	132.524	-1.27622	-10.7663
NEU1	12.7835	35.7897	1.48527	10.735
IL1B	0.910641	35.2653	5.27522	10.7219
GNL3L	23.6181	8.07393	-1.54855	-10.6877
UNC5B	4.80889	1.84733	-1.38026	-10.664
GBP2	1.51717	10.8299	2.83556	10.6414
RP13-463N16.6	5.85382	18.7056	1.67602	10.6231
CD24P4	107.072	292.466	1.44969	10.608
FNDC4	1.89414	10.0404	2.40621	10.5858
DPYD	2.49023	10.5163	2.07828	10.5714
CSRP1	11.9752	38.1873	1.67305	10.5131
NDUFB1	35.2535	65.7837	0.899962	10.4705
CST4	4.18007	14.9365	1.83724	10.4339
TONSL	25.9544	11.2487	-1.20622	-10.4229
LAMA3	36.3607	113.828	1.64641	10.4137
PDCD1LG2	0.688351	5.60526	3.02557	10.3893
Metazoa_SRP	4241.31	2709.39	-0.64654	-10.3866
RPL22L1	290.205	86.4654	-1.74688	-10.362
ASS1	36.5824	104.546	1.51491	10.3337
GSTK1	65.3343	183.115	1.48684	10.3256
LAMC2	102.721	325.323	1.66314	10.3025
HIST2H2AC	671.421	334.263	-1.00623	-10.2991
NOP56	373.467	109.204	-1.77395	-10.2986
HLA-A	39.6568	100.372	1.33972	10.294
IL8	2.11769	17.0007	3.00503	10.2595
FAM214B	1.00562	5.49696	2.45055	10.2557
PADI3	2.94389	0.286188	-3.36269	-10.2513
RUVBL2	181.474	74.9067	-1.27659	-10.2266
GABARAPL1	7.41029	20.8033	1.48921	10.1969
PARP12	10.0113	32.8619	1.71479	10.1676
LAMB3	74.6933	211.818	1.50377	10.0406
FAM43A	1.93262	0.353938	-2.44899	-10.029
AKR1B10	564.213	214.981	-1.39203	-10.0265
FLNC	3.82834	13.791	1.84894	10.0136
MYH14	10.0664	24.655	1.29233	9.99784

FOXA1	41.0651	15.9242	-1.36669	-9.96093
SLFN5	4.64969	18.524	1.99419	9.95628
RAC2	14.6211	42.8285	1.55052	9.93942
ZNF239	6.31346	1.85514	-1.7669	-9.918
PDHA1	146.919	42.5747	-1.78695	-9.88544
UNC5A	4.28275	1.48738	-1.52577	-9.86433
IL1RN	5.44406	16.3264	1.58445	9.84269
BEND3	4.14867	1.56722	-1.40444	-9.81448
SLC2A6	4.5881	16.5269	1.84885	9.79836
TRIM29	26.9085	99.7802	1.89069	9.79573
FAM123B	2.27301	0.598875	-1.92428	-9.78997
HBE1	1.93782	42.9526	4.47024	9.78071
NIPSNAP3A	6.70684	17.2971	1.36683	9.76798
OTUD1	6.64098	14.0498	1.08108	9.7667
SH3BGRL3	34.9974	104.749	1.58162	9.75803
HDAC9	4.51229	20.3872	2.17573	9.7457
HEPHL1	0.103959	1.92687	4.21217	9.72636
NAT8L	2.33003	0.318094	-2.87282	-9.7153
AEN	17.922	6.52652	-1.45734	-9.68945
CITED2	28.1643	67.0059	1.25042	9.66232
HIST1H2BJ	622.763	245.989	-1.34009	-9.63264
SLAIN1	15.1358	3.81624	-1.98775	-9.62316
FAM83D	52.8437	23.8837	-1.14571	-9.61646
ATP11C	9.93443	3.00193	-1.72654	-9.60205
CHCHD10	114.385	64.9673	-0.81611	-9.57182

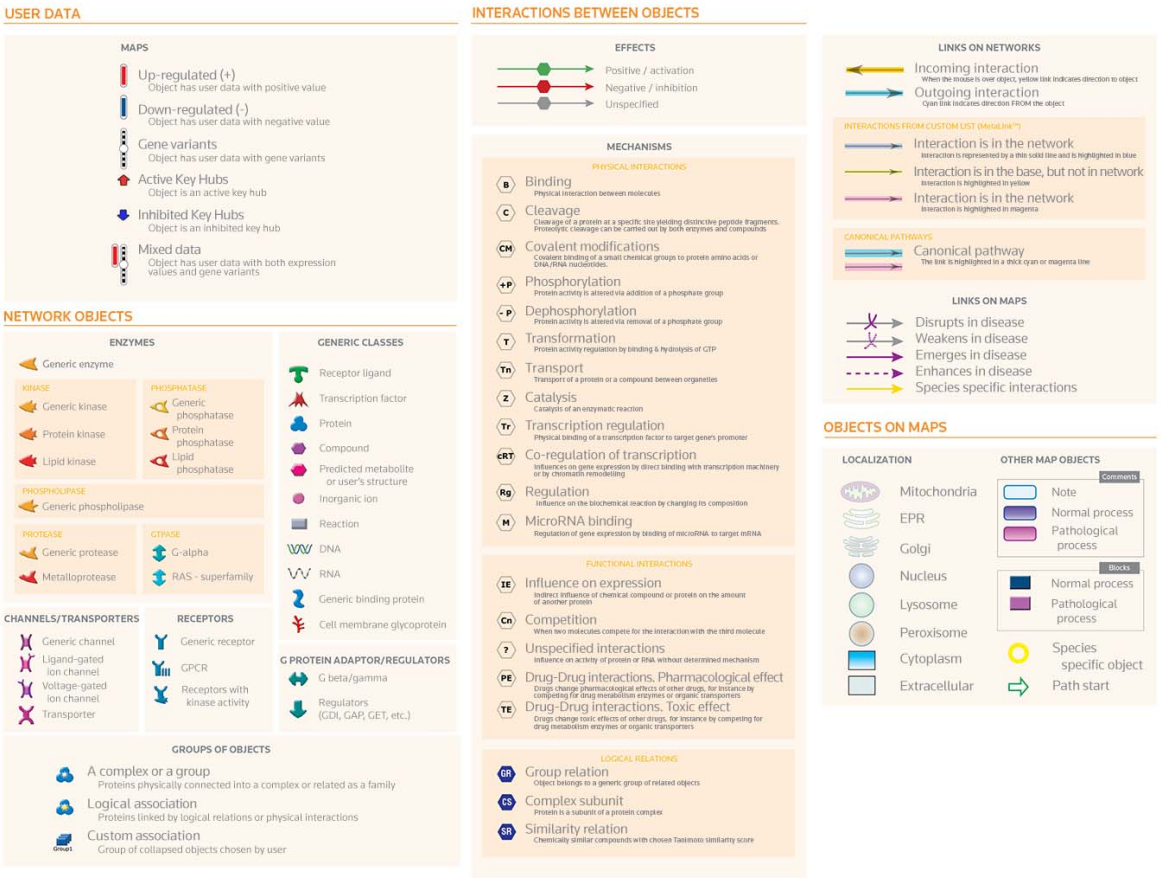
[1]p value of all genes $\leq 5x10^{-5}$
[2]Q value of all genes $\leq x10^{-4}$

Supplementary Table 2: Key pathways differentially regulated between PC-9 and SO25 cells.

These are the key pathways differentially regulated in the RNA-sequencing analysis conducted between PC-9 and SO25 cells as determined using Metacore Key Pathway Analysis (KPA).

#	Name	Input Data p-value	Key Hubs p-value	Union p-value	stacked / grouped
1	Cell cycle_Role of APC in cell cycle regulation	9.479E-10	1.452E-10	6.103E-16	
2	Cell cycle_ESR1 regulation of G1/S transition	8.315E-4	2.406E-10	8.48E-11	
3	DNA damage_ATM/ATR regulation of G1/S checkpoint	0.003796	2.056E-9	4.994E-10	
4	Cell cycle_Role of Nek in cell cycle regulation	1.014E-5	1.686E-5	2.862E-9	
5	Cytoskeleton remodeling_TGF, WNT and cytoskeletal remodeling	0.00218	5.378E-7	3.054E-9	
6	Development_WNT signaling pathway. Part 2	8.693E-4	2.743E-7	4.292E-9	
7	Cell cycle_Cell cycle (generic schema)	3.564E-4	5.14E-6	4.564E-9	
8	Cell cycle_Regulation of G1/S transition (part 1)	0.001995	2.32E-7	1.467E-8	
9	Cell cycle_Influence of Ras and Rho proteins on G1/S Transition	0.03815	2.778E-8	1.845E-8	
10	Regulation of degradation of deltaF508-CFTR in CF	0.002333	3.197E-7	2.374E-8	
11	Cell cycle_Spindle assembly and chromosome separation	1.314E-4	2.034E-4	8.107E-8	
12	Apoptosis and survival_Role of IAP-proteins in apoptosis	0.01345	1.374E-6	1.47E-7	
13	Transcription_Epigenetic regulation of gene expression	6.006E-5	0.007407	4.267E-7	
14	Mitogenic action of Estradiol / ESR1 (nuclear) in breast cancer	3.639E-5	6.587E-7	4.464E-7	
15	Transcription_Role of heterochromatin protein 1 (HP1) family in transcriptional silencing	1.418E-6	0.04801	1.14E-6	
16	Transport_RAN regulation pathway	0.009561	1.951E-4	1.212E-6	
17	DNA damage_ATM / ATR regulation of G2 / M checkpoint	0.007267	3.143E-5	1.357E-6	
18	Cell cycle_Regulation of G1/S transition (part 2)	0.03451	3.143E-5	1.357E-6	
19	CFTR folding and maturation (normal and CF)	1.021E-5	1.621E-5	4.128E-6	
20	Apoptosis and survival_Role of PKR in stress-induced apoptosis	0.01313	6.239E-5	4.191E-6	
21	Tau pathology in Alzheimer disease	0.04134	1.132E-5	4.191E-6	
22	Cell cycle_Initiation of mitosis	1.307E-4	0.00137	6.743E-6	
23	Immune response _IFN gamma signaling pathway	0.04134	6.239E-5	1.91E-5	

24	Cell cycle_Transition and termination of DNA replication	0.001858	0.01295	2.488E-5	
25	Apoptosis and survival_Role of nuclear PI3K in NGF/ TrkA signaling	7.816E-4	0.006631	3.197E-5	
26	Apoptosis and survival_Granzyme A signaling	0.04901	5.26E-4	3.668E-5	
27	Apoptosis and survival_p53-dependent apoptosis	0.04901	5.26E-4	3.668E-5	
28	Development_Thromboxane A2 signaling pathway	0.001229	0.007533	4.354E-5	
29	Apoptosis and survival_BAD phosphorylation	0.002713	0.01551	4.878E-5	
30	Apoptosis and survival_TNF-alpha-induced Caspase-8 signaling	0.04202	1.514E-4	4.878E-5	
31	Immune response_CD137 signaling in immune cell	0.04901	5.26E-4	2.103E-4	
32	Immune response_IL-33 signaling pathway	0.04822	0.006638	4.631E-4	
33	Development_Endothelin-1/EDNRA signaling	0.02953	0.01196	4.763E-4	
34	Immune response_Platelet activating factor/ PTAFR pathway signaling	0.002821	0.01477	7.23E-4	
35	Cell adhesion_Integrin inside-out signaling	0.03815	0.01634	8.819E-4	
36	Development_Epigenetic and transcriptional regulation of oligodendrocyte precursor cell differentiation and myelination	0.02244	0.007038	8.885E-4	
37	Cell cycle_The metaphase checkpoint	0.02813	0.002061	0.001446	
38	Transcription_Transcription regulation of aminoacid metabolism	0.03032	0.03703	0.00159	
39	G-protein signaling_Regulation of p38 and JNK signaling mediated by G-proteins	0.007951	0.03948	0.001817	
40	Development_TGF-beta receptor signaling	0.03224	0.01332	0.002016	
41	Reproduction_Progesterone-mediated oocyte maturation	0.03464	0.002852	0.00226	
42	Translation _Regulation of EIF2 activity	0.03464	0.01216	0.00226	
43	Development_Non-genomic action of Retinoic acid in cell differentiation	0.03512	0.01477	0.002414	
44	Development_Osteopontin signaling in osteoclasts	0.008574	0.04744	0.002751	
45	Development_Adenosine A2A receptor signaling	0.04604	0.01741	0.00413	
46	Development_Delta- and kappa-type opioid receptors signaling via beta-arrestin	0.02289	0.02809	0.004273	
47	Androgen receptor activation and downstream signaling in Prostate cancer	0.03346	0.02124	0.005297	
48	G-protein signaling_G-Protein alpha-12 signaling pathway	0.02813	0.03559	0.005376	



Supplementary Figure 1: Legend for cell cycle schematic.

Legend for cell cycle schematic shown in Figure 3.12 that was produced using Metacore KPA to analyse RNA-sequencing data. From Metacore KPA software.